Journal of High Energy Astrophysics 32 (2021) 28–64

Contents lists available at ScienceDirect

Journal of High Energy Astrophysics

www.elsevier.com/locate/jheap

Dissecting the H_0 and S_8 tensions with Planck + BAO + supernova type Ia in multi-parameter cosmologies

Luis A. Anchordoqui [a,b,c], Eleonora Di Valentino [d,*], Supriya Pan [e], Weiqiang Yang [f]

[a] Department of Physics and Astronomy, Lehman College, City University of New York, NY 10468, USA
[b] Department of Physics, Graduate Center, City University of New York, NY 10016, USA
[c] Department of Astrophysics, American Museum of Natural History, NY 10024, USA
[d] Institute for Particle Physics Phenomenology, Department of Physics, Durham University, Durham DH1 3LE, UK
[e] Department of Mathematics, Presidency University, 86/1 College Street, Kolkata 700073, India
[f] Department of Physics, Liaoning Normal University, Dalian, 116029, PR China

ARTICLE INFO

Article history:
Received 3 August 2021
Accepted 3 August 2021

ABSTRACT

The mismatch between the locally measured expansion rate of the universe and the one inferred from observations of the cosmic microwave background (CMB) assuming the canonical ΛCDM model has become the new cornerstone of modern cosmology, and many new-physics set ups are rising to the challenge. Concomitant with the so-called H_0 problem, there is evidence of a growing tension between the CMB-preferred value and the local determination of the weighted amplitude of matter fluctuations S_8. It would be appealing and compelling if both the H_0 and S_8 tensions were resolved at once, but as yet none of the proposed new-physics models have done so to a satisfactory degree. Herein, we adopt a systematic approach to investigate the possible interconnection among the free parameters in several classes of models that typify the main theoretical frameworks tackling the tensions on the universe expansion rate and the clustering of matter. Our calculations are carried out using the publicly available Boltzmann solver CAMB in combination with the sampler CosmoMC. We show that even after combining the leading classes of models sampling modifications of both the early and late-time universe a simultaneous solution to the H_0 and S_8 tensions remains elusive.

1. Introduction

The standard Λ-cold dark matter (ΛCDM) cosmological model provides an exceptional description of a wide range of astrophysical and astronomical observations (Zyla et al., 2020). The parameters governing the ΛCDM cosmology have been constrained with unprecedented accuracy using measurements of galaxy clusters (Alam et al., 2017; Beutler et al., 2011; Ross et al., 2015), weak lensing (Abbott et al., 2021; Asgari et al., 2020), supernovae type Ia (Scolnic et al., 2018), and anisotropies in the cosmic microwave background (CMB) temperature and polarization fields (Aghanim et al., 2020a,b). However, the enhanced precision of the various steps in the local distance-ladder measurements of the Hubble constant, $H_0 \equiv 100\ h$ km/s/Mpc, has recently opened a crack in the ΛCDM model. Indeed, a combination of the latest Supernovae $H0$ for the Equation of State (SH0ES) measurements with constraints of medium-to-high redshift probes have revealed a 4.2σ discrepancy between the ΛCDM inferred $H_0 = 67.27 \pm 0.60$ km/s/Mpc using data from the Planck satellite (Aghanim et al., 2020a,b) and the local measured value $H_0 = 73.2 \pm 1.3$ km/s/Mpc (Riess et al., 2019, 2021). Moreover, these measurements are supported by other early and late time observables, as shown in Verde et al. (2019); Di Valentino et al. (2021a); Riess (2019); Di Valentino (2021); Freedman (2021) and references therein.

Adding fuel to fire, the ΛCDM inferred value of the amplitude of mass fluctuations σ_8 has been consistently higher than the one measured in gravitational lensing (Abbott et al., 2021; Asgari et al., 2020). This leads to a tension that is quantified in terms of the $S_8 \equiv \sigma_8\sqrt{\Omega_m/0.3}$ parameter, where Ω_m is the present day value of the nonrelativistic matter density; see e.g. Di Valentino et al. (2021d). Strictly speaking, on the assumption of ΛCDM the Planck Collaboration estimated $S_8 = 0.834 \pm 0.016$, which is in more than 3σ tension with the result reported by KiDS-1000: $S_8 = 0.766^{+0.020}_{-0.014}$ (Asgari et al., 2020). The tension becomes 3.4σ if we consider a combination of BOSS and KV450: $S_8 = 0.728 \pm 0.026$ (Tröster et al., 2020). However, some data sets point to higher values of S_8, e.g. KiDS-450+GAMA for which

* Corresponding author.
E-mail addresses: luis.anchordoqui@gmail.com (L.A. Anchordoqui), eleonora.di-valentino@durham.ac.uk (E. Di Valentino), supriya.maths@presiuniv.ac.in (S. Pan), d11102004@163.com (W. Yang).

https://doi.org/10.1016/j.jheap.2021.08.001
2214-4048/

$S_8 = 0.800^{+0.029}_{-0.027}$ (van Uitert et al., 2018) or HSC SSP finding $S_8 = 0.804^{+0.032}_{-0.029}$ (Hamana et al., 2020).

Models addressing the H_0 tension either reduce the size of the sound horizon at recombination modifying the expansion rate in the early-universe, or else shift the matter-dark energy equality to earlier times than it otherwise would in ΛCDM with new physics in the post-recombination universe. Then, to keep the locations of the peaks in the CMB angular power spectrum fixed, H_0 increases diminishing the tension. Models addressing the S_8 tension are either based on late-universe physics processes that yield a suppression of the linear matter power spectrum, or else decrease the CMB-predicted value of Ω_m. It would be appealing and compelling if both the H_0 and σ_8 tensions were resolved simultaneously, but as yet none of the extant new physics models on this front have done so to a satisfactory degree (Di Valentino et al., 2021h).

In the recent H_0 olympics of Schöneberg et al. (2021), spanning both early- and late-time modifications of the universe expansion rate, the "gold medal" for the best scenario has been given to a varying effective electron mass in a curved universe (Sekiguchi and Takahashi, 2021). However, the so-called "interacting dark energy - dark matter (IDE) models" did not participate in this competition. It has long been suspected that IDE is a compelling framework settling several cosmological issues (see e.g., Wetterich, 1995; Amendola, 2000; Comelli et al., 2003; Franca and Rosenfeld, 2004; Anchordoqui et al., 2007; Chimento and Richarte, 2012; Bolotin et al., 2014; Wang et al., 2016) and recently it gained significant attention for ameliorating the H_0 and S_8 tensions (see e.g. Kumar and Nunes, 2016, 2017; Di Valentino et al., 2017; Yang et al., 2018c,a; Kumar et al., 2019; Pan et al., 2019b,a; Di Valentino et al., 2020b,c; Yang et al., 2020e; Gao et al., 2021; Pan et al., 2020c; Lucca and Hooper, 2020; Wang et al., 2021; Kumar, 2021; Lucca, 2021a). In this paper we adopt a systematic approach to study the possible interconnection among the free parameters in 24 combinations that typify the various theoretical frameworks tackling the H_0 and S_8 tensions, including both early- and late-time modifications of the universe expansion rate, as well as IDE and curved-space models. Hence, the results presented herein are complementary to those reported in Schöneberg et al. (2021).

The layout of the paper is as follows. We begin in Sec. 2 by introducing the classes of cosmological models to be explored and discussing the relevant phenomenology. In Sec. 3 we first describe the observational data sets used in our study together with the method of data analysis and the priors imposed on the cosmological parameters. After that, for each class of models, we use the Boltzmann solver `CAMB` (Lewis et al., 2000) in combination with `CosmoMC` (Lewis and Bridle, 2002; Lewis, 2013) to establish which regions of parameter space are empirically viable to resolve the H_0 and S_8 tensions. Armed with our findings, in Sec. 4 we investigate the crosscorrelation between parameters. The paper wraps up with some conclusions in Sec. 5.

2. ΛCDM and beyond

Experiments show that the distribution of matter and radiation in the observable universe is almost homogeneous and isotropic. Thus, the evolution of the universe is well-described by the maximally-symmetric Friedmann-Lamaître-Robertson-Walker (FLRW) line element

$$ds^2 = dt^2 - a^2(t)\left[\frac{dr^2}{1-kr^2} + r^2\,(d\theta^2 + \sin^2\phi\, d\phi^2)\right], \tag{1}$$

where (t, r, θ, ϕ) are comoving coordinates, $a(t)$ is the cosmic scale factor, and k $(= -1, 0, 1)$ parametrizes the curvature of the homogeneous and isotropic spatial sections (Kolb and Turner, 1990). It is often convenient to express the line element as

$$ds^2 = a^2(\eta)\left\{d\eta^2 - \left[\frac{dr^2}{1-kr^2} + r^2(d\theta^2 + \sin^2\phi d\phi^2)\right]\right\}, \tag{2}$$

where $\eta = \int_0^t dt'/a(t')$ is the "conformal time." Small deviations from homogeneity and isotropy are generally modeled as perturbations over the background metric given in (2).

The cosmic expansion is driven by the first Friedmann equation for the Hubble parameter H,

$$H^2(a) = \frac{8\pi G}{3}\left\{\sum_i \rho_i(a)\right\} - \frac{k}{a^2}, \tag{3}$$

where G is the gravitational constant and the sum runs over the energy densities ρ_i of the various components of the cosmic fluid: dark energy (DE), CDM (c), baryons (b), photons (γ), and three flavors of one helicity state neutrinos (left-handed ν_L along with their right-handed $\overline{\nu}_R$, that we denote ν for short). Equation (3) can be rewritten as

$$H^2(z) = H_0^2\Bigg[(\Omega_c + \Omega_b)(1+z)^3 + \Omega_\gamma(1+z)^4 + \Omega_k(1+z)^2 + \Omega_{\rm DE}\exp\left(3\int_0^z \frac{1+w}{1+z'}dz'\right) + \frac{\rho_\nu(z)}{\rho_{\rm crit,0}}\Bigg], \tag{4}$$

where $z = a_0/a - 1$ is the redshift, $\rho_{\rm crit,0} = 3H_0^2/(8\pi G)$ is the present day value of the critical density, and $\Omega_i = \rho_{i,0}/\rho_{\rm crit,0}$ denotes the present-day density parameters. Throughout the article we use the subscript 0 to indicate the quantities evaluated today, with $a_0 = 1$. Since we always refer to the present day density parameters, we omit the subscript 0 in this case. The energy densities of non-relativistic matter and radiation scale as a^{-3} and a^{-4} respectively, and set the scalings with $(1+z)$. The scaling of $\Omega_{\rm DE}$ is usually described by an "equation-of-state" parameter $w \equiv p_{\rm DE}/\rho_{\rm DE}$, the ratio of the spatially-homogeneous dark energy pressure to its energy density $\rho_{\rm DE}$. To accommodate the observed cosmic acceleration we should have $w < -1/3$. The most economic explanation for dark energy is the cosmological constant Λ, for which $w = -1$. An alternative possibility is to consider a cosmic scalar field slowly rolling to the minimum of its potential (Wetterich, 1988; Peebles and Ratra, 1988; Ratra and Peebles, 1988), the so-called "quintessence field" (Caldwell et al., 1998). For this class of models, $-1 < w < -1/3$ and the dark-energy density decreases as $\rho_q \propto a^{-3(1+w)}$. Yet another possibility is to consider "phantom dark energy" for which $w < -1$ (Caldwell, 2002). A point worth noting at this juncture is that phantom DE models violate the dominant energy condition (Carroll et al., 2003; Caldwell et al., 2003; Carroll et al., 2005; Sawicki and Vikman, 2013) a cherished notion adopted to prohibit wormholes and time machines (Morris et al., 1988). However, it is hard to envision how wormholes and time machines could originate from phantom energy. In (4) we have left open the possibility for an arbitrary (albeit constant) value of w. For ρ_ν, we could not write a simple scaling with z because the equation-of-state parameter is not constant. The curvature density parameter is defined as $\Omega_k = -k/H_0^2$.

For the benchmark spatially-flat ΛCDM 6-parameter model, we have: $\Omega_k = 0$, $\Omega_{\rm DE} = \Omega_\Lambda$, and $w = -1$. The Hubble constant is inferred from one of these free parameters: the angular size of the sound horizon at recombination θ_*, which is given by the ratio of the comoving sound horizon to the comoving angular diameter distance to last-scattering surface

$$\theta_* = \frac{r_s(z_{\rm LS})}{D_M(z_{\rm LS})}. \tag{5}$$

The comoving linear size of the sound horizon and the comoving angular diameter distance are linked to the expansion history of the universe via

$$r_s(z) = \int_z^\infty \frac{c_s(z')}{H(z')}\, dz' \tag{6}$$

and

$$D_M(z) = \int_0^z \frac{1}{H(z')}\, dz' \tag{7}$$

respectively, with c_s the speed of sound (Aghanim et al., 2020a). The set of free parameters that describe the ΛCDM model is:

$$\mathcal{P}_0 \equiv \left\{\Omega_b h^2, \Omega_c h^2, 100\theta_{\rm MC}, \tau, n_s, \ln[10^{10} A_s]\right\}, \tag{8}$$

where τ is the reionization optical depth, n_s is the scalar spectral index, A_s is the amplitude of the scalar primordial power spectrum, and the $\theta_{\rm MC}$ parameter is an approximation of θ_* (which is adopted in CosmoMC (Lewis and Bridle, 2002; Lewis, 2013) and is based on fitting formulae given in Hu and Sugiyama (1996)).

A class of spatially-flat extensions to the base ΛCDM model that can reduce the H_0 tension is based on the addition of relativistic degrees-of-freedom in the early universe. The presence of any additional light species (such as sterile neutrinos (Anchordoqui and Goldberg, 2012; Anchordoqui et al., 2013; Jacques et al., 2013; Di Valentino et al., 2016b), axions (Giusarma et al., 2014; Di Valentino et al., 2015, 2016a; Baumann et al., 2016; Poulin et al., 2018; D'Eramo et al., 2018; Giarè et al., 2020), massless Goldstone bosons (Weinberg, 2013), or any other massless fields from the dark sector (Anchordoqui, 2021)) can be characterized by the number of "equivalent" light neutrino species

$$N_{\rm eff} \equiv \frac{\rho_{\rm R} - \rho_\gamma}{\rho_\nu} \tag{9}$$

in units of the density of a single Weyl neutrino ρ_ν, where $\rho_{\rm R}$ is the total energy density in relativistic particles and ρ_γ is the energy density of photons (Steigman et al., 1977). For three families of massless (Standard Model) neutrinos, $N_{\rm eff} = 3.046$ (Mangano et al., 2005; de Salas and Pastor, 2016; Akita and Yamaguchi, 2020; Froustey et al., 2020; Bennett et al., 2021). The set of free parameters describing this class of models is given by

$$\mathcal{P}_1 \equiv \left\{\Omega_b h^2, \Omega_c h^2, 100\theta_{\rm MC}, \tau, n_s, \ln[10^{10} A_s], N_{\rm eff}\right\}. \tag{10}$$

Note that by adding dark relativistic degrees-of-freedom into the early universe we are increasing the expansion rate $H(z)$, which in turn reduces $r_s(z_{\rm LS})$. The accurate measurement of the location of the acoustic peaks by the Planck mission sets the value of the ΛCDM free parameter θ_*, and so to maintain the ratio in (5) we must increase H_0 to decrease $D_M(z_{\rm LS})$. However, adding relativistic degrees-of-freedom into the early universe also affects the damping scale θ_D of the CMB power spectrum, with $\theta_D/\theta_* \propto \sqrt{H(z_{\rm LS})}$ (Hou et al., 2013). Therefore, while we increase $N_{\rm eff}$ for a faster expansion rate $H(z_{\rm LS})$ at θ_* fixed we also increase θ_D, with the damping contributing at larger scales to reduce the power in the damping tail. The main limiting factor in constraining $N_{\rm eff}$ from CMB data is a degeneracy with the primordial helium fraction $Y_P \equiv n_{\rm He}/n_b$. Namely, for fixed $\Omega_b h^2$, by increasing Y_P at the end of big bang nucleosynthesis (BBN) we decrease the number density of free electrons and increase the diffusion length. Altogether this reduces the power in the damping tail (Baumann, 2018). Using $\mathcal{P}_1$ to accommodate CMB + BAO data and BBN observations (Aver et al., 2015; Cooke et al., 2018) the Planck Collaboration reported $N_{\rm eff} = 3.12^{+0.25}_{-0.26}$ at the 95% CL (Aghanim et al., 2020a). Herein we will take this bound as an external constraint to our numerical analysis for spatially-flat models.

Other attempts to resolve the H_0 tension involve tweaking ΛCDM somehow to slow down the late-time expansion rate without making radical changes to the early-time expansion rate. Within this class of models the value of $r_s(z_{\rm LS})$ does not differ appreciably from that obtained assuming ΛCDM for the same choice of cosmological parameters. Now, a consistently lower value of $H(z)$ at low redshifts leads to a larger value of $D_M(z_{\rm LS})$, which in turn would result in a smaller value of θ_*. Thus, we must (re)-decrease $D_M(z_{\rm LS})$ to keep θ_* unchanged, and this can be accomplished by increasing H_0. A straightforward extension of the standard cosmology within this class of models emerges when considering $w < -1$. It is easily seen in (4) that by considering $w < -1$ we lower the expansion rate for $z > 0$ with respect to the case where the DE is in the form of a cosmological constant. From now on, we denote with $w_q > -1$ and $w_p < -1$ the equation-of-state of quintessence and phantom models, which are analyzed separately. The sets of free parameters describing these classes of models are given by

$$\mathcal{P}_2 \equiv \left\{\Omega_b h^2, \Omega_c h^2, 100\theta_{\rm MC}, \tau, n_s, \ln[10^{10} A_s], w_q, \right\}, \tag{11}$$

and

$$\mathcal{P}_3 \equiv \left\{\Omega_b h^2, \Omega_c h^2, 100\theta_{\rm MC}, \tau, n_s, \ln[10^{10} A_s], w_p, \right\}. \tag{12}$$

It is worth recalling that models with $w_p < -1$ violate the null energy condition and are typically unstable; though with optimistic assumptions the instability time scale can be greater than the age of the universe. Quintessence models for which $r_s(z_{\rm LS})$ is unmodified from ΛCDM exacerbate the H_0 tension. This is because for $w \geq -1$, the DE can only redshift faster than the cosmological constant, yielding a smaller contribution to the energy density today than it would have been in ΛCDM with the same value of $H(z_{\rm LS})$, and so it is easily seen from (4) that H_0 must also be smaller (Raveri et al., 2019; Colgáin and Yavartanoo, 2019). A different quintessence scenario appears if the scalar field speeds up $H(z)$ and reduces the sound horizon during the era leading up to recombination (Pettorino et al., 2013; Poulin et al., 2019; Agrawal et al., 2019a; Gogoi et al., 2021; Gómez-Valent et al., 2021). As in the class of models characterized by $N_{\rm eff}$, these early dark energy models lead to larger H_0 values as compared to ΛCDM. However, early dark energy models increase the tension with large scale structure data. It is easy to detect the source that increases S_8 in this class of models, because the early dark energy slightly suppresses the growth of perturbations during the period in which it contributes non-negligibly to the cosmic energy density. Therefore, to properly match the CMB data we must increase the CDM component to compensate for the suppression in the efficiency of perturbation growth (Hill et al., 2020).

A fourth class of models incorporates a coupling between the DE and the dark matter (DM) sectors, altering ΛCDM late-universe-based predictions (Cai and Wang, 2005; Barrow and Clifton, 2006; Valiviita et al., 2008; Gavela et al., 2009, 2010; Salvatelli et al., 2013; Li and Zhang, 2014; Yang and Xu, 2014a,b; Salvatelli et al., 2014; Yang and Xu, 2014c; Väliviita and Palmgren, 2015; Pan et al., 2015; Nunes et al., 2016; Ferreira et al., 2017; Kumar and Nunes, 2016; Murgia et al., 2016; Pan and Sharov, 2017; vom Marttens et al., 2017; Sharov et al., 2017, Yang et al., 2017a, 2018b, 2017b; Guo et al., 2018; Pan et al., 2018; Kumar and Nunes, 2017; Di Valentino et al., 2017; Li et al., 2017; Feng et al., 2019; Yang et al., 2019c,b; von Marttens et

al., 2019; Yang et al., 2018c; Pan et al., 2019a; Martinelli et al., 2019; Paliathanasis et al., 2019; Yang et al., 2020d,e; Pan et al., 2019b, 2020c; Yang et al., 2019a; Kumar et al., 2019; Agrawal et al., 2019b; Di Valentino et al., 2020b,c; Anchordoqui et al., 2020; Yao and Meng, 2020; Pan et al., 2020a,b; Gómez-Valent et al., 2020; Lucca and Hooper, 2020; Yao and Meng, 2021; Di Valentino, 2021; Anchordoqui, 2020; Anchordoqui et al., 2021; Amirhashchi and Yadav, 2020; von Marttens et al., 2020; Sinha, 2021; Gao et al., 2021; Bonilla et al., 2021; Kumar, 2021; Lucca, 2021a; Yang et al., 2021c; Paliathanasis et al., 2021; Mukherjee and Banerjee, 2021; Lucca, 2021b; Nunes and Di Valentino, 2021). At the background level, the DM-DE coupling modifies the functional form of the continuity equation of the dark fluids as

$$\dot{\rho}_c + 3\mathcal{H}\rho_c = Q \tag{13}$$

and

$$\dot{\rho}_{\rm DE} + 3\mathcal{H}(1+w)\rho_{\rm DE} = -Q\,, \tag{14}$$

where the dot denotes derivative with respect to η, $\mathcal{H} \equiv \dot{a}/a$ is the conformal Hubble rate, and Q is the interaction rate or the interaction function which characterizes the transfer of energy or/and momentum between the dark sectors, and where $Q < 0$ and $Q > 0$ indicate energy transfer from DE to DM and vice versa. Although the choice of the interaction function is not unique, a classical functional form is given by

$$Q = \xi \mathcal{H} \rho_{\rm DE}\,, \tag{15}$$

where ξ is a dimensionless coupling parameter quantifying the strength of the DM-DE interaction. Since the sign of ξ could be either positive or negative, this defines two sub-classes of models driven by ξ_+ (for which $\xi > 0$) and ξ_- (for which $\xi < 0$). The presence of the DM-DE coupling also modifies the evolution at the level of perturbations. Assuming the synchronous gauge, the evolution of the DM and DE density perturbations as well as velocity divergences have been computed in Refs. Valiviita et al. (2008); Gavela et al. (2009, 2010). Following Di Valentino et al. (2020b), we adopt adiabatic initial conditions in our Boltzmann system for all species. At this stage, it is worthwhile to note that when considering a coupling between the DE and DM sectors, the interacting system could be unstable. Indeed, DE-DM interactions suffer from gravitational instabilities if $w = -1$ (Valiviita et al., 2008; He et al., 2009). We circumvent the instability problem by taking $w = -0.999$. This approximation is justified because for $w \to -1$, the effect of DE perturbations is basically unnoticeable (Salvatelli et al., 2013; Di Valentino et al., 2017, 2020c). Therefore, the interacting system essentially captures the effect of the DM-DE coupling, while at the same time ensuring the absence of gravitational instabilities. In addition, in this case we require $\xi < 0$, in order to avoid the early-time instabilities (Valiviita et al., 2008; Gavela et al., 2009; Clemson et al., 2012; Gavela et al., 2010; He et al., 2009; Jackson et al., 2009). The set of free parameters describing this class of models are given by

$$\mathcal{P}_4 \equiv \left\{\Omega_b h^2, \Omega_c h^2, 100\theta_{\rm MC}, \tau, n_s, \ln[10^{10}A_s], \xi_-, \right\}. \tag{16}$$

Finally, we can open Pandora's box to construct another class of models that could resolve the H_0 tension. By inspection of (4) we can immediately see that the increase of the effective fractional contribution of spatial curvature to the energy budget yields a faster expansion rate. The set of free parameters describing this class of models is given by

$$\mathcal{P}_5 \equiv \left\{\Omega_b h^2, \Omega_c h^2, 100\theta_{\rm MC}, \tau, n_s, \ln[10^{10}A_s], \Omega_k\right\} \tag{17}$$

Observational data from the Planck mission point to a 3.4σ evidence for a closed universe: $-0.095 < \Omega_k < -0.007$ at 99% CL (Aghanim et al., 2020a; Di Valentino et al., 2019; Handley, 2021; Di Valentino et al., 2021b). If this were the case, we can immediately infer from (4) that the parameter set $\mathcal{P}_5$ would actually exacerbate the H_0 tension.

In what follows we consider the cosmological models that can be characterized by the 18 additional possible combinations of the extra 6 free parameters discussed above ($N_{\rm eff}$, w_q, w_p, $\xi_\pm$, Ω_k). In order to avoid the early-time instabilities (Valiviita et al., 2008; Gavela et al., 2009; Clemson et al., 2012; Gavela et al., 2010; He et al., 2009; Jackson et al., 2009) we will have ξ_- when $w_q > -1$, and ξ_+ when $w_p < -1$. The set of free parameters describing these classes of models are given by

$$\mathcal{P}_6 \equiv \left\{\Omega_b h^2, \Omega_c h^2, 100\theta_{\rm MC}, \tau, n_s, \ln[10^{10}A_s], N_{\rm eff}, w_q\right\}, \tag{18}$$

$$\mathcal{P}_7 \equiv \left\{\Omega_b h^2, \Omega_c h^2, 100\theta_{\rm MC}, \tau, n_s, \ln[10^{10}A_s], N_{\rm eff}, w_p\right\}, \tag{19}$$

$$\mathcal{P}_8 \equiv \left\{\Omega_b h^2, \Omega_c h^2, 100\theta_{\rm MC}, \tau, n_s, \ln[10^{10}A_s], N_{\rm eff}, \xi_-\right\}, \tag{20}$$

$$\mathcal{P}_9 \equiv \left\{\Omega_b h^2, \Omega_c h^2, 100\theta_{\rm MC}, \tau, n_s, \ln[10^{10}A_s], N_{\rm eff}, \Omega_k\right\}, \tag{21}$$

$$\mathcal{P}_{10} \equiv \left\{\Omega_b h^2, \Omega_c h^2, 100\theta_{\rm MC}, \tau, n_s, \ln[10^{10}A_s], w_q, \xi_-\right\}, \tag{22}$$

$$\mathcal{P}_{11} \equiv \left\{\Omega_b h^2, \Omega_c h^2, 100\theta_{\rm MC}, \tau, n_s, \ln[10^{10}A_s], w_p, \xi_+\right\}, \tag{23}$$

$$\mathcal{P}_{12} \equiv \left\{\Omega_b h^2, \Omega_c h^2, 100\theta_{\rm MC}, \tau, n_s, \ln[10^{10}A_s], w_q, \Omega_k\right\}, \tag{24}$$

$$\mathcal{P}_{13} \equiv \left\{\Omega_b h^2, \Omega_c h^2, 100\theta_{\rm MC}, \tau, n_s, \ln[10^{10}A_s], w_p, \Omega_k\right\}, \tag{25}$$

$$\mathcal{P}_{14} \equiv \left\{\Omega_b h^2, \Omega_c h^2, 100\theta_{\rm MC}, \tau, n_s, \ln[10^{10}A_s], \xi_-, \Omega_k\right\}, \tag{26}$$

$$\mathcal{P}_{15} \equiv \left\{\Omega_b h^2, \Omega_c h^2, 100\theta_{\rm MC}, \tau, n_s, \ln[10^{10}A_s], N_{\rm eff}, w_q, \xi_-\right\}, \tag{27}$$

$$\mathcal{P}_{16} \equiv \left\{\Omega_b h^2, \Omega_c h^2, 100\theta_{\rm MC}, \tau, n_s, \ln[10^{10}A_s], N_{\rm eff}, w_p, \xi_+\right\}, \tag{28}$$

$$\mathcal{P}_{17} \equiv \left\{\Omega_b h^2, \Omega_c h^2, 100\theta_{\rm MC}, \tau, n_s, \ln[10^{10}A_s], N_{\rm eff}, w_q, \Omega_k\right\}, \tag{29}$$

$$\mathcal{P}_{18} \equiv \left\{\Omega_b h^2, \Omega_c h^2, 100\theta_{\rm MC}, \tau, n_s, \ln[10^{10}A_s], N_{\rm eff}, w_p, \Omega_k\right\}, \tag{30}$$

$$\mathcal{P}_{19} \equiv \left\{\Omega_b h^2, \Omega_c h^2, 100\theta_{\rm MC}, \tau, n_s, \ln[10^{10}A_s], N_{\rm eff}, \xi_-, \Omega_k\right\}, \tag{31}$$

$$\mathcal{P}_{20} \equiv \left\{\Omega_b h^2, \Omega_c h^2, 100\theta_{\rm MC}, \tau, n_s, \ln[10^{10}A_s], w_q, \xi_-, \Omega_k\right\}, \tag{32}$$

$$\mathcal{P}_{21} \equiv \left\{\Omega_b h^2, \Omega_c h^2, 100\theta_{\rm MC}, \tau, n_s, \ln[10^{10}A_s], w_p, \xi_+, \Omega_k\right\}, \tag{33}$$

$$\mathcal{P}_{22} \equiv \left\{\Omega_b h^2, \Omega_c h^2, 100\theta_{\rm MC}, \tau, n_s, \ln[10^{10}A_s], N_{\rm eff}, w_q, \xi_-, \Omega_k\right\}, \tag{34}$$

and

$$\mathcal{P}_{23} \equiv \left\{\Omega_b h^2, \Omega_c h^2, 100\theta_{\rm MC}, \tau, n_s, \ln[10^{10}A_s], N_{\rm eff}, w_p, \xi_+, \Omega_k\right\}. \tag{35}$$

Most of the combined models described in (17) to (27) have been previously discussed in the literature, see e.g. Vagnozzi (2020); Yang et al. (2020c,b,a); Di Valentino et al. (2020a, 2021g); Yang et al. (2021a); Benaoum et al. (2020); Di Valentino and Mena (2020); Vagnozzi et al. (2020); Di Valentino (2021); Di Valentino et al. (2021e); Yang et al. (2021b,d). In this work we adopt a systematic approach in which we (re)examine all of these models with the goal of establishing possible intercorrelations among the free parameters.

For extensive reviews about possible solutions of the H_0 and S_8 tensions see Di Valentino et al. (2021a,d,h); Jedamzik et al. (2021); Knox and Millea (2020); Saridakis et al. (2021); Perivolaropoulos and Skara (2021); Schöneberg et al. (2021) and references therein.

3. Observational data, statistical methodology, and numerical analysis

We begin with a brief description of the cosmological data sets used in this work.

- **Planck 2018 CMB data**: The CMB temperature and polarization angular power spectra *plikTTTEEE+lowl+lowE* from the Planck 2018 legacy release (Aghanim et al., 2020a,b).
- **BAO**: Measurements of baryon acoustic oscillations (BAO) from different galaxy surveys: 6dFGS (Beutler et al., 2011), SDSS-MGS (Ross et al., 2015), and BOSS DR12 (Alam et al., 2017). This is the same combination of BAO data considered by the Planck Collaboration in Aghanim et al. (2020a).
- **Pantheon**: The 1048 supernovae type Ia data points which are distributed in the redshift interval $0.01 \leq z \leq 2.3$, dubbed the Pantheon sample (Scolnic et al., 2018).
- **R20**: A gaussian prior on the Hubble constant in agreement with the measurement obtained by the SH0ES collaboration in Riess et al. (2021).

We note in passing that associated to the H_0 tension there is the question of the roles played by the sound horizon scale and the local expansion rate as distance anchors (Cuesta et al., 2015). In particular, the so-called "inverse distance ladder calibration" of Pantheon sample (Scolnic et al., 2018) based on the CMB-inferred sound-horizon scale as an anchor cannot be made compatible with the direct distance ladder calibration of R20 (Riess et al., 2021). This has emerged as a redefinition of the H_0 tension gauging the calibration of the intrinsic supernova magnitude M_B adopted in the local distance ladder H_0 measurement, while testing the consistency of the corresponding observed fluxes from the Pantheon catalogue with the underlying cosmological model (Camarena and Marra, 2021; Efstathiou, 2021). However, we note that the M_B tension is only referring to the mismatch observed in SH0ES vs Planck data analyses, without considering all the other probes and cannot test modifications of the expansion rate in the early universe. For this reason, herein we center the analysis on the H_0 tension.

For the numerical analysis, we adopt a modified version of the well known cosmological package `CosmoMC` (Lewis and Bridle, 2002; Lewis, 2013), which is publicly available (http://cosmologist.info/cosmomc/). This package is equipped with a convergence diagnostic based on the Gelman-Rubin criterion (Gelman and Rubin, 1992) and includes the support for the 2018 Planck data release (Aghanim et al., 2020b). The flat priors on the free parameters of the classes of models analyzed herein are listed in Table 1. The results of our numerical analysis are encapsulated in Tables 2 to 13 and Figs. 1 to 24.

A point worth noting at this juncture is that the acoustic peaks which are prominently observed in the CMB anisotropy spectra, are also visible as BAO peaks in the galaxy power spectra and carry the footprints of a new standard ruler: the sound horizon at the epoch of baryon decoupling, $r_{\rm drag}$, when the photon drag on baryons becomes unimportant. The estimated sound horizon at the end of the baryonic-drag epoch is $r_{\rm drag} = (137 \pm 3^{\rm stat} \pm 2^{\rm syst})$ Mpc (Arendse et al., 2020). This estimate is based on data from low-redshift probes and a set of polynomial parametrizations which are almost independent of the underlying cosmology. None of the combination of classes of models analyzed herein can accommodate the $r_{\rm drag}$ estimate of Arendse et al. (2020) at the 1σ level; see Tables 2 to 13.

Table 1
Flat priors on various cosmological parameters coming from several cosmological scenarios.

Parameter	Prior
$\Omega_b h^2$	$[0.005, 0.1]$
$\Omega_c h^2$	$[0.001, 0.99]$
$100\theta_{\rm MC}$	$[0.5, 10]$
τ	$[0.01, 0.8]$
n_s	$[0.8, 1.2]$
$\ln[10^{10} A_s]$	$[1.61, 3.91]$
$N_{\rm eff}$	$[0.05, 10]$
w_q	$[-1, 1]$
w_p	$[-3, -1]$
ξ_+	$[0, 1]$
ξ_-	$[-1, 0]$
Ω_k	$[-0.3, 0.3]$

4. Discussion of the results

In this section we summarize the results obtained for the different extended cosmological classes of models, highlighting the indication for new physics beyond the ΛCDM model or the possible solution of the H_0 and/or S_8 tension. For each case, we show the constraints obtained from Planck alone (CMB), CMB + BAO + Pantheon (labeled by 'all'), CMB + R20, and CMB +BAO + R20.

4.1. Planck, BAO and Pantheon

In Table 2 we show the results obtained for a ΛCDM model ($\mathcal{P}_0$) and two wCDM classes of models, divided into two different regions based on the DE equation of state parameter: when the DE equation of state lies in the quintessence regime, i.e. $w_q > -1$ ($\mathcal{P}_2$) and when the DE equation of state lies in the phantom regime, i.e. $w_p < -1$ ($\mathcal{P}_3$). We can see that, with respect to the ΛCDM model, in the $\mathcal{P}_2$ scenario the CMB + BAO + Pantheon dataset combination decreases the tension with the weak lensing data, but there is no indication for $w \neq -1$ and the Hubble constant tension cannot be eliminated. In the $\mathcal{P}_3$ scenario, for CMB + BAO + Pantheon dataset combination the tension with the weak lensing data is restored with an indication of a phantom DE at more than 1σ. Additionally, we see a very mild increase in H_0 for this dataset compared to the recorded value of H_0 in the $\mathcal{P}_0$ for the same dataset and hence the H_0 tension is very mildly alleviated in this case. This increment in the Hubble constant is mainly driven by the phantom DE. In order to understand the behavior of the parameters in these classes of models, we have displayed the one dimensional posterior distributions and the two dimensional joint contours in Figs. 1 (for $\mathcal{P}_0$), 3 (for $\mathcal{P}_2$), and 4 (for $\mathcal{P}_3$).

In Table 3 we show the cosmological constraints for the classes of models described by ΛCDM + $N_{\rm eff}$ model ($\mathcal{P}_1$), IDE ($\mathcal{P}_4$), and IDE + $N_{\rm eff}$ ($\mathcal{P}_8$). As already shown in the literature, extra relativistic degrees of freedom at recombination are not favored by data, and in the $\mathcal{P}_1$ framework the Hubble tension cannot be resolved. On the contrary, H_0 is naturally in agreement with SH0ES in the IDE scenario, at the price of a coupling between DM and DE at more than 99% CL for Planck-data alone. The H_0 tension is, however, restored above 3σ when BAO and Pantheon data are included, i.e. for the dataset CMB + BAO + Pantheon, and the evidence for the coupling is reduced to 1σ. The combination of the two extensions in

Table 2
68% CL constraints on various free and derived parameters of the parameter spaces $\mathcal{P}_0 \equiv \left\{\Omega_b h^2, \Omega_c h^2, 100\theta_{\rm MC}, \tau, n_s, \ln[10^{10} A_s]\right\}$, $\mathcal{P}_2 \equiv \left\{\Omega_b h^2, \Omega_c h^2, 100\theta_{\rm MC}, \tau, n_s, \ln[10^{10} A_s], w_q, \right\}$ and $\mathcal{P}_3 \equiv \left\{\Omega_b h^2, \Omega_c h^2, 100\theta_{\rm MC}, \tau, n_s, \ln[10^{10} A_s], w_p, \right\}$.

Model	$\mathcal{P}_0$	$\mathcal{P}_0$	$\mathcal{P}_2$	$\mathcal{P}_2$	$\mathcal{P}_3$	$\mathcal{P}_3$
	CMB	all	CMB	all	CMB	all
$\Omega_{\rm b}h^2$	0.02236 ± 0.00015	0.02243 ± 0.00013	0.02235 ± 0.00015	0.02246 ± 0.00014	0.02240 ± 0.00015	0.02237 ± 0.00014
$\Omega_{\rm c}h^2$	0.1202 ± 0.0014	0.11918 ± 0.00097	0.1203 ± 0.0014	0.1188 ± 0.0010	0.1199 ± 0.0013	0.1200 ± 0.0011
$100\theta_{MC}$	1.04090 ± 0.00031	1.04102 ± 0.00029	1.04088 ± 0.00031	1.04106 ± 0.00030	1.04095 ± 0.00031	1.04093 ± 0.00030
τ	0.0546 ± 0.0078	$0.0558^{+0.0070}_{-0.0078}$	$0.0547^{+0.0074}_{-0.0082}$	$0.0563^{+0.0072}_{-0.0081}$	0.0540 ± 0.0078	0.0545 ± 0.0077
n_s	0.9648 ± 0.0043	0.9671 ± 0.0038	0.9645 ± 0.0044	0.9682 ± 0.0038	0.9656 ± 0.0043	0.9651 ± 0.0040
$\ln(10^{10} A_s)$	3.045 ± 0.016	$3.046^{+0.014}_{-0.016}$	3.046 ± 0.016	3.046 ± 0.016	3.044 ± 0.016	3.045 ± 0.016
w	-1	-1	< -0.879	< -0.977	$-1.60^{+0.16}_{-0.33}$	$-1.039^{+0.037}_{-0.011}$
Ω_{m0}	0.3166 ± 0.0085	0.3102 ± 0.0058	$0.347^{+0.013}_{-0.034}$	0.3129 ± 0.0063	$0.194^{+0.015}_{-0.051}$	0.3046 ± 0.0069
σ_8	0.8122 ± 0.0073	0.8095 ± 0.0071	$0.785^{+0.029}_{-0.013}$	0.8029 ± 0.0088	$0.976^{+0.090}_{-0.044}$	$0.822^{+0.010}_{-0.012}$
H_0[km/s/Mpc]	67.27 ± 0.61	67.73 ± 0.43	$64.4^{+2.9}_{-1.2}$	$67.35^{+0.56}_{-0.49}$	> 83.2	$68.53^{+0.60}_{-0.74}$
S_8	0.834 ± 0.016	0.823 ± 0.012	0.842 ± 0.018	0.809 ± 0.012	$1.29^{+0.17}_{-0.45}$	0.828 ± 0.013
$r_{\rm drag}$ [Mpc]	147.05 ± 0.30	147.24 ± 0.24	147.04 ± 0.30	147.32 ± 0.25	147.08 ± 0.29	147.10 ± 0.26

Table 3
68% CL constraints on various free and derived parameters of the parameter spaces $\mathcal{P}_1 \equiv \left\{\Omega_b h^2, \Omega_c h^2, 100\theta_{\rm MC}, \tau, n_s, \ln[10^{10} A_s], N_{\rm eff}\right\}$, $\mathcal{P}_4 \equiv \left\{\Omega_b h^2, \Omega_c h^2, 100\theta_{\rm MC}, \tau, n_s, \ln[10^{10} A_s], \xi_-\right\}$ and $\mathcal{P}_8 \equiv \left\{\Omega_b h^2, \Omega_c h^2, 100\theta_{\rm MC}, \tau, n_s, \ln[10^{10} A_s], N_{\rm eff}, \xi_-\right\}$.

Model	$\mathcal{P}_1$	$\mathcal{P}_1$	$\mathcal{P}_4$	$\mathcal{P}_4$	$\mathcal{P}_8$	$\mathcal{P}_8$
	CMB	all	CMB	all	CMB	all
$\Omega_{\rm b}h^2$	0.02226 ± 0.00022	0.02241 ± 0.00018	0.02239 ± 0.00015	0.02237 ± 0.00014	0.02228 ± 0.00023	0.02229 ± 0.00019
$\Omega_{\rm c}h^2$	0.1184 ± 0.0030	0.1187 ± 0.0031	< 0.0634	$0.106^{+0.011}_{-0.005}$	< 0.0657	$0.103^{+0.012}_{-0.008}$
$100\theta_{MC}$	1.04110 ± 0.00043	1.04108 ± 0.00045	$1.0458^{+0.0033}_{-0.0021}$	$1.04174^{+0.00045}_{-0.00066}$	$1.0458^{+0.0032}_{-0.0023}$	$1.04205^{+0.00064}_{-0.00082}$
τ	0.0536 ± 0.0078	$0.0557^{+0.0072}_{-0.0080}$	0.0541 ± 0.0076	0.0545 ± 0.0078	0.0528 ± 0.0081	0.0538 ± 0.0077
n_s	0.9600 ± 0.0085	0.9661 ± 0.0071	0.9655 ± 0.0043	0.9652 ± 0.0039	0.9610 ± 0.0088	0.9616 ± 0.0074
$\ln(10^{10} A_s)$	3.039 ± 0.018	3.044 ± 0.018	3.044 ± 0.016	3.045 ± 0.016	3.037 ± 0.019	3.039 ± 0.018
ξ	0	0	$-0.54^{+0.12}_{-0.28}$	$-0.13^{+0.12}_{-0.04}$	$-0.53^{+0.13}_{-0.30}$	$-0.14^{+0.12}_{-0.06}$
$N_{\rm eff}$	2.92 ± 0.19	3.02 ± 0.18	3.046	3.046	2.93 ± 0.20	2.94 ± 0.18
Ω_{m0}	0.320 ± 0.010	0.3106 ± 0.0067	$0.139^{+0.034}_{-0.095}$	$0.274^{+0.029}_{-0.017}$	$0.15^{+0.04}_{-0.10}$	$0.271^{+0.029}_{-0.019}$
σ_8	0.806 ± 0.011	0.808 ± 0.011	$2.3^{+0.4}_{-1.4}$	$0.92^{+0.04}_{-0.10}$	$2.2^{+0.4}_{-1.4}$	$0.93^{+0.05}_{-0.11}$
H_0[km/s/Mpc]	66.4 ± 1.4	67.6 ± 1.1	$72.8^{+3.0}_{-1.5}$	$68.60^{+0.62}_{-0.82}$	$71.8^{+3.3}_{-2.6}$	68.1 ± 1.2
S_8	0.833 ± 0.016	0.822 ± 0.014	$1.30^{+0.17}_{-0.44}$	$0.876^{+0.025}_{-0.047}$	$1.28^{+0.17}_{-0.45}$	$0.879^{+0.027}_{-0.050}$
$r_{\rm drag}$ [Mpc]	148.3 ± 1.9	147.6 ± 1.8	147.08 ± 0.30	$147.09^{+0.27}_{-0.24}$	148.3 ± 2.0	148.2 ± 1.8

Table 4
68% CL constraints on various free and derived parameters of the parameter spaces $\mathcal{P}_5 \equiv \left\{\Omega_b h^2, \Omega_c h^2, 100\theta_{\rm MC}, \tau, n_s, \ln[10^{10} A_s], \Omega_k\right\}$, $\mathcal{P}_{12} \equiv \left\{\Omega_b h^2, \Omega_c h^2, 100\theta_{\rm MC}, \tau, n_s, \ln[10^{10} A_s], w_q, \Omega_k\right\}$ and $\mathcal{P}_{13} \equiv \left\{\Omega_b h^2, \Omega_c h^2, 100\theta_{\rm MC}, \tau, n_s, \ln[10^{10} A_s], w_p, \Omega_k\right\}$.

Model	$\mathcal{P}_5$	$\mathcal{P}_5$	$\mathcal{P}_{12}$	$\mathcal{P}_{12}$	$\mathcal{P}_{13}$	$\mathcal{P}_{13}$
	CMB	all	CMB	all	CMB	all
$\Omega_{\rm b}h^2$	0.02259 ± 0.00017	0.02240 ± 0.00016	0.02260 ± 0.00017	0.02240 ± 0.00016	0.02260 ± 0.00017	0.02240 ± 0.00015
$\Omega_{\rm c}h^2$	0.1182 ± 0.0015	0.1196 ± 0.0014	0.1182 ± 0.0015	0.1195 ± 0.0014	0.1180 ± 0.0015	0.1197 ± 0.0014
$100\theta_{MC}$	1.04115 ± 0.00033	1.04097 ± 0.00030	1.04116 ± 0.00032	1.04096 ± 0.00031	1.04117 ± 0.00033	1.04095 ± 0.00030
τ	$0.0489^{+0.0078}_{-0.0071}$	$0.0553^{+0.0071}_{-0.0078}$	$0.0483^{+0.0082}_{-0.0069}$	0.0558 ± 0.0079	$0.0478^{+0.0087}_{-0.0076}$	0.0544 ± 0.0076
n_s	0.9703 ± 0.0047	0.9662 ± 0.0044	0.9706 ± 0.0047	0.9661 ± 0.0046	0.9709 ± 0.0049	0.9657 ± 0.0044
$\ln(10^{10} A_s)$	$3.029^{+0.017}_{-0.015}$	3.046 ± 0.016	$3.028^{+0.017}_{-0.015}$	3.046 ± 0.016	$3.026^{+0.019}_{-0.016}$	3.044 ± 0.016
Ω_k	$-0.043^{+0.018}_{-0.014}$	0.0009 ± 0.0019	$-0.080^{+0.041}_{-0.026}$	0.0017 ± 0.0020	$-0.028^{+0.019}_{-0.008}$	-0.0004 ± 0.0020
w	-1	-1	$-0.59^{+0.24}_{-0.28}$	< -0.973	> -1.98	> -1.05
Ω_{m0}	$0.479^{+0.055}_{-0.065}$	0.3087 ± 0.0064	$0.70^{+0.14}_{-0.19}$	0.3114 ± 0.0067	$0.314^{+0.07}_{-0.15}$	0.3041 ± 0.0070
σ_8	0.776 ± 0.015	0.8115 ± 0.0083	$0.690^{+0.045}_{-0.056}$	$0.8050^{+0.0099}_{-0.0090}$	$0.926^{+0.07}_{-0.14}$	$0.822^{+0.010}_{-0.012}$
H_0[km/s/Mpc]	$54.6^{+3.2}_{-3.8}$	68.00 ± 0.66	$45.8^{+4.2}_{-6.4}$	67.68 ± 0.68	70^{+9}_{-20}	68.53 ± 0.77
S_8	0.978 ± 0.046	0.823 ± 0.012	$1.040^{+0.060}_{-0.054}$	0.820 ± 0.013	0.915 ± 0.069	0.827 ± 0.012
$r_{\rm drag}$ [Mpc]	147.34 ± 0.31	147.15 ± 0.30	147.32 ± 0.31	147.19 ± 0.31	147.35 ± 0.31	147.14 ± 0.30

$\mathcal{P}_8$ leaves unaltered the previous results, because $N_{\rm eff}$ is very well constrained and in agreement with the Standard Model expectation. The tension in the S_8 parameter is not addressed by any of these classes of models when BAO and Pantheon are included. In fact, for all these extensions, the S_8 parameter takes a higher value when compared to the classes of models characterized by $\mathcal{P}_1$ and $\mathcal{P}_0$ (see Table 2). In a similar fashion, the one dimensional posterior distributions and the two dimensional joint contours for these classes of models are shown in Figs. 2 (for $\mathcal{P}_1$), 5 (for $\mathcal{P}_4$), and 9 (for $\mathcal{P}_8$).

In Table 4 we show the cosmological constraints at 68% CL for the classes of models marked out by kΛCDM ($\mathcal{P}_5$) and kwCDM, with the latter divided again into two different regions based on the nature of the DE equation of state: quintessence regime, i.e.

Table 5
68% CL constraints on various free and derived parameters of the parameter spaces $\mathcal{P}_6 \equiv \left\{\Omega_b h^2, \Omega_c h^2, 100\theta_{\rm MC}, \tau, n_s, \ln[10^{10} A_s], N_{\rm eff}, w_q\right\}$, $\mathcal{P}_{10} \equiv \left\{\Omega_b h^2, \Omega_c h^2, 100\theta_{\rm MC}, \tau, n_s, \ln[10^{10} A_s], w_q, \xi_-\right\}$ and $\mathcal{P}_{15} \equiv \left\{\Omega_b h^2, \Omega_c h^2, 100\theta_{\rm MC}, \tau, n_s, \ln[10^{10} A_s], N_{\rm eff}, w_q, \xi_-\right\}$.

Model	$\mathcal{P}_6$	$\mathcal{P}_6$	$\mathcal{P}_{10}$	$\mathcal{P}_{10}$	$\mathcal{P}_{15}$	$\mathcal{P}_{15}$
	CMB	all	CMB	all	CMB	all
$\Omega_b h^2$	0.02222 ± 0.00022	0.02245 ± 0.00019	0.02237 ± 0.00015	0.02239 ± 0.00014	0.02226 ± 0.00022	0.02233 ± 0.00020
$\Omega_c h^2$	0.1185 ± 0.0030	0.1189 ± 0.0030	< 0.0456	< 0.0599	< 0.0431	< 0.0577
$100\theta_{MC}$	1.04109 ± 0.00043	1.04107 ± 0.00044	$1.0467^{+0.0031}_{-0.0014}$	$1.0461^{+0.0034}_{-0.0019}$	$1.0470^{+0.0031}_{-0.0014}$	$1.0462^{+0.0031}_{-0.0020}$
τ	$0.0539^{+0.0072}_{-0.0081}$	0.0561 ± 0.0077	0.0535 ± 0.0076	0.0544 ± 0.0077	0.0530 ± 0.0078	0.0536 ± 0.0077
n_s	0.9591 ± 0.0086	0.9682 ± 0.0070	0.9650 ± 0.0044	0.9660 ± 0.0040	0.9600 ± 0.0087	0.9631 ± 0.0077
$\ln(10^{10} A_s)$	3.039 ± 0.019	3.045 ± 0.018	3.043 ± 0.016	3.044 ± 0.016	3.037 ± 0.019	3.039 ± 0.018
ξ	0	0	$-0.62^{+0.07}_{-0.22}$	$-0.56^{+0.11}_{-0.27}$	$-0.64^{+0.07}_{-0.22}$	$-0.57^{+0.11}_{-0.25}$
$N_{\rm eff}$	2.91 ± 0.19	3.05 ± 0.18	3.046	3.046	2.92 ± 0.19	2.96 ± 0.18
w_q	< -0.877	< -0.978	< -0.836	$-0.841^{+0.093}_{-0.054}$	< -0.835	$-0.843^{+0.087}_{-0.054}$
Ω_{m0}	$0.353^{+0.014}_{-0.036}$	0.3132 ± 0.0069	$0.127^{+0.022}_{-0.081}$	$0.146^{+0.037}_{-0.093}$	$0.125^{+0.021}_{-0.079}$	$0.144^{+0.037}_{-0.088}$
σ_8	$0.779^{+0.030}_{-0.016}$	0.803 ± 0.012	$2.56^{+0.7}_{-1.7}$	$2.2^{+0.5}_{-1.3}$	$2.6^{+0.7}_{-1.7}$	$2.2^{+0.4}_{-1.3}$
H_0[km/s/Mpc]	$63.5^{+3.2}_{-2.0}$	67.3 ± 1.1	$69.7^{+3.9}_{-2.6}$	68.33 ± 0.81	$68.8^{+4.1}_{-3.0}$	68.0 ± 1.2
S_8	0.843 ± 0.017	0.821 ± 0.013	$1.42^{+0.27}_{-0.46}$	$1.31^{+0.20}_{-0.45}$	$1.43^{+0.28}_{-0.47}$	$1.31^{+0.19}_{-0.42}$
$r_{\rm drag}$ [Mpc]	148.4 ± 1.9	147.3 ± 1.8	147.06 ± 0.29	147.14 ± 0.26	148.3 ± 1.9	148.0 ± 1.9

Table 6
68% CL constraints on various free and derived parameters of the parameter spaces $\mathcal{P}_7 \equiv \left\{\Omega_b h^2, \Omega_c h^2, 100\theta_{\rm MC}, \tau, n_s, \ln[10^{10} A_s], N_{\rm eff}, w_p\right\}$, $\mathcal{P}_{11} \equiv \left\{\Omega_b h^2, \Omega_c h^2, 100\theta_{\rm MC}, \tau, n_s, \ln[10^{10} A_s], w_p, \xi_+\right\}$ and $\mathcal{P}_{16} \equiv \left\{\Omega_b h^2, \Omega_c h^2, 100\theta_{\rm MC}, \tau, n_s, \ln[10^{10} A_s], N_{\rm eff}, w_p, \xi_+\right\}$.

Model	$\mathcal{P}_7$	$\mathcal{P}_7$	$\mathcal{P}_{11}$	$\mathcal{P}_{11}$	$\mathcal{P}_{16}$	$\mathcal{P}_{16}$
	CMB	all	CMB	all	CMB	all
$\Omega_b h^2$	0.02227 ± 0.00022	0.02229 ± 0.00019	0.02239 ± 0.00015	0.02239 ± 0.00014	0.02227 ± 0.00022	0.02231 ± 0.00020
$\Omega_c h^2$	0.1178 ± 0.0029	0.1183 ± 0.0030	$0.133^{+0.005}_{-0.012}$	$0.133^{+0.006}_{-0.012}$	$0.130^{+0.006}_{-0.012}$	$0.131^{+0.007}_{-0.011}$
$100\theta_{MC}$	1.04118 ± 0.00044	1.04113 ± 0.00044	$1.04026^{+0.00065}_{-0.00049}$	$1.04023^{+0.00059}_{-0.00050}$	$1.04052^{+0.00070}_{-0.00059}$	$1.04043^{+0.00067}_{-0.00058}$
τ	0.0528 ± 0.0080	0.0540 ± 0.0075	0.0539 ± 0.0078	0.0548 ± 0.0080	0.0529 ± 0.0078	0.0543 ± 0.0080
n_s	0.9597 ± 0.0083	0.9616 ± 0.0074	0.9654 ± 0.0043	0.9659 ± 0.0040	0.9597 ± 0.0085	0.9622 ± 0.0076
$\ln(10^{10} A_s)$	3.035 ± 0.019	3.039 ± 0.018	3.043 ± 0.016	3.045 ± 0.016	3.036 ± 0.018	3.040 ± 0.019
ξ	0	0	< 0.134	< 0.181	< 0.132	< 0.171
$N_{\rm eff}$	2.90 ± 0.19	2.94 ± 0.18	3.046	3.046	2.90 ± 0.19	2.95 ± 0.18
w_p	$-1.65^{+0.19}_{-0.34}$	$-1.044^{+0.038}_{-0.016}$	$-1.59^{+0.19}_{-0.34}$	$-1.076^{+0.049}_{-0.033}$	$-1.62^{+0.23}_{-0.36}$	$-1.081^{+0.049}_{-0.036}$
Ω_{m0}	$0.192^{+0.017}_{-0.051}$	0.3056 ± 0.0072	$0.220^{+0.025}_{-0.066}$	$0.334^{+0.018}_{-0.024}$	$0.219^{+0.027}_{-0.068}$	$0.334^{+0.017}_{-0.023}$
σ_8	$0.978^{+0.091}_{-0.045}$	0.818 ± 0.013	0.881 ± 0.085	$0.750^{+0.051}_{-0.045}$	0.881 ± 0.086	$0.751^{+0.050}_{-0.040}$
H_0[km/s/Mpc]	> 83.1	68.0 ± 1.2	> 80.9	68.38 ± 0.78	> 80.2	67.9 ± 1.2
S_8	$0.771^{+0.024}_{-0.035}$	0.826 ± 0.014	0.742 ± 0.039	0.791 ± 0.026	0.740 ± 0.040	$0.791^{+0.028}_{-0.025}$
$r_{\rm drag}$ [Mpc]	148.6 ± 1.9	148.2 ± 1.9	147.09 ± 0.29	147.14 ± 0.27	148.5 ± 1.9	148.1 ± 1.9

Table 7
68% CL constraints on various free and derived parameters of the parameter spaces $\mathcal{P}_9 \equiv \left\{\Omega_b h^2, \Omega_c h^2, 100\theta_{\rm MC}, \tau, n_s, \ln[10^{10} A_s], N_{\rm eff}, \Omega_k\right\}$, $\mathcal{P}_{14} \equiv \left\{\Omega_b h^2, \Omega_c h^2, 100\theta_{\rm MC}, \tau, n_s, \ln[10^{10} A_s], \xi_-, \Omega_k\right\}$, and $\mathcal{P}_{19} \equiv \left\{\Omega_b h^2, \Omega_c h^2, 100\theta_{\rm MC}, \tau, n_s, \ln[10^{10} A_s], N_{\rm eff}, \xi_-, \Omega_k\right\}$.

Model	$\mathcal{P}_9$	$\mathcal{P}_9$	$\mathcal{P}_{14}$	$\mathcal{P}_{14}$	$\mathcal{P}_{19}$	$\mathcal{P}_{19}$
	CMB	all	CMB	all	CMB	all
$\Omega_b h^2$	0.02259 ± 0.00025	0.02233 ± 0.00023	0.02261 ± 0.00017	0.02240 ± 0.00016	0.02262 ± 0.00025	0.02231 ± 0.00023
$\Omega_c h^2$	0.1180 ± 0.0031	0.1187 ± 0.0030	$0.077^{+0.035}_{-0.019}$	$0.105^{+0.012}_{-0.006}$	$0.074^{+0.035}_{-0.021}$	$0.103^{+0.013}_{-0.007}$
$100\theta_{MC}$	1.04120 ± 0.00045	1.04109 ± 0.00044	$1.0437^{+0.0012}_{-0.0023}$	$1.04179^{+0.00050}_{-0.00075}$	$1.0439^{+0.0014}_{-0.0023}$	$1.04203^{+0.00059}_{-0.00088}$
τ	0.0485 ± 0.0083	0.0547 ± 0.0079	$0.0481^{+0.0085}_{-0.0076}$	0.0546 ± 0.0078	$0.0468^{+0.0085}_{-0.0075}$	$0.0543^{+0.0072}_{-0.0082}$
n_s	0.9701 ± 0.0094	0.9632 ± 0.0088	0.9708 ± 0.0047	0.9660 ± 0.0045	0.9714 ± 0.0093	0.9623 ± 0.0088
$\ln(10^{10} A_s)$	3.027 ± 0.020	3.042 ± 0.019	$3.027^{+0.017}_{-0.016}$	3.044 ± 0.016	$3.028^{+0.020}_{-0.018}$	3.040 ± 0.019
ξ	0	0	< -0.385	> -0.171	< -0.414	$-0.15^{+0.14}_{-0.04}$
$N_{\rm eff}$	3.04 ± 0.20	2.97 ± 0.19	3.046	3.046	3.05 ± 0.20	2.95 ± 0.20
Ω_k	$-0.044^{+0.020}_{-0.015}$	0.0013 ± 0.0022	$-0.036^{+0.017}_{-0.013}$	-0.0005 ± 0.0020	$-0.035^{+0.018}_{-0.012}$	-0.0002 ± 0.0023
Ω_{m0}	$0.484^{+0.057}_{-0.070}$	0.3097 ± 0.0066	0.30 ± 0.11	$0.273^{+0.029}_{-0.017}$	$0.29^{+0.11}_{-0.13}$	$0.271^{+0.032}_{-0.019}$
σ_8	0.774 ± 0.017	0.808 ± 0.011	$1.31^{+0.10}_{-0.54}$	$0.93^{+0.04}_{-0.10}$	$1.36^{+0.11}_{-0.59}$	$0.93^{+0.04}_{-0.11}$
H_0[km/s/Mpc]	$54.4^{+3.4}_{-4.0}$	67.6 ± 1.1	$58.7^{+4.1}_{-5.2}$	68.52 ± 0.75	$59.1^{+4.5}_{-5.1}$	68.1 ± 1.2
S_8	0.980 ± 0.051	0.821 ± 0.013	$1.20^{+0.10}_{-0.22}$	$0.878^{+0.025}_{-0.050}$	$1.21^{+0.10}_{-0.24}$	$0.881^{+0.026}_{-0.055}$
$r_{\rm drag}$ [Mpc]	147.5 ± 2.0	147.9 ± 1.9	147.34 ± 0.31	147.14 ± 0.30	147.3 ± 2.0	148.1 ± 2.0

$w_q > -1$ ($\mathcal{P}_{12}$) and phantom regime, i.e. $w_p < -1$ ($\mathcal{P}_{13}$). As already shown in the literature, a closed universe is preferred at more than 3σ by Planck-data alone (Aghanim et al., 2020a; Di Valentino et al., 2019; Handley, 2021), but this trademark increases the tension with H_0. The evidence for a closed universe disappears completely by the inclusion of the BAO and Pantheon data

Table 8
68% CL constraints on various free and derived parameters of the parameter spaces $\mathcal{P}_{17} \equiv \left\{\Omega_b h^2, \Omega_c h^2, 100\theta_{\rm MC}, \tau, n_s, \ln[10^{10} A_s], N_{\rm eff}, w_q, \Omega_k\right\}$, $\mathcal{P}_{20} \equiv \left\{\Omega_b h^2, \Omega_c h^2, 100\theta_{\rm MC}, \tau, n_s, \ln[10^{10} A_s], w_q, \xi_-, \Omega_k\right\}$ and $\mathcal{P}_{22} \equiv \left\{\Omega_b h^2, \Omega_c h^2, 100\theta_{\rm MC}, \tau, n_s, \ln[10^{10} A_s], N_{\rm eff}, w_q, \xi_-, \Omega_k\right\}$.

Model	$\mathcal{P}_{17}$	$\mathcal{P}_{17}$	$\mathcal{P}_{20}$	$\mathcal{P}_{20}$	$\mathcal{P}_{22}$	$\mathcal{P}_{22}$
	CMB	all	CMB	all	CMB	all
$\Omega_b h^2$	0.02258 ± 0.00025	0.02234 ± 0.00023	0.02260 ± 0.00017	0.02240 ± 0.00016	0.02260 ± 0.00025	0.02231 ± 0.00023
$\Omega_c h^2$	0.1182 ± 0.0030	0.1187 ± 0.0030	$0.078^{+0.036}_{-0.018}$	< 0.0555	$0.076^{+0.036}_{-0.021}$	< 0.0569
$100\theta_{MC}$	1.04117 ± 0.00044	1.04106 ± 0.00043	$1.0437^{+0.0012}_{-0.0023}$	$1.0463^{+0.0031}_{-0.0019}$	$1.0438^{+0.0013}_{-0.0024}$	$1.0463^{+0.0034}_{-0.0019}$
τ	0.0482 ± 0.0082	$0.0550^{+0.0073}_{-0.0083}$	0.0481 ± 0.0080	0.0546 ± 0.0078	0.0484 ± 0.0083	0.0540 ± 0.0077
n_s	0.9703 ± 0.0093	0.9633 ± 0.0088	0.9706 ± 0.0046	0.9661 ± 0.0046	0.9708 ± 0.0092	0.9623 ± 0.0087
$\ln(10^{10} A_s)$	3.027 ± 0.019	3.042 ± 0.019	3.027 ± 0.017	3.044 ± 0.016	3.028 ± 0.019	3.039 ± 0.018
ξ	0	0	< -0.415	$-0.58^{+0.10}_{-0.25}$	< -0.426	$-0.57^{+0.10}_{-0.26}$
w_q	< -0.476	< -0.972	$-0.55^{+0.26}_{-0.29}$	$-0.834^{+0.084}_{-0.054}$	$-0.55^{+0.26}_{-0.31}$	$-0.838^{+0.094}_{-0.056}$
$N_{\rm eff}$	3.04 ± 0.20	2.98 ± 0.19	3.046	3.046	3.05 ± 0.20	2.95 ± 0.19
Ω_k	$-0.077^{+0.042}_{-0.023}$	0.0021 ± 0.0023	$-0.072^{+0.047}_{-0.021}$	0.0000 ± 0.0023	$-0.072^{+0.050}_{-0.020}$	0.0004 ± 0.0024
Ω_{m0}	$0.69^{+0.12}_{-0.19}$	0.3123 ± 0.0070	$0.47^{+0.16}_{-0.23}$	$0.139^{+0.035}_{-0.086}$	$0.46^{+0.16}_{-0.23}$	$0.144^{+0.035}_{-0.091}$
σ_8	0.694 ± 0.048	0.802 ± 0.012	$1.08^{+0.09}_{-0.43}$	$2.2^{+0.5}_{-1.3}$	$1.11^{+0.09}_{-0.45}$	$2.2^{+0.5}_{-1.4}$
H_0[km/s/Mpc]	$46.2^{+4.6}_{-6.4}$	67.4 ± 1.1	48^{+6}_{-8}	68.33 ± 0.84	49^{+6}_{-8}	67.9 ± 1.2
S_8	1.037 ± 0.056	0.819 ± 0.014	$1.21^{+0.08}_{-0.18}$	$1.33^{+0.20}_{-0.44}$	$1.22^{+0.09}_{-0.19}$	$1.32^{+0.20}_{-0.45}$
$r_{\rm drag}$ [Mpc]	147.4 ± 1.9	147.9 ± 1.9	147.33 ± 0.30	147.15 ± 0.30	147.3 ± 1.9	148.1 ± 1.9

Table 9
68% CL constraints on various free and derived parameters of the parameter spaces $\mathcal{P}_{18} \equiv \left\{\Omega_b h^2, \Omega_c h^2, 100\theta_{\rm MC}, \tau, n_s, \ln[10^{10} A_s], N_{\rm eff}, w_p, \Omega_k\right\}$, $\mathcal{P}_{21} \equiv \left\{\Omega_b h^2, \Omega_c h^2, 100\theta_{\rm MC}, \tau, n_s, \ln[10^{10} A_s], w_p, \xi_+, \Omega_k\right\}$ and $\mathcal{P}_{23} \equiv \left\{\Omega_b h^2, \Omega_c h^2, 100\theta_{\rm MC}, \tau, n_s, \ln[10^{10} A_s], N_{\rm eff}, w_p, \xi_+, \Omega_k\right\}$.

Model	$\mathcal{P}_{18}$	$\mathcal{P}_{18}$	$\mathcal{P}_{21}$	$\mathcal{P}_{21}$	$\mathcal{P}_{23}$	$\mathcal{P}_{23}$
	CMB	all	CMB	all	CMB	all
$\Omega_b h^2$	0.02259 ± 0.00025	0.02229 ± 0.00023	0.02262 ± 0.00017	0.02239 ± 0.00016	0.02261 ± 0.00025	0.02231 ± 0.00023
$\Omega_c h^2$	0.1178 ± 0.0029	0.1182 ± 0.0030	$0.131^{+0.006}_{-0.011}$	$0.134^{+0.007}_{-0.012}$	$0.131^{+0.007}_{-0.011}$	$0.132^{+0.008}_{-0.011}$
$100\theta_{MC}$	1.04120 ± 0.00044	1.04112 ± 0.00044	$1.04049^{+0.00062}_{-0.00049}$	1.04021 ± 0.00056	$1.04052^{+0.00067}_{-0.00058}$	$1.04039^{+0.00067}_{-0.00061}$
τ	$0.0488^{+0.0083}_{-0.0075}$	0.0540 ± 0.0079	$0.0477^{+0.0084}_{-0.0071}$	0.0549 ± 0.0076	$0.0478^{+0.0084}_{-0.0074}$	0.0544 ± 0.0077
n_s	0.9702 ± 0.0092	0.9614 ± 0.0090	0.9711 ± 0.0046	0.9661 ± 0.0045	0.9708 ± 0.0095	0.9624 ± 0.0087
$\ln(10^{10} A_s)$	$3.028^{+0.019}_{-0.018}$	3.039 ± 0.019	$3.026^{+0.017}_{-0.015}$	3.045 ± 0.016	3.025 ± 0.019	3.040 ± 0.018
ξ	0	0	< 0.288	< 0.188	< 0.287	< 0.180
w_p	> -2.0	> -1.06	< -1.94	$-1.078^{+0.056}_{-0.035}$	> -1.92	$-1.079^{+0.054}_{-0.036}$
$N_{\rm eff}$	3.03 ± 0.20	2.94 ± 0.19	3.046	3.046	3.04 ± 0.20	$2.95^{+0.18}_{-0.20}$
Ω_k	$-0.026^{+0.018}_{-0.008}$	0.0001 ± 0.0023	$-0.031^{+0.020}_{-0.009}$	-0.0002 ± 0.0022	$-0.031^{+0.020}_{-0.010}$	0.0002 ± 0.0022
Ω_{m0}	$0.31^{+0.07}_{-0.14}$	0.3053 ± 0.0075	$0.37^{+0.11}_{-0.15}$	$0.335^{+0.019}_{-0.025}$	$0.38^{+0.11}_{-0.15}$	$0.335^{+0.018}_{-0.024}$
σ_8	$0.93^{+0.08}_{-0.15}$	$0.818^{+0.012}_{-0.014}$	$0.82^{+0.06}_{-0.12}$	0.748 ± 0.044	$0.82^{+0.06}_{-0.12}$	$0.748^{+0.051}_{-0.042}$
H_0[km/s/Mpc]	71^{+9}_{-20}	68.0 ± 1.2	68^{+8}_{-20}	68.34 ± 0.82	67^{+8}_{-20}	67.9 ± 1.2
S_8	0.907 ± 0.066	0.825 ± 0.014	$0.879^{+0.088}_{-0.074}$	0.790 ± 0.026	$0.883^{+0.088}_{-0.074}$	0.789 ± 0.025
$r_{\rm drag}$ [Mpc]	147.5 ± 1.9	148.2 ± 1.9	147.37 ± 0.30	147.16 ± 0.30	147.5 ± 2.0	148.1 ± 1.9

Table 10
68% CL constraints on various free and derived parameters of the parameter spaces $\mathcal{P}_3 \equiv \left\{\Omega_b h^2, \Omega_c h^2, 100\theta_{\rm MC}, \tau, n_s, \ln[10^{10} A_s], w_p, \right\}$, $\mathcal{P}_4 \equiv \left\{\Omega_b h^2, \Omega_c h^2, 100\theta_{\rm MC}, \tau, n_s, \ln[10^{10} A_s], \xi_-, \right\}$, $\mathcal{P}_{10} \equiv \left\{\Omega_b h^2, \Omega_c h^2, 100\theta_{\rm MC}, \tau, n_s, \ln[10^{10} A_s], w_q, \xi_-\right\}$, $\mathcal{P}_{11} \equiv \left\{\Omega_b h^2, \Omega_c h^2, 100\theta_{\rm MC}, \tau, n_s, \ln[10^{10} A_s], w_p, \xi_+\right\}$ and $\mathcal{P}_{13} \equiv \left\{\Omega_b h^2, \Omega_c h^2, 100\theta_{\rm MC}, \tau, n_s, \ln[10^{10} A_s], w_p, \Omega_k\right\}$ for CMB + R20 dataset only.

Model	$\mathcal{P}_3$	$\mathcal{P}_4$	$\mathcal{P}_{10}$	$\mathcal{P}_{11}$	$\mathcal{P}_{13}$
	CMB + R20	CMB + R20	CMB + R20	CMB + R20	CMB + R20
$\Omega_b h^2$	0.02237 ± 0.00015	0.02238 ± 0.00014	0.02240 ± 0.00015	0.02237 ± 0.00015	0.02262 ± 0.00017
$\Omega_c h^2$	0.1201 ± 0.0013	$0.039^{+0.018}_{-0.024}$	< 0.0276	$0.133^{+0.006}_{-0.012}$	0.1181 ± 0.0015
$100\theta_{MC}$	1.04090 ± 0.00031	1.0463 ± 0.0017	$1.0479^{+0.0020}_{-0.0010}$	$1.04021^{+0.00061}_{-0.00051}$	1.04115 ± 0.00033
τ	0.0540 ± 0.0080	0.0533 ± 0.0080	0.0539 ± 0.0077	0.0536 ± 0.0077	$0.0489^{+0.0082}_{-0.0072}$
n_s	0.9650 ± 0.0044	0.9653 ± 0.0042	0.9658 ± 0.0042	0.9647 ± 0.0043	0.9707 ± 0.0048
$\ln(10^{10} A_s)$	3.044 ± 0.016	3.042 ± 0.016	3.043 ± 0.016	3.043 ± 0.016	$3.029^{+0.017}_{-0.016}$
w	-1.200 ± 0.048	-0.999	$-0.939^{+0.020}_{-0.054}$	-1.240 ± 0.055	$-1.88^{+0.42}_{-0.23}$
ξ	0	$-0.60^{+0.11}_{-0.16}$	$-0.71^{+0.05}_{-0.012}$	< 0.162	0
Ω_k	0	0	0	0	$-0.0203^{+0.0063}_{-0.0072}$
Ω_{m0}	0.2660 ± 0.0097	$0.117^{+0.033}_{-0.050}$	$0.085^{+0.013}_{-0.040}$	$0.291^{+0.015}_{-0.023}$	0.2642 ± 0.0097
σ_8	0.867 ± 0.016	$2.3^{+0.4}_{-1.1}$	$3.2^{+0.9}_{-1.5}$	$0.794^{+0.062}_{-0.041}$	0.953 ± 0.035
H_0[km/s/Mpc]	73.4 ± 1.3	$73.4^{+1.4}_{-1.1}$	$72.8^{+1.2}_{-1.1}$	73.3 ± 1.3	73.2 ± 1.3
S_8	0.816 ± 0.015	$1.34^{+0.15}_{-0.33}$	1.58 ± 0.28	$0.780^{+0.032}_{-0.026}$	0.894 ± 0.031
$r_{\rm drag}$ [Mpc]	147.06 ± 0.29	147.07 ± 0.29	147.10 ± 0.29	147.05 ± 0.29	147.34 ± 0.32

Table 11
68% CL constraints on various free and derived parameters of the parameter spaces $\mathcal{P}_7 \equiv \left\{\Omega_b h^2, \Omega_c h^2, 100\theta_{\rm MC}, \tau, n_s, \ln[10^{10} A_s], N_{\rm eff}, w_p\right\}$, $\mathcal{P}_8 \equiv \left\{\Omega_b h^2, \Omega_c h^2, 100\theta_{\rm MC}, \tau, n_s, \ln[10^{10} A_s], N_{\rm eff}, \xi_-\right\}$ and $\mathcal{P}_{18} \equiv \left\{\Omega_b h^2, \Omega_c h^2, 100\theta_{\rm MC}, \tau, n_s, \ln[10^{10} A_s], N_{\rm eff}, w_p, \Omega_k\right\}$ when R20 is considered.

Model	$\mathcal{P}_7$	$\mathcal{P}_7$	$\mathcal{P}_8$	$\mathcal{P}_8$	$\mathcal{P}_{18}$	$\mathcal{P}_{18}$
	CMB + R20	CMB + BAO + R20	CMB + R20	CMB + BAO + R20	CMB + R20	CMB + BAO + R20
$\Omega_b h^2$	0.02224 ± 0.00022	0.02236 ± 0.00020	0.02230 ± 0.00019	0.02253 ± 0.00018	0.02260 ± 0.00025	0.02247 ± 0.00022
$\Omega_c h^2$	0.1179 ± 0.0030	0.1207 ± 0.0028	< 0.0421	$0.0997^{+0.013}_{-0.011}$	0.1180 ± 0.0031	0.1203 ± 0.0029
$100\theta_{MC}$	1.04118 ± 0.00044	1.04085 ± 0.00041	$1.0470^{+0.0023}_{-0.0017}$	$1.04198^{+0.00073}_{-0.00092}$	1.04119 ± 0.00045	1.04090 ± 0.00042
τ	0.0532 ± 0.0079	0.0539 ± 0.0078	0.0528 ± 0.0076	0.0555 ± 0.0079	0.0479 ± 0.0082	0.0542 ± 0.0078
n_s	0.9591 ± 0.0084	0.9643 ± 0.0079	0.9620 ± 0.0073	0.9718 ± 0.0066	0.9701 ± 0.0093	0.9682 ± 0.0083
$\ln(10^{10} A_s)$	3.036 ± 0.019	3.045 ± 0.018	3.037 ± 0.018	3.053 ± 0.018	3.026 ± 0.019	3.045 ± 0.018
w	-1.238 ± 0.070	-1.200 ± 0.048	-1	-1	$-1.90^{+0.41}_{-0.25}$	$-1.188^{+0.080}_{-0.071}$
$N_{\rm eff}$	2.89 ± 0.19	3.06 ± 0.18	2.95 ± 0.16	3.22 ± 0.16	3.04 ± 0.20	3.10 ± 0.18
ξ	0	0	$-0.65^{+0.09}_{-0.18}$	$-0.20^{+0.10}_{0.09}$	0	0
Ω_k	0	0	0	0	$-0.0207^{+0.0065}_{-0.0075}$	-0.0028 ± 0.0024
Ω_{m0}	$0.262^{+0.010}_{-0.012}$	0.2818 ± 0.0090	$0.106^{+0.022}_{-0.057}$	$0.247^{+0.029}_{-0.024}$	$0.264^{+0.010}_{-0.012}$	0.2782 ± 0.0096
σ_8	0.869 ± 0.016	0.853 ± 0.016	$2.6^{+0.5}_{-1.4}$	$1.01^{+0.07}_{-0.13}$	0.954 ± 0.035	0.861 ± 0.018
H_0[km/s/Mpc]	73.3 ± 1.3	71.4 ± 1.1	73.2 ± 1.2	70.50 ± 0.90	73.2 ± 1.3	71.8 ± 1.1
S_8	0.812 ± 0.015	0.826 ± 0.013	$1.42^{+0.25}_{-0.57}$	$0.909^{+0.036}_{-0.059}$	0.895 ± 0.034	0.829 ± 0.014
$r_{\rm drag}$ [Mpc]	148.6 ± 1.9	146.9 ± 1.8	148.1 ± 1.7	145.4 ± 1.5	147.5 ± 2.0	146.7 ± 1.8

Table 12
68% CL constraints on various free and derived parameters of the parameter spaces $\mathcal{P}_{16} \equiv \left\{\Omega_b h^2, \Omega_c h^2, 100\theta_{\rm MC}, \tau, n_s, \ln[10^{10} A_s], N_{\rm eff}, w_p, \xi_+\right\}$, $\mathcal{P}_{21} \equiv \left\{\Omega_b h^2, \Omega_c h^2, 100\theta_{\rm MC}, \tau, n_s, \ln[10^{10} A_s], w_p, \xi_+, \Omega_k\right\}$ and $\mathcal{P}_{23} \equiv \left\{\Omega_b h^2, \Omega_c h^2, 100\theta_{\rm MC}, \tau, n_s, \ln[10^{10} A_s], N_{\rm eff}, w_p, \xi_+, \Omega_k\right\}$ when R20 is considered.

Model	$\mathcal{P}_{16}$	$\mathcal{P}_{16}$	$\mathcal{P}_{21}$	$\mathcal{P}_{23}$	$\mathcal{P}_{23}$
	CMB + R20	CMB + BAO + R20	CMB + R20	CMB + R20	CMB + BAO + R20
$\Omega_b h^2$	0.02224 ± 0.00021	0.02254 ± 0.00019	0.02262 ± 0.00017	0.02262 ± 0.00025	0.02257 ± 0.00021
$\Omega_c h^2$	$0.130^{+0.007}_{-0.012}$	$0.137^{+0.008}_{-0.012}$	$0.132^{+0.007}_{-0.012}$	$0.132^{+0.008}_{-0.012}$	$0.1368^{+0.008}_{-0.012}$
$100\theta_{MC}$	$1.04051^{+0.00068}_{-0.00060}$	$1.03992^{+0.00067}_{-0.00060}$	$1.04045^{+0.00065}_{-0.00053}$	$1.04043^{+0.00069}_{-0.00062}$	$1.03992^{+0.00070}_{-0.00062}$
τ	0.0530 ± 0.0079	0.0558 ± 0.0079	$0.0480^{+0.0085}_{-0.0073}$	0.0486 ± 0.0083	0.0560 ± 0.0082
n_s	0.9590 ± 0.0084	0.9724 ± 0.0069	0.9709 ± 0.0048	0.9713 ± 0.0093	0.9729 ± 0.0082
$\ln(10^{10} A_s)$	3.036 ± 0.019	3.054 ± 0.018	$3.026^{+0.018}_{-0.016}$	3.027 ± 0.020	3.054 ± 0.018
w	-1.279 ± 0.075	$-1.101^{+0.047}_{-0.042}$	$-1.99^{+0.40}_{-0.29}$	$-2.00^{+0.40}_{-0.26}$	$-1.101^{+0.052}_{-0.042}$
$N_{\rm eff}$	2.89 ± 0.19	3.24 ± 0.16	3.046	3.05 ± 0.20	3.24 ± 0.17
ξ	< 0.160	< 0.176	< 0.269	< 0.279	< 0.179
Ω_k	0	0	$-0.0214^{+0.0053}_{-0.0073}$	$-0.0217^{+0.0058}_{-0.0069}$	-0.0001 ± 0.0022
Ω_{m0}	$0.285^{+0.017}_{-0.022}$	$0.322^{+0.016}_{-0.025}$	$0.290^{+0.017}_{-0.023}$	$0.291^{+0.019}_{-0.023}$	$0.323^{+0.016}_{-0.024}$
σ_8	$0.797^{+0.059}_{-0.043}$	$0.765^{+0.058}_{-0.041}$	$0.861^{+0.070}_{-0.064}$	0.860 ± 0.065	$0.763^{+0.056}_{-0.042}$
H_0[km/s/Mpc]	73.3 ± 1.3	70.41 ± 0.91	73.1 ± 1.3	73.1 ± 1.3	70.43 ± 0.88
S_8	$0.776^{+0.032}_{-0.026}$	$0.791^{+0.030}_{-0.026}$	0.844 ± 0.043	0.844 ± 0.044	$0.790^{+0.030}_{-0.026}$
$r_{\rm drag}$ [Mpc]	148.6 ± 1.9	145.3 ± 1.6	147.36 ± 0.31	147.4 ± 1.9	145.2 ± 1.6

Table 13
68% CL constraints on various free and derived parameters of the parameter spaces $\mathcal{P}_{15} \equiv \left\{\Omega_b h^2, \Omega_c h^2, 100\theta_{\rm MC}, \tau, n_s, \ln[10^{10} A_s], N_{\rm eff}, w_q, \xi_-\right\}$, $\mathcal{P}_{19} \equiv \left\{\Omega_b h^2, \Omega_c h^2, 100\theta_{\rm MC}, \tau, n_s, \ln[10^{10} A_s], N_{\rm eff}, \xi_-, \Omega_k\right\}$ and $\mathcal{P}_{22} \equiv \left\{\Omega_b h^2, \Omega_c h^2, 100\theta_{\rm MC}, \tau, n_s, \ln[10^{10} A_s], N_{\rm eff}, w_q, \xi_-, \Omega_k\right\}$ when R20 is considered.

Model	$\mathcal{P}_{15}$	$\mathcal{P}_{15}$	$\mathcal{P}_{19}$	$\mathcal{P}_{22}$
	CMB + R20	CMB + BAO + R20	CMB + BAO + R20	CMB + BAO + R20
$\Omega_b h^2$	0.02238 ± 0.00019	0.02256 ± 0.00019	0.02255 ± 0.00021	0.02257 ± 0.00021
$\Omega_c h^2$	< 0.0259	< 0.0538	$0.099^{+0.015}_{-0.011}$	< 0.0569
$100\theta_{MC}$	$1.0480^{+0.0020}_{-0.0009}$	$1.0462^{+0.0032}_{-0.0018}$	$1.04200^{+0.00073}_{-0.00099}$	$1.0460^{+0.0030}_{-0.0020}$
τ	0.0536 ± 0.0078	0.0555 ± 0.0079	0.0556 ± 0.0078	0.0553 ± 0.0080
n_s	0.9545 ± 0.0073	0.9727 ± 0.0069	0.9722 ± 0.0080	0.9731 ± 0.0079
$\ln(10^{10} A_s)$	3.041 ± 0.018	3.054 ± 0.018	3.053 ± 0.018	3.053 ± 0.018
w	< -0.928	$-0.859^{+0.081}_{-0.050}$	-1	$-0.862^{+0.080}_{-0.058}$
$N_{\rm eff}$	3.01 ± 0.17	3.24 ± 0.17	3.23 ± 0.17	3.25 ± 0.18
ξ	$-0.72^{+0.05}_{-0.13}$	$-0.59^{+0.09}_{-0.23}$	$-0.20^{+0.12}_{-0.09}$	$-0.58^{+0.10}_{-0.24}$
Ω_k	0	0	-0.0003 ± 0.0022	0.0000 ± 0.0022
Ω_{m0}	$0.084^{+0.011}_{-0.039}$	$0.129^{+0.032}_{-0.079}$	$0.247^{+0.032}_{-0.023}$	$0.133^{+0.035}_{-0.081}$
σ_8	$3.3^{+0.9}_{-1.5}$	$2.4^{+0.5}_{-1.4}$	$1.02^{+0.07}_{-0.15}$	$2.3^{+0.5}_{-1.4}$
H_0[km/s/Mpc]	72.7 ± 1.1	70.43 ± 0.91	70.47 ± 0.92	70.45 ± 0.89
S_8	$1.59^{+0.34}_{-0.27}$	$1.37^{+0.20}_{-0.45}$	$0.912^{+0.036}_{-0.067}$	$1.34^{+0.20}_{-0.43}$
$r_{\rm drag}$ [Mpc]	147.5 ± 1.7	145.2 ± 1.6	145.4 ± 1.6	145.1 ± 1.6

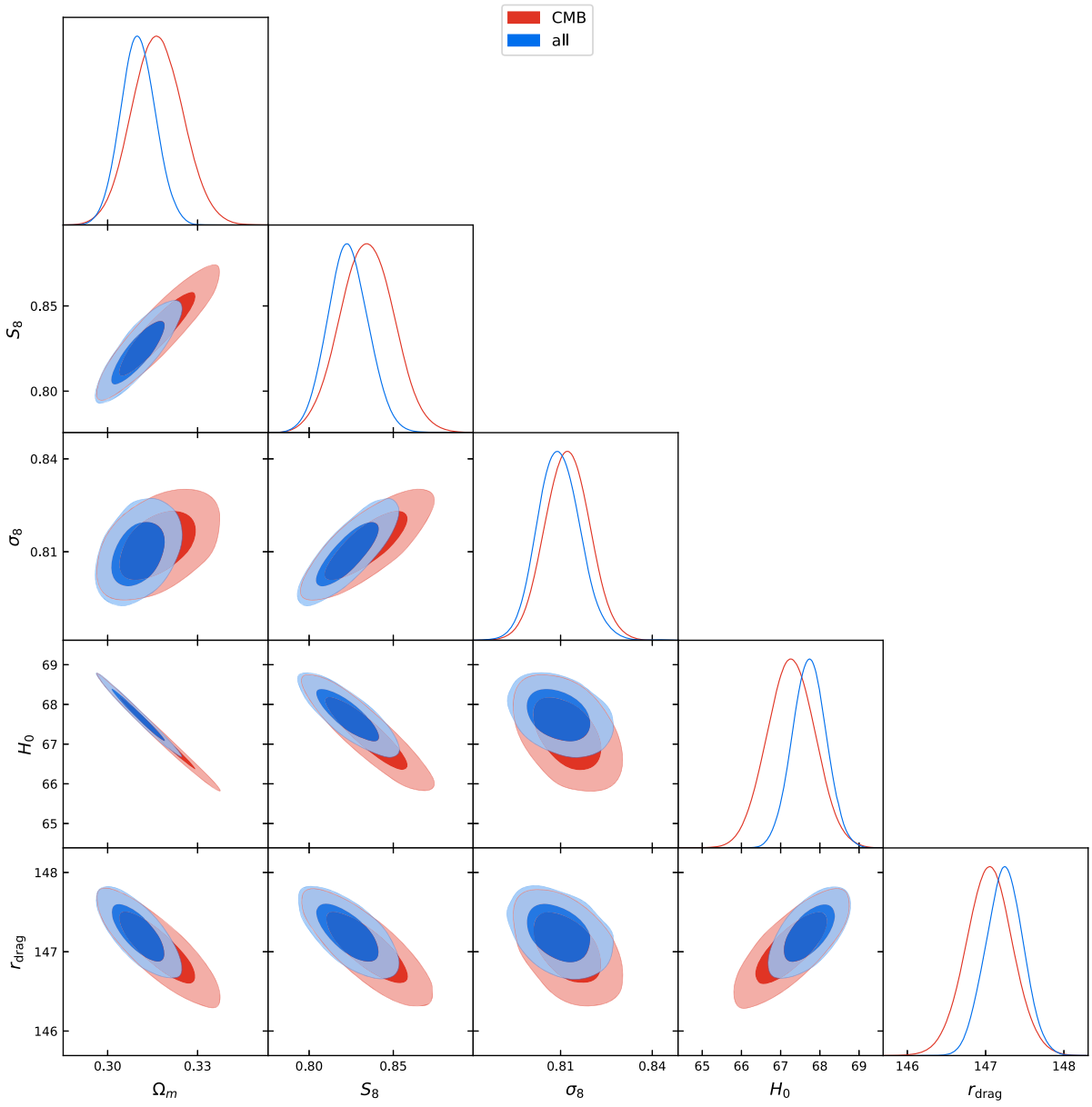

Fig. 1. One dimensional posterior distributions and two dimensional joint contours for the parameter space $\mathcal{P}_0 \equiv \left\{\Omega_b h^2, \Omega_c h^2, 100\theta_{\rm MC}, \tau, n_s, \ln[10^{10} A_s]\right\}$ for CMB alone and CMB + BAO + Pantheon (referred to as 'all') dataset. The H_0 and $r_{\rm drag}$ parameters are respectively measured in [km/s/Mpc] and [Mpc] in all the triangular plots of this work.

samples. The inclusion of the DE equation of state free to vary in the quintessence region, i.e. $w_q > -1$ ($\mathcal{P}_{12}$) yields evidence for a closed universe at more than 3σ along with a $w_q > -1$ at more than 68% CL and an increased Hubble constant discrepancy with respect to the ΛCDM model, for Planck-data alone. On the contrary, if we consider a phantom DE equation of state (i.e. $w_p < -1$) free to vary in this regime ($\mathcal{P}_{13}$), we obtain $\Omega_k < 0$ at more than 99% CL, w_p is in agreement with a cosmological constant, and the Hubble constant is consistent with SH0ES, for the Planck-data alone. However, for all the cases, all these features disappear for the combined dataset CMB + BAO + Pantheon data, which perfectly restores a flat ΛCDM model. Similarly, aiming to understand the correlations between the model parameters, we again show the one dimensional posterior distributions and the two dimensional joint contours for these classes of models in Figs. 6 (for $\mathcal{P}_5$), 13 (for $\mathcal{P}_{12}$), and 14 (for $\mathcal{P}_{13}$).

In Table 5 we present the constraint on the cosmological parameters for the classes of models characterized by w_qCDM + $N_{\rm eff}$ ($\mathcal{P}_6$), w_qIDE ($\mathcal{P}_{10}$), and w_qIDE + $N_{\rm eff}$ ($\mathcal{P}_{15}$), where the DE equation of state is always in the quintessence regime, i.e. $w_q > -1$. The $\mathcal{P}_6$ framework does not show any deviation from the standard ΛCDM scenario. However, in the w_qIDE scenario we find some interesting results. First of all, for the Planck-data alone case, the introduction of a w_q free to vary reduces the overlap with the Hubble constant measured by SH0ES, even if this is still in agreement within 1σ. Secondly, even if w_q is consistent with a cosmological constant, the evidence for the coupling between DM and DE increases in significance. Lastly, the inclusion of the BAO and Pantheon data does not restore the usual ΛCDM model concordance. In fact, for the combined dataset CMB + BAO + Pantheon we have a coupling still at more than 99% CL, a $w_q \neq -1$ above 95% CL, but H_0 is still in tension with SH0ES at more than 3 standard deviations. Finally, the extended scenario w_qIDE + $N_{\rm eff}$ (the last two columns of Table 5) does not modify the previous findings about the free parameters, because $N_{\rm eff}$ is completely consistent with the standard value of 3.046. However, we have slightly larger error bars for an increased

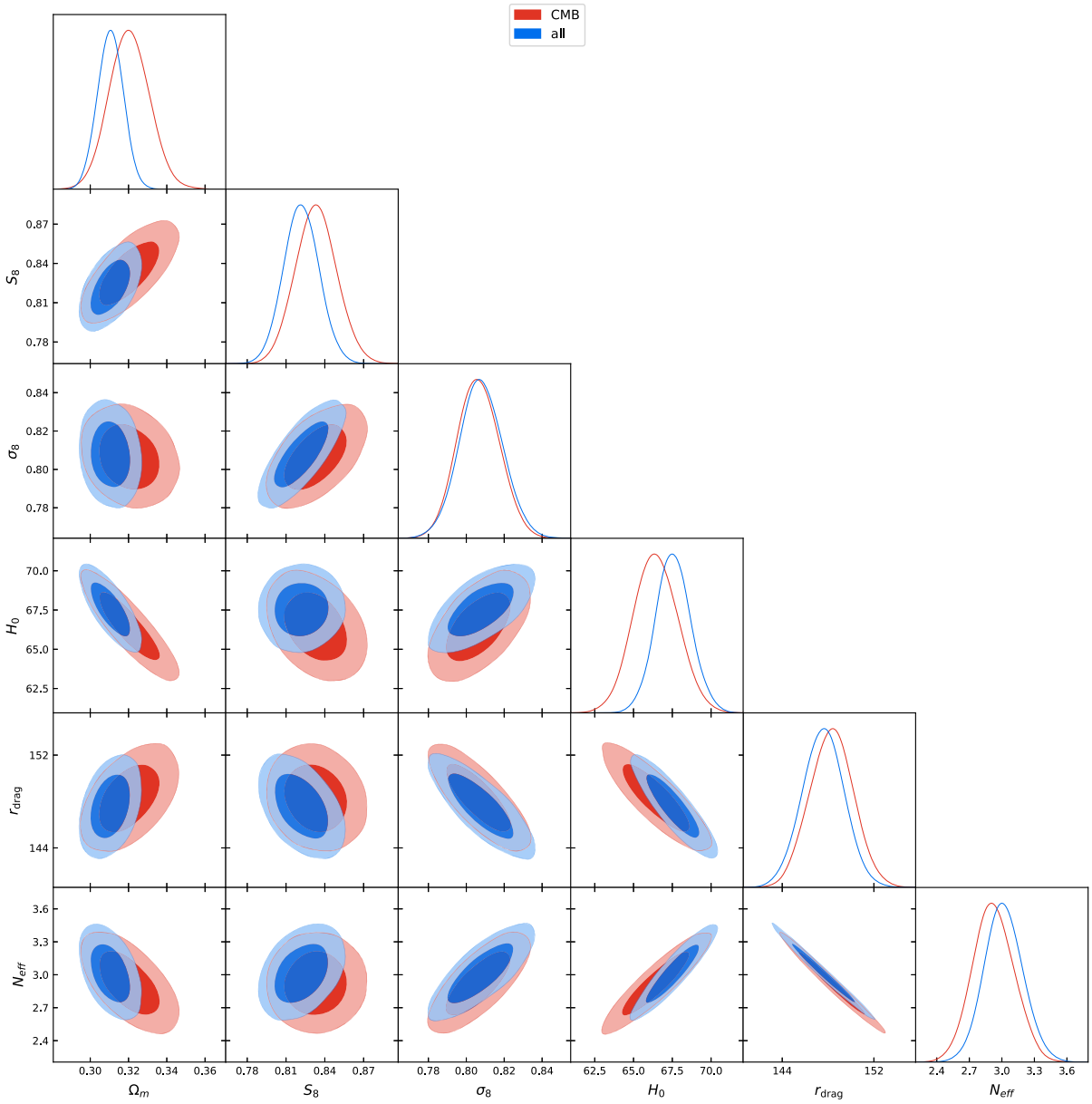

Fig. 2. One dimensional posterior distributions and two dimensional joint contours for the parameter space $\mathcal{P}_1 \equiv \left\{\Omega_b h^2, \Omega_c h^2, 100\theta_{MC}, \tau, n_s, \ln[10^{10} A_s], N_{eff}\right\}$ for CMB alone and CMB + BAO + Pantheon (referred to as 'all') dataset.

volume of the parameter space. The one dimensional posterior distributions and the two dimensional joint contours for these classes of models are shown in Figs. 7 (for $\mathcal{P}_6$), 11 (for $\mathcal{P}_{10}$), and 16 (for $\mathcal{P}_{15}$).

Complementary, in Table 6 we present the constraint on the cosmological parameters for the classes of models specified by w_pCDM + N_{eff} ($\mathcal{P}_7$), w_pIDE ($\mathcal{P}_{11}$) and w_pIDE + N_{eff} ($\mathcal{P}_{16}$), where the DE equation of state is always in the phantom regime, i.e. $w_p < -1$. In this case, for the scenario $\mathcal{P}_7$ we find evidence for a phantom $w_p < -1$ at more than 99% CL when considering Planck-data alone. In addition, we find that the S_8 parameter is in agreement with the weak lensing experiments within 1σ, and the H_0 tension is certainly alleviated within the 95% CL. However, even though the evidence for $w_p < -1$ at more than 1σ still persists when the full combination CMB + BAO + Pantheon is considered, the H_0 and S_8 tensions strike back. For the $\mathcal{P}_{11}$ scenario, we do not find any indication for a coupling $\xi \neq 0$, and our analysis confirms the same salient features present in the $\mathcal{P}_7$ classes of models for the Planck data only. On the other hand, when the combined dataset CMB + BAO + Pantheon is considered, $w_p < -1$ is still preferred at more than 1σ and the S_8 tension is alleviated. However, in this case the H_0 tension is only reduced down to 3.2σ. The inclusion of the N_{eff} parameter free to vary in the last scenario $\mathcal{P}_{16}$ does not modify the previous findings, because N_{eff} is in complete agreement with the Standard Model value. The one dimensional posterior distributions and the two dimensional joint contours for these classes of models are shown in Figs. 8 (for $\mathcal{P}_7$), 12 (for $\mathcal{P}_{11}$), and 17 (for $\mathcal{P}_{16}$).

In Table 7 we show the results for the classes of models headlining kΛCDM + N_{eff} ($\mathcal{P}_9$), kIDE ($\mathcal{P}_{14}$), and kIDE + N_{eff} ($\mathcal{P}_{19}$). For the Planck-data alone, evidence for a closed universe at more than 95% CL is clearly visible for all three scenarios. However, such an evidence disappears when BAO and Pantheon data samples are included. Both the H_0 and S_8 tensions are exacerbated when considering just the Planck data sample, but N_{eff} is always found to be in agreement with the Standard Model value. In addition, when

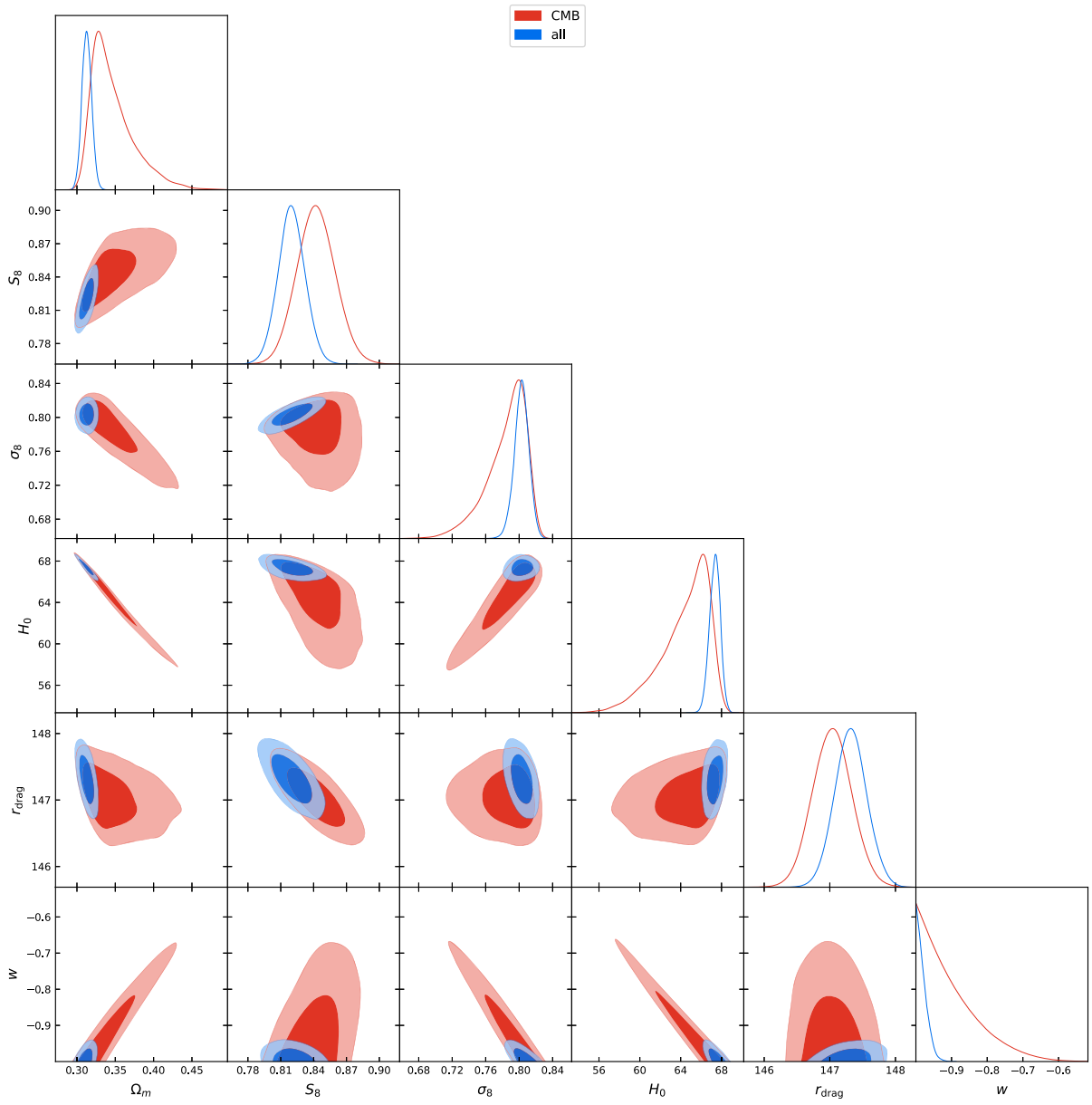

Fig. 3. One dimensional posterior distributions and two dimensional joint contours for the parameter space $\mathcal{P}_2 \equiv \left\{\Omega_b h^2, \Omega_c h^2, 100\theta_{\rm MC}, \tau, n_s, \ln[10^{10} A_s], w_q, \right\}$ for CMB alone and CMB + BAO + Pantheon (referred to as 'all') dataset.

considering only the CMB-data sample for $\mathcal{P}_{14}$ and $\mathcal{P}_{19}$, we find evidence for a coupling of DE and DM through an upper limit for ξ. However, for the combined dataset CMB + BAO + Pantheon, $\xi \neq 0$ remains true around 1σ for the $\mathcal{P}_{19}$ (kIDE + $N_{\rm eff}$). Further, we see that for the combined dataset the classes of models typify by $\mathcal{P}_{14}$ and $\mathcal{P}_{19}$ do not offer any alleviation of the S_8 tension, rather the tension in S_8 increases significantly. These classes of models, however, lead to a mild alleviation of the H_0 tension. For the $\mathcal{P}_{14}$ and $\mathcal{P}_{19}$ classes of models, the H_0 tension is reduced down to 3.1σ and 2.8σ, for the combined CMB + BAO + Pantheon dataset. The one dimensional posterior distributions and the two dimensional joint contours for these classes of models are shown in Figs. 10 (for $\mathcal{P}_9$), 15 (for $\mathcal{P}_{14}$), and 20 (for $\mathcal{P}_{19}$).

In Table 8 we show the results of the classes of models featuring kw_qCDM + $N_{\rm eff}$ ($\mathcal{P}_{17}$), kw_qIDE ($\mathcal{P}_{20}$) and the kw_qIDE + $N_{\rm eff}$ ($\mathcal{P}_{22}$), where the DE equation of state has been freely varying in the quintessence regime, i.e. $w_q > -1$. For the CMB dataset, we find for all the classes of models evidence for a closed universe at more than 95% CL. However, this evidence disappears when we combine BAO and Pantheon with CMB data. Focusing on the tensions on H_0 and S_8 parameters, we find that for both CMB and CMB + BAO + Pantheon, the H_0 and S_8 tensions cannot be resolved. In fact, for CMB alone, both the H_0 and S_8 tensions significantly increase. However, for CMB + BAO + Pantheon, we see that for $\mathcal{P}_{17}$, $\mathcal{P}_{20}$ and $\mathcal{P}_{22}$ classes of models, the tension on H_0 is reduced down to 3.4σ, 3.1σ and slightly below 3σ respectively. Similar to the other cases, the graphical extraction for these scenarios are shown in Figs. 18 (for $\mathcal{P}_{17}$), 21 (for $\mathcal{P}_{20}$), and 23 (for $\mathcal{P}_{22}$).

Finally, in Table 9 we compare the classes of models characterized by kw_pCDM + $N_{\rm eff}$ ($\mathcal{P}_{18}$), kw_pIDE ($\mathcal{P}_{21}$), and kw_pIDE + $N_{\rm eff}$ ($\mathcal{P}_{23}$), where the DE equation of state is always in the phantom regime, i.e. $w_p < -1$. Similar to the classes of models summarized in Table 8, for all the three extended cases, Planck alone suggests an indication for a closed universe and this evidence goes away when BAO and Pantheon are added to CMB, that means for the

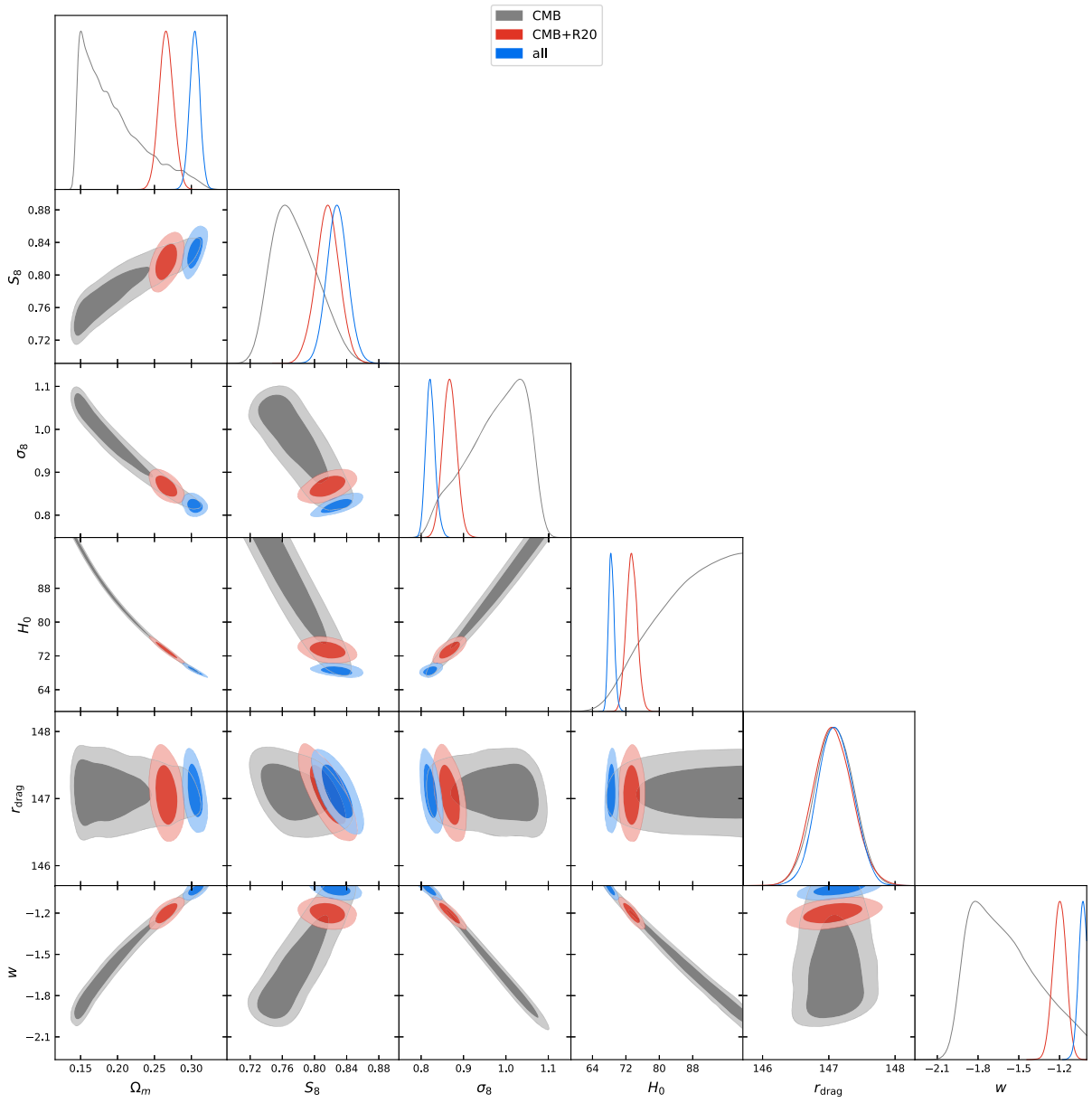

Fig. 4. One dimensional posterior distributions and two dimensional joint contours for the parameter space $\mathcal{P}_3 \equiv \left\{\Omega_b h^2, \Omega_c h^2, 100\theta_{\rm MC}, \tau, n_s, \ln[10^{10} A_s], w_p, \right\}$ for CMB alone, CMB + R20 and CMB + BAO + Pantheon (referred to as 'all') dataset.

combined analysis CMB + BAO + Pantheon. However, due to the phantom behavior of the DE, the Hubble tension is solved within 1σ, even if w_p is consistent with a cosmological constant. Interestingly, for the CMB + BAO + Pantheon combination and the $\mathcal{P}_{21}$ and $\mathcal{P}_{23}$ cosmological models, while the agreement with a flat universe is restored, an indication for a $w_p < -1$ appears at more than 68% CL, and at the same time both the S_8 and H_0 tension are reduced. The one dimensional posterior distributions and the two dimensional joint contours for these models are shown in Figs. 19 (for $\mathcal{P}_{18}$), 22 (for $\mathcal{P}_{21}$), and 24 (for $\mathcal{P}_{23}$).

4.2. Including the R20 prior

In this section we study the effects of adding a gaussian prior R20 (Riess et al., 2021) on the classes of models (described in Table 2 – Table 8) which alleviate the Hubble tension below 3σ for Planck or CMB + BAO + Pantheon datasets. To make this selection we adopt a back-of-the-envelope definition of the H_0 tension,

$$T = (x_1 - x_2)/\sqrt{(\mathrm{err}\, x_1)^2 + (\mathrm{err}\, x_2)^2}\,, \tag{36}$$

where $x_1 \pm \mathrm{err}\, x_1$ is the R20 H_0 measurement and $x_2 \pm \mathrm{err}\, x_2$ is the corresponding H_0 prediction from model $\mathcal{P}_i$, with $i = 0, \cdots, 23$. To avoid double counting, when using the R20 prior we do not consider the Pantheon catalog.

For the case of study, the data samples are divided into two subgroups: CMB + R20 and CMB + BAO + R20. The results are shown in Tables 10 to 13. We can see that in all the selected cases the H_0 tension is reduced down to 1σ, as expected when a gaussian prior is included and datasets are not in strong tension. In particular, the agreement in the CMB + R20 analyses takes place at the price of a phantom DE ($\mathcal{P}_3$ and $\mathcal{P}_{7,11,16,18}$), a coupling for IDE ($\mathcal{P}_4$ and $\mathcal{P}_{8,15}$), a quintessence DE interacting with DM ($\mathcal{P}_{10}$), and a phantom closed scenario ($\mathcal{P}_{13}$ and the extended $\mathcal{P}_{21,23}$). Alternatively, the agreement in the CMB + BAO + R20 analyses takes place at the price of a phantom DE ($\mathcal{P}_7$), an IDE framework with additional dark radiation ($\mathcal{P}_8$ and $\mathcal{P}_{19}$), an interacting quintessence DE with DM in presence of additional dark radiation ($\mathcal{P}_{15}$ and $\mathcal{P}_{22}$),

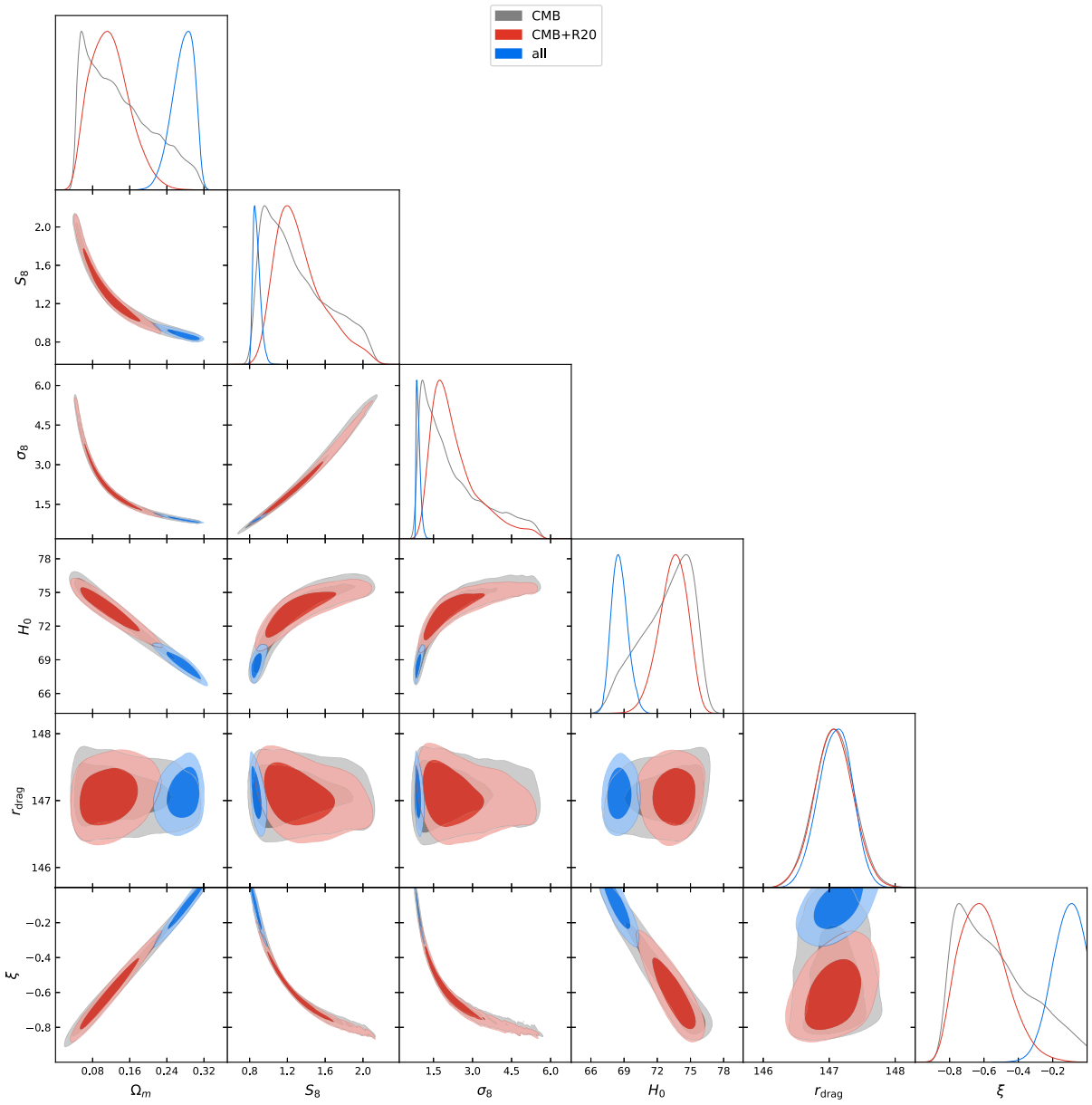

Fig. 5. One dimensional posterior distributions and two dimensional joint contours for the parameter space $\mathcal{P}_4 \equiv \left\{\Omega_b h^2, \Omega_c h^2, 100\theta_{\rm MC}, \tau, n_s, \ln[10^{10} A_s], \xi_-, \right\}$ for CMB alone, CMB + R20 and CMB + BAO + Pantheon (referred to as 'all') dataset.

a phantom DE with additional dark radiation ($\mathcal{P}_{16}$ and $\mathcal{P}_{23}$), and a phantom closed universe ($\mathcal{P}_{18}$). However, only the class of models characterized by $\mathcal{P}_{16}$ and $\mathcal{P}_{23}$ can resolve the H_0 tension at 1σ level, while relaxing also the S_8 and the r_{drag} tensions for the CMB + BAO + R20 combination.

In closing, we note that the phantom DE can address the H_0 problem, but does not solve the M_B tension (Camarena and Marra, 2021; Efstathiou, 2021). On the contrary, the IDE classes of models can solve simultaneously the H_0 and M_B tensions (Nunes and Di Valentino, 2021), but it is not supported by a full dataset combination.

5. Conclusions

We have investigated the possible interconnection among the free parameters in several classes of cosmological models that typify the main theoretical frameworks tackling the tensions on the universe expansion rate and the clustering of matter. This meta-analysis features interesting results on the global cosmological picture which can be summarized as follows:

- The estimate of $r_{\rm drag}$ from low-redshift probes (Knox and Millea, 2020; Arendse et al., 2020) poses a challenge for beyond ΛCDM models trying to address the Hubble tension. Since the baryonic-drag epoch takes place at a somewhat lower redshift than recombination, by comparing the ΛCDM value of $r_{\rm drag}$ in Table 2 with the estimate of Ref. Arendse et al. (2020) we can conclude that in order to accommodate $r_{\rm drag} = (137 \pm 3^{\rm stat} \pm 2^{\rm syst})$ Mpc we need a modification of the sound horizon at recombination. Actually, for ΛCDM the two standard rulers are related according to $r_{\rm drag} \sim 1.0184\, r_*$, and the proportionality factor is essentially the same in all analyzed classes of models introducing modifications in the expansion rate pre-recombination. In our study we have considered the latest Planck 2018 data sample which contains both temperature and polarization measurements, together with a new optical depth estimate which strongly correlates with $N_{\rm eff}$ keep-

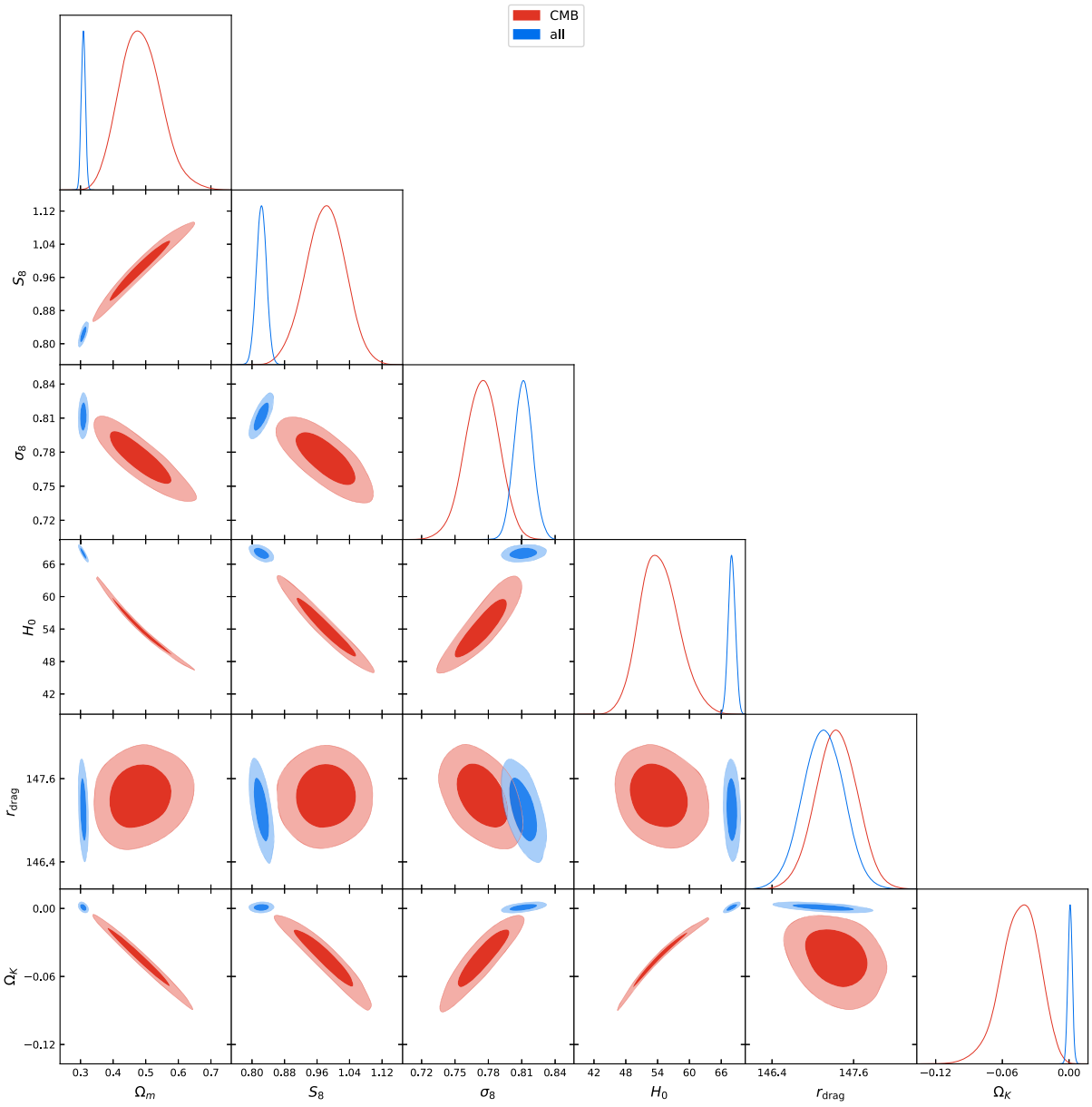

Fig. 6. One dimensional posterior distributions and two dimensional joint contours for the parameter space $\mathcal{P}_5 \equiv \left\{\Omega_b h^2, \Omega_c h^2, 100\theta_{\rm MC}, \tau, n_s, \ln[10^{10} A_s], \Omega_k, \right\}$ for CMB alone, and CMB + BAO + Pantheon (referred to as 'all') dataset.

ing its value near 3.046, and thereby the sound horizon at the epoch of baryon decoupling near the ΛCDM prediction, $r_{\rm drag} = 147.24 \pm 0.24$ Mpc. Altogether our conclusion points towards the need of new-physics at $z_{\rm drag} \lesssim z \lesssim z_*$, or else some unaccounted systematic effects are at play. Note that our conclusion is complementary to the statements presented in Jedamzik et al. (2021); Bernal et al. (2021) because our study includes combination of classes of models modifying both the early and late-time expansion rate of the universe. It should be noticed here that models involving only modifications pre-recombination of early universe physics alone are disfavored (Lin et al., 2021).

- For considerations of CMB + BAO + Pantheon data, string-inspired models with coupling between the DE and DM sectors characterized by $\mathcal{P}_{10}$ tend to fall short of fully resolving the H_0 tension (Agrawal et al., 2019b). The addition of extra-relativistic degrees of freedom (e.g., by considering 3 right-handed Dirac neutrinos ubiquitous in D-brane constructs (Anchordoqui et al., 2020; Anchordoqui, 2020), or thermal axions (Giusarma et al., 2014; Di Valentino et al., 2015, 2016a; Baumann et al., 2016; Poulin et al., 2018; D'Eramo et al., 2018; Giarè et al., 2020), or sterile neutrinos (Anchordoqui and Goldberg, 2012; Anchordoqui et al., 2013; Jacques et al., 2013; Di Valentino et al., 2016b), or any other light species) tend to exacerbate the tension; see $\mathcal{P}_{15}$ in Table 5. However, when considering Planck data and the R20 prior both, the scenarios $\mathcal{P}_{10}$ and $\mathcal{P}_{15}$ can resolve the H_0 tension at the 1σ level; see Tables 10 and 13. One would expect that the transfer from DM to DE (a.k.a. fading DM) could ameliorate the S_8 tension. However, this happens because of the larger error bars instead of a stronger overlap. In particular, for the $\mathcal{P}_{15}$ scenario in Table 13, $N_{\rm eff}$ saturates the Planck limit. Since $N_{\rm eff}$ is correlated with Ω_m, the effect of a non-negligible dark radiation shifts the S_8 parameter towards higher values, even if with large errors.

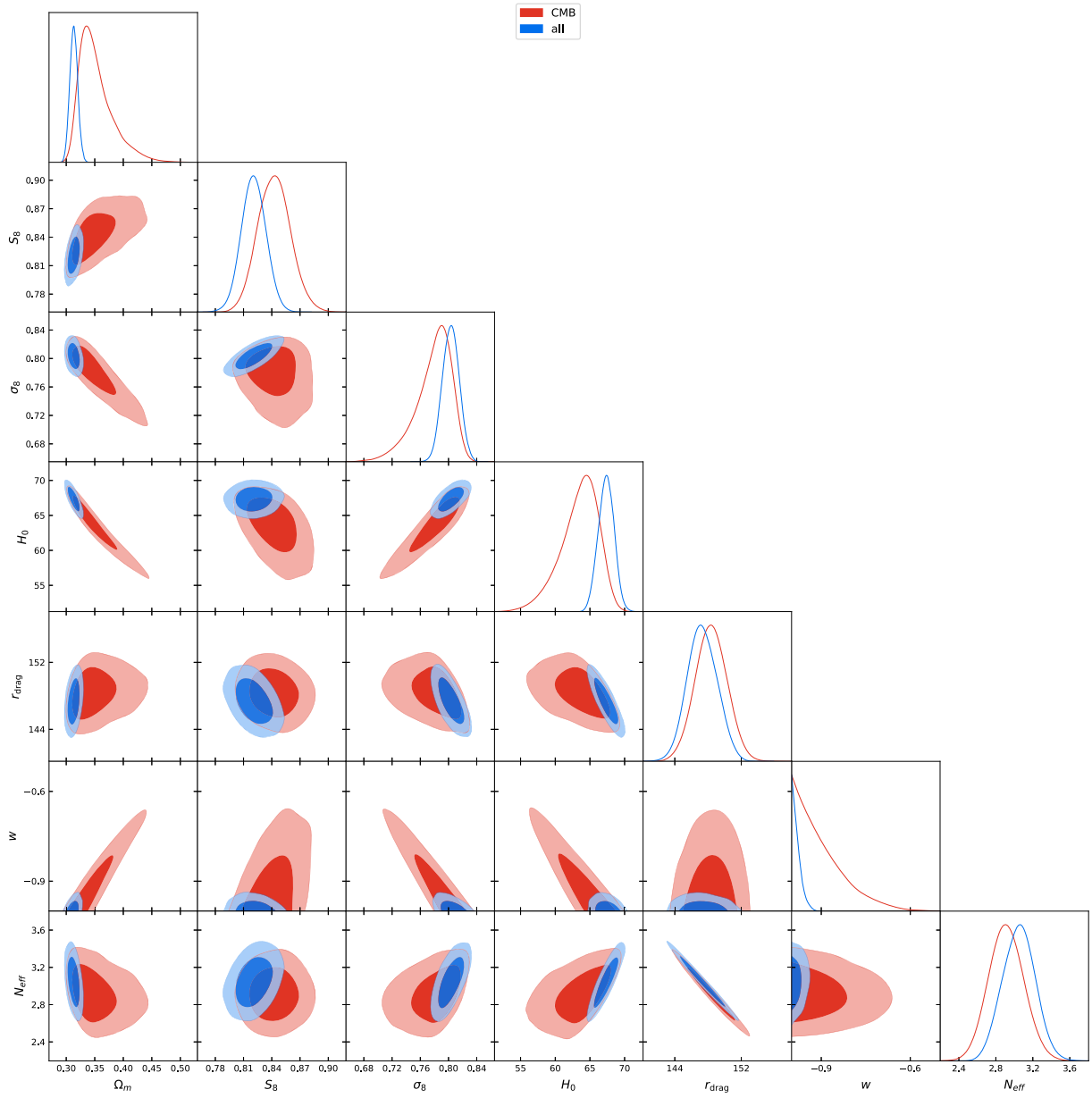

Fig. 7. One dimensional posterior distributions and two dimensional joint contours for the parameter space $\mathcal{P}_6 \equiv \left\{\Omega_b h^2, \Omega_c h^2, 100\theta_{MC}, \tau, n_s, \ln[10^{10} A_s], N_{\rm eff}, w_q\right\}$ for CMB alone and CMB + BAO + Pantheon (referred to as 'all') dataset.

- Frameworks featuring phantom dark energy characterize the classes of models with a potential to accommodate simultaneously the H_0 and S_8 local measurements (but not the M_B tension (Camarena and Marra, 2021)). Classes of models with a transfer of energy from DE to DM (e.g. $\mathcal{P}_{16}$) keep the value of $N_{\rm eff}$ consistent with the Standard Model expectation of 3.046, and can resolve the S_8 tension while ameliorating the H_0 tension, see Table 6 and Fig. 17. Notably, the IDE model also accommodates the M_B tension (Nunes and Di Valentino, 2021). When including the R20 prior the value of $N_{\rm eff}$ saturates the Planck limit, but the H_0 is resolved at the 1σ level and S_8 remains consistent with local measurements; see Table 12.
- The latest observations of the Planck satellite have confirmed the presence of an enhanced lensing amplitude in CMB power spectra compared to that predicted in the standard ΛCDM model. It was noted in Di Valentino et al. (2019) that a closed universe can provide a physical explanation for this effect, with the 2018 Planck CMB spectra preferring a positive curvature at more than 99% CL (Aghanim et al., 2020a; Di Valentino et al., 2019; Handley, 2021; Di Valentino et al., 2021b). Altogether this motivated our consideration of Ω_k as a free parameter in the likelihood analysis. Scenarios favoring a closed universe also favor a smaller value of the expansion rate than the H_0 measurement by SH0ES, see e.g. Tables 7 and 8. An exception is the class of models featuring extra-relativistic degrees of freedom in the early universe and a phantom DE, which is described by $\mathcal{P}_{23}$, and can simultaneously ameliorate the H_0 and S_8 tensions (i.e. a phantom closed model Di Valentino et al., 2021f; Shirokov and Baryshev, 2020).

In summary, the H_0 and S_8 tensions present a daunting challenge. In this paper we have collected some of the best insights

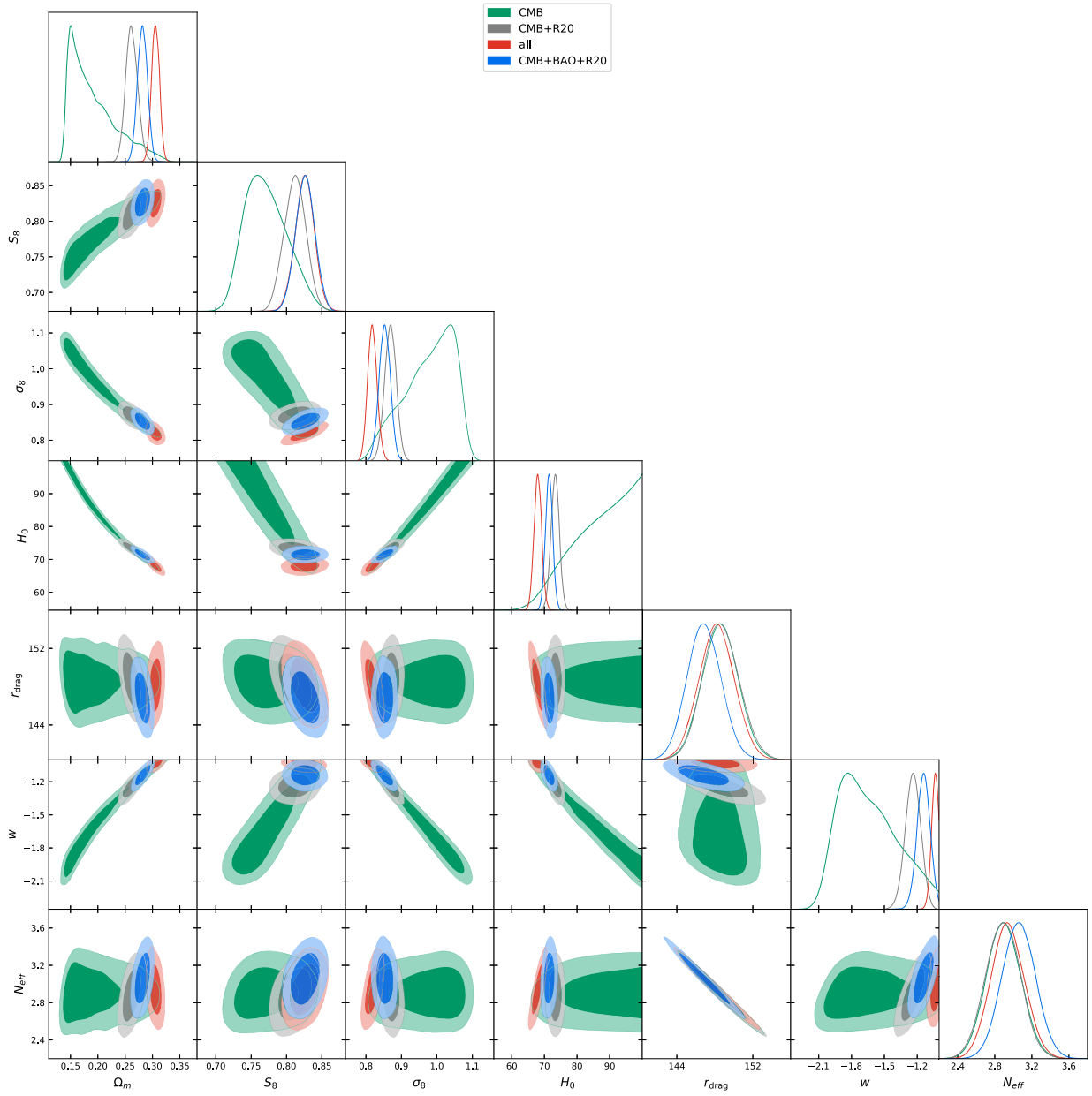

Fig. 8. One dimensional posterior distributions and two dimensional joint contours for the parameter space $\mathcal{P}_7 \equiv \left\{\Omega_b h^2, \Omega_c h^2, 100\theta_{\rm MC}, \tau, n_s, \ln[10^{10} A_s], N_{\rm eff}, w_p\right\}$ for CMB alone, CMB + R20, CMB + BAO + Pantheon (referred to as 'all'), and CMB + BAO + R20 datasets.

to extend the standard ΛCDM model and studied the interconnections among free parameters of these classes of models. So far, all these insights have drawbacks and herein we have shown that the extended multi-parameter cosmologies could only help to narrow down (though not fully eliminate) the tensions. It is crystal-clear that to unlock Pandora's box a coordinated effort involving theory, interpretation, and data analysis would be needed to exploit the large data sets to be collected by the next-generation experiments (Di Valentino et al., 2021c).

Declaration of competing interest

The authors declare that they have no known competing financial interests or personal relationships that could have appeared to influence the work reported in this paper.

Acknowledgments

LAA was supported by the U.S. National Science Foundation (NSF Grant PHY-2112527). EDV acknowledges the support of the Addison-Wheeler Fellowship awarded by the Institute of Advanced Study at Durham University. SP acknowledges the financial supports from the Science and Engineering Research Board, Govt. of India under Mathematical Research Impact-Centric Support Scheme (File No. MTR/2018/000940) and the Department of Science and Technology (DST), Govt. of India under the Scheme "Fund for Improvement of S&T Infrastructure (FIST)" [File No. SR/FST/MS-I/2019/41]. WY was supported by the National Natural Science Foundation of China under Grants No. 11705079 and No. 11647153.

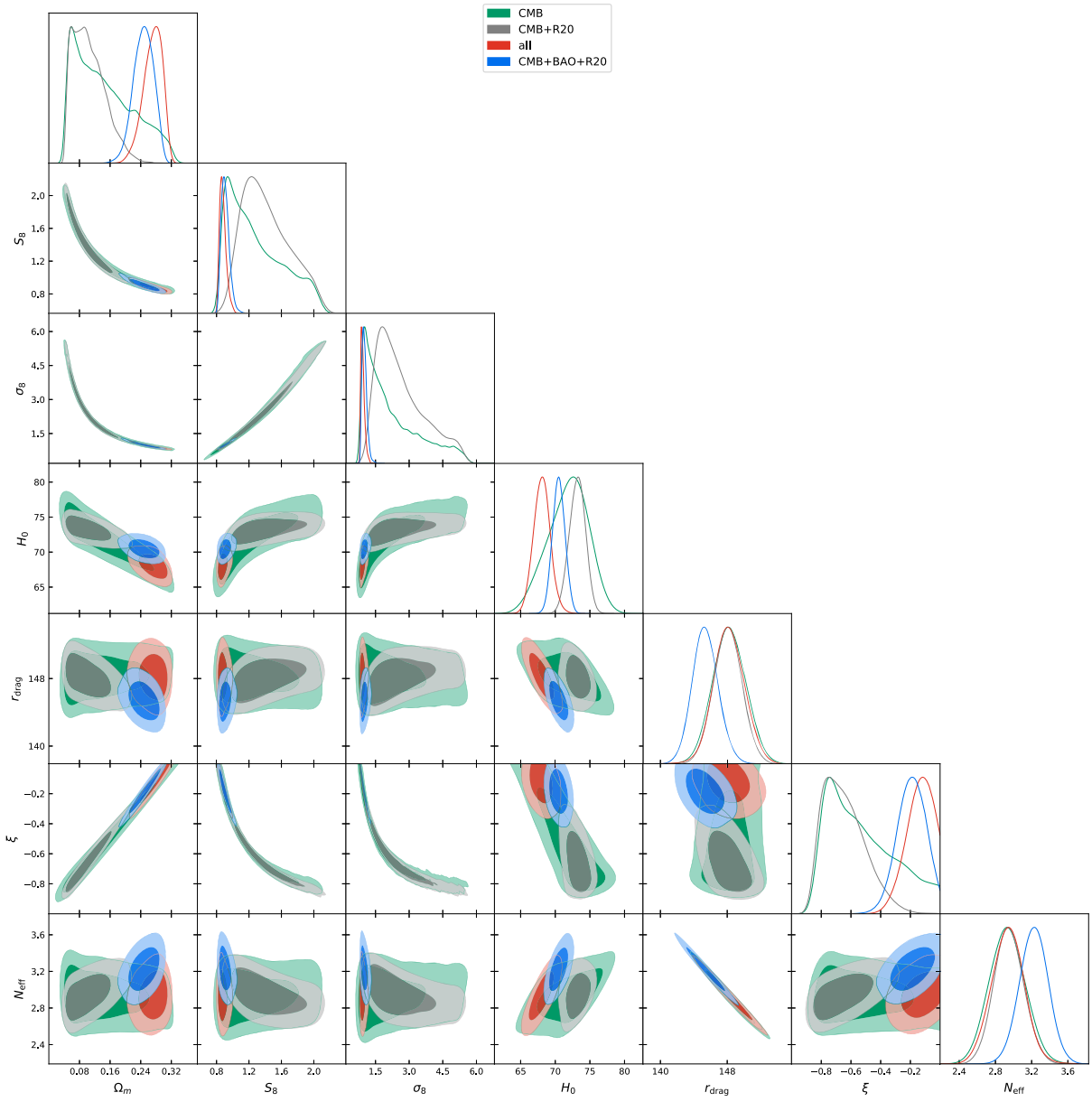

Fig. 9. One dimensional posterior distributions and two dimensional joint contours for the parameter space $\mathcal{P}_8 \equiv \left\{\Omega_b h^2, \Omega_c h^2, 100\theta_{MC}, \tau, n_s, \ln[10^{10} A_s], N_{eff}, \xi_-\right\}$ for CMB alone, CMB + R20, CMB + BAO + Pantheon (referred to as 'all'), and CMB + BAO + R20 datasets.

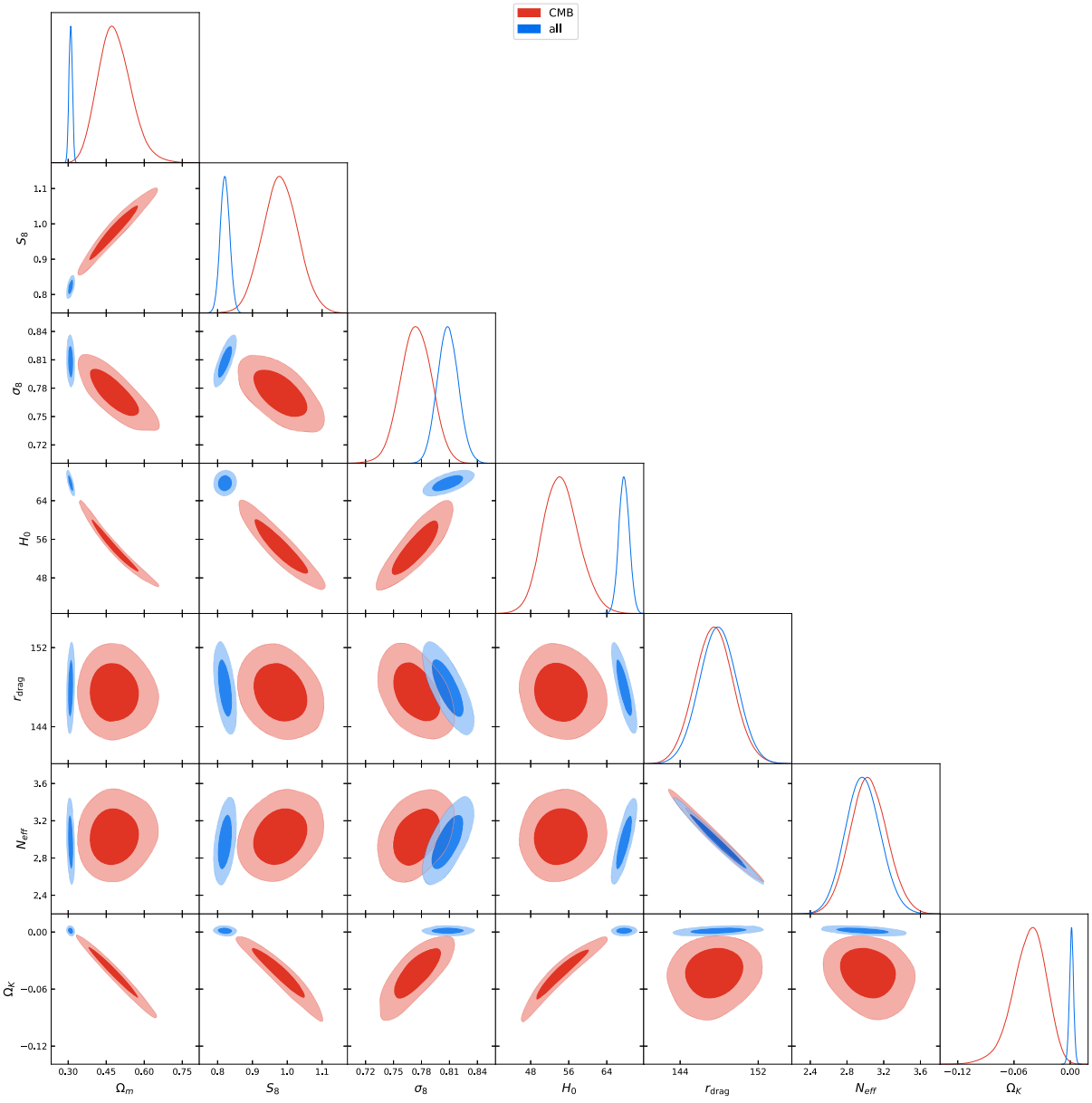

Fig. 10. One dimensional posterior distributions and two dimensional joint contours for the parameter space $\mathcal{P}_9 \equiv \left\{\Omega_b h^2, \Omega_c h^2, 100\theta_{\rm MC}, \tau, n_s, \ln[10^{10} A_s], N_{\rm eff}, \Omega_k\right\}$ for CMB alone and CMB + BAO + Pantheon (referred to as 'all') dataset.

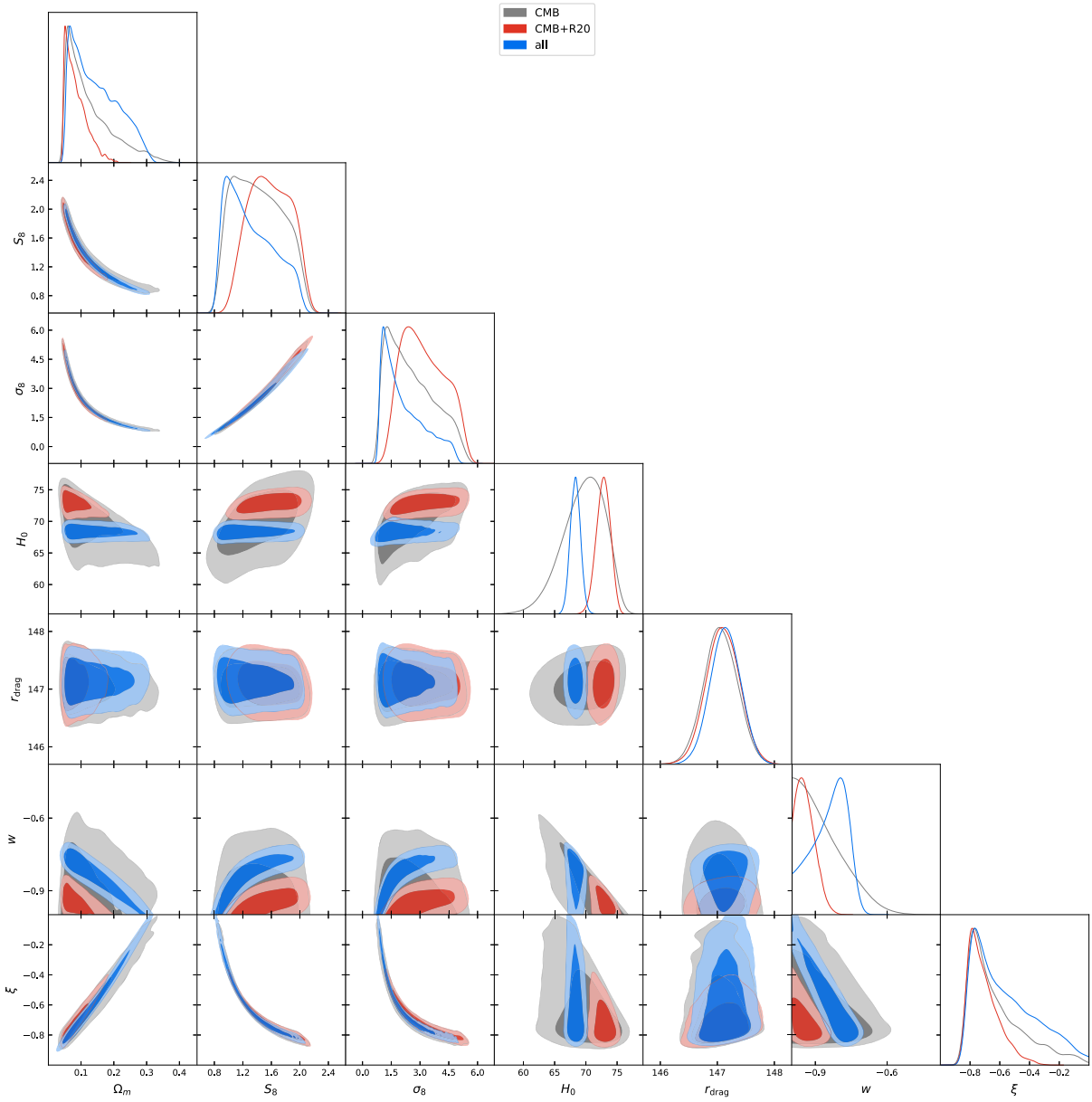

Fig. 11. One dimensional posterior distributions and two dimensional joint contours for the parameter space $\mathcal{P}_{10} \equiv \left\{\Omega_b h^2, \Omega_c h^2, 100\theta_{MC}, \tau, n_s, \ln[10^{10} A_s], w_q, \xi_-\right\}$ for CMB alone, CMB + R20 and CMB + BAO + Pantheon (referred to as 'all') dataset.

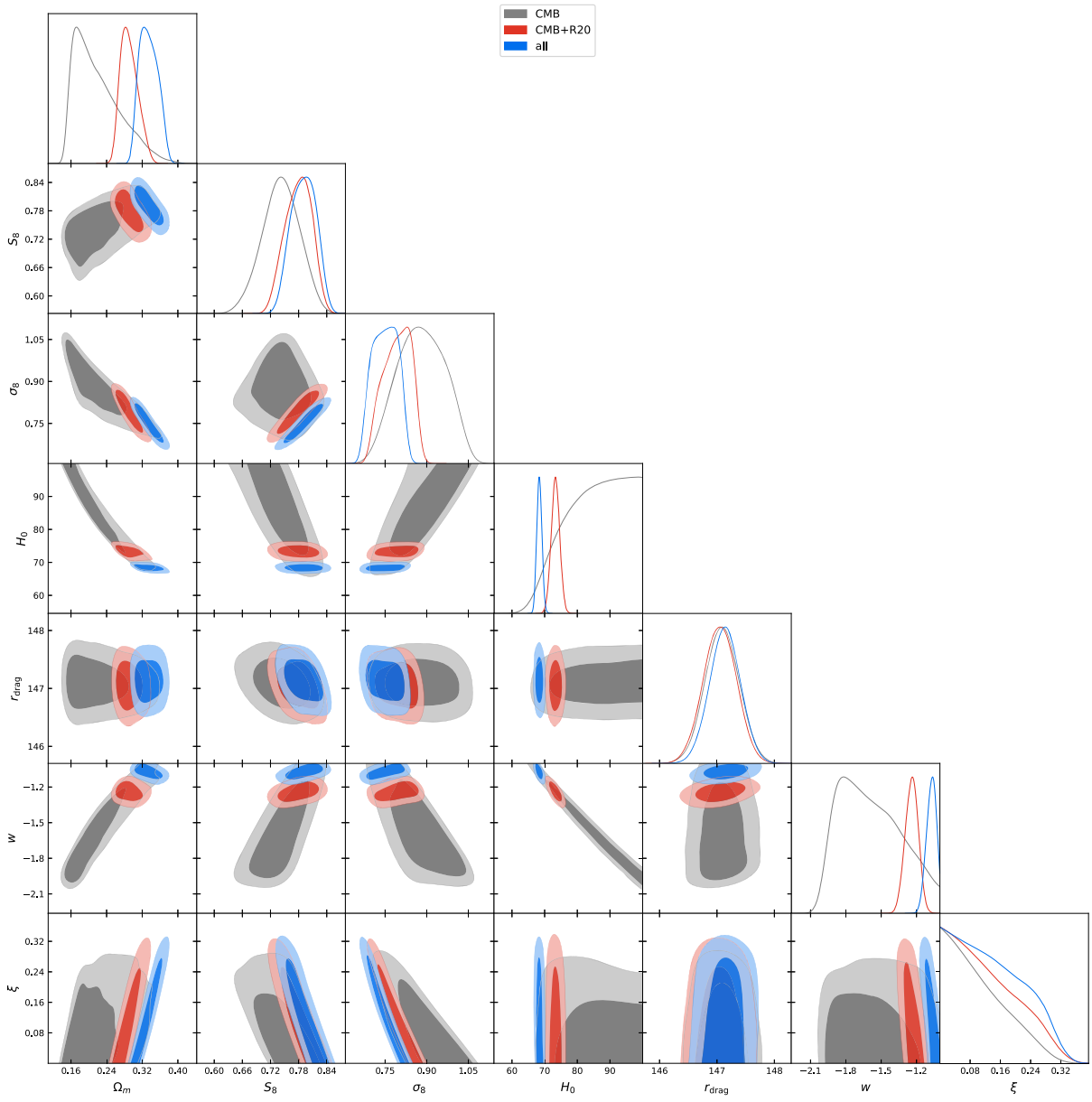

Fig. 12. One dimensional posterior distributions and two dimensional joint contours for the parameter space $\mathcal{P}_{11} \equiv \left\{\Omega_b h^2, \Omega_c h^2, 100\theta_{MC}, \tau, n_s, \ln[10^{10} A_s], w_p, \xi_+\right\}$ for CMB alone, CMB + R20 and CMB + BAO + Pantheon (referred to as 'all') dataset.

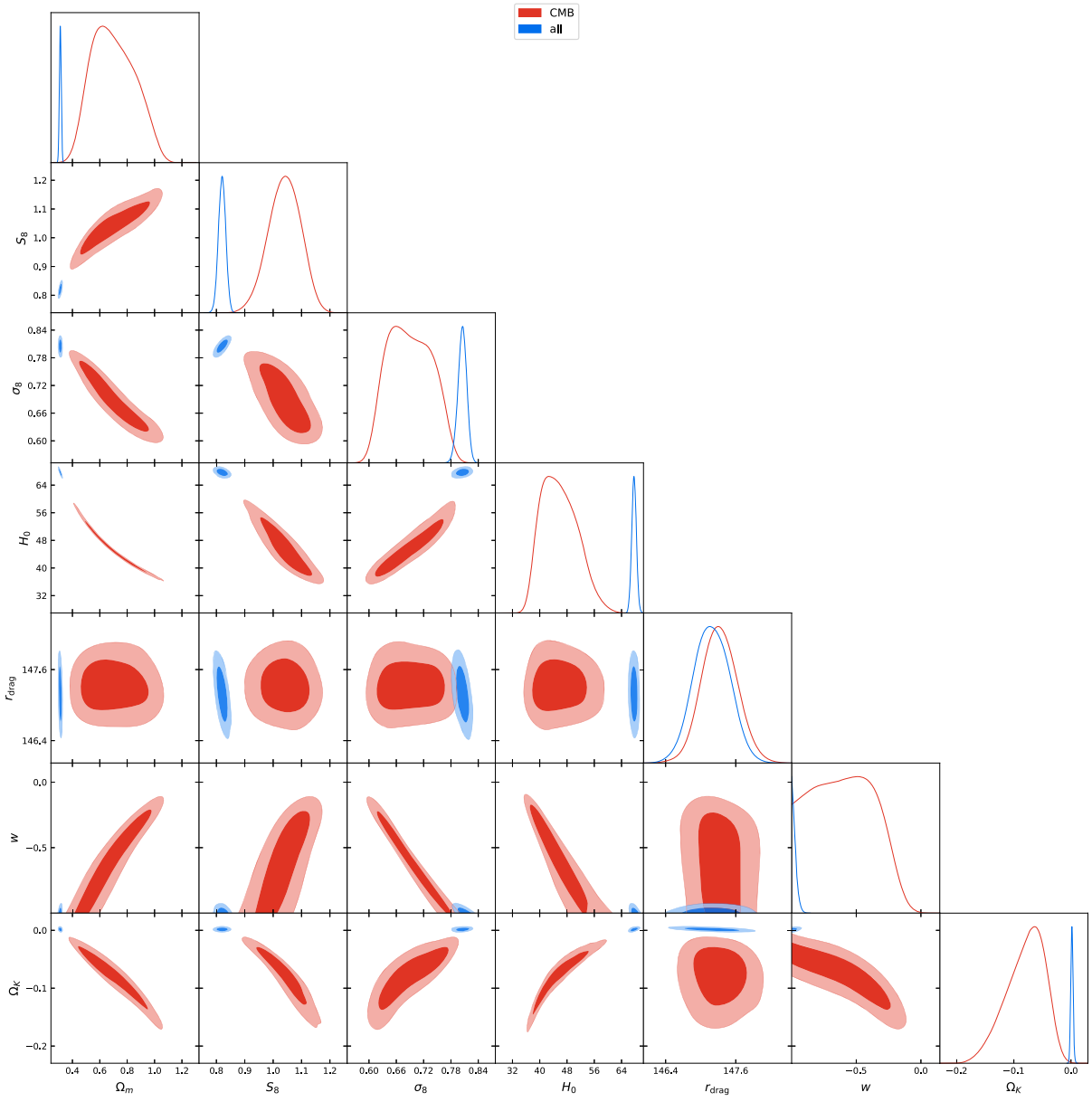

Fig. 13. One dimensional posterior distributions and two dimensional joint contours for the parameter space $\mathcal{P}_{12} \equiv \left\{\Omega_b h^2, \Omega_c h^2, 100\theta_{MC}, \tau, n_s, \ln[10^{10} A_s], w_q, \Omega_k\right\}$ for CMB alone and CMB + BAO + Pantheon (referred to as 'all') dataset.

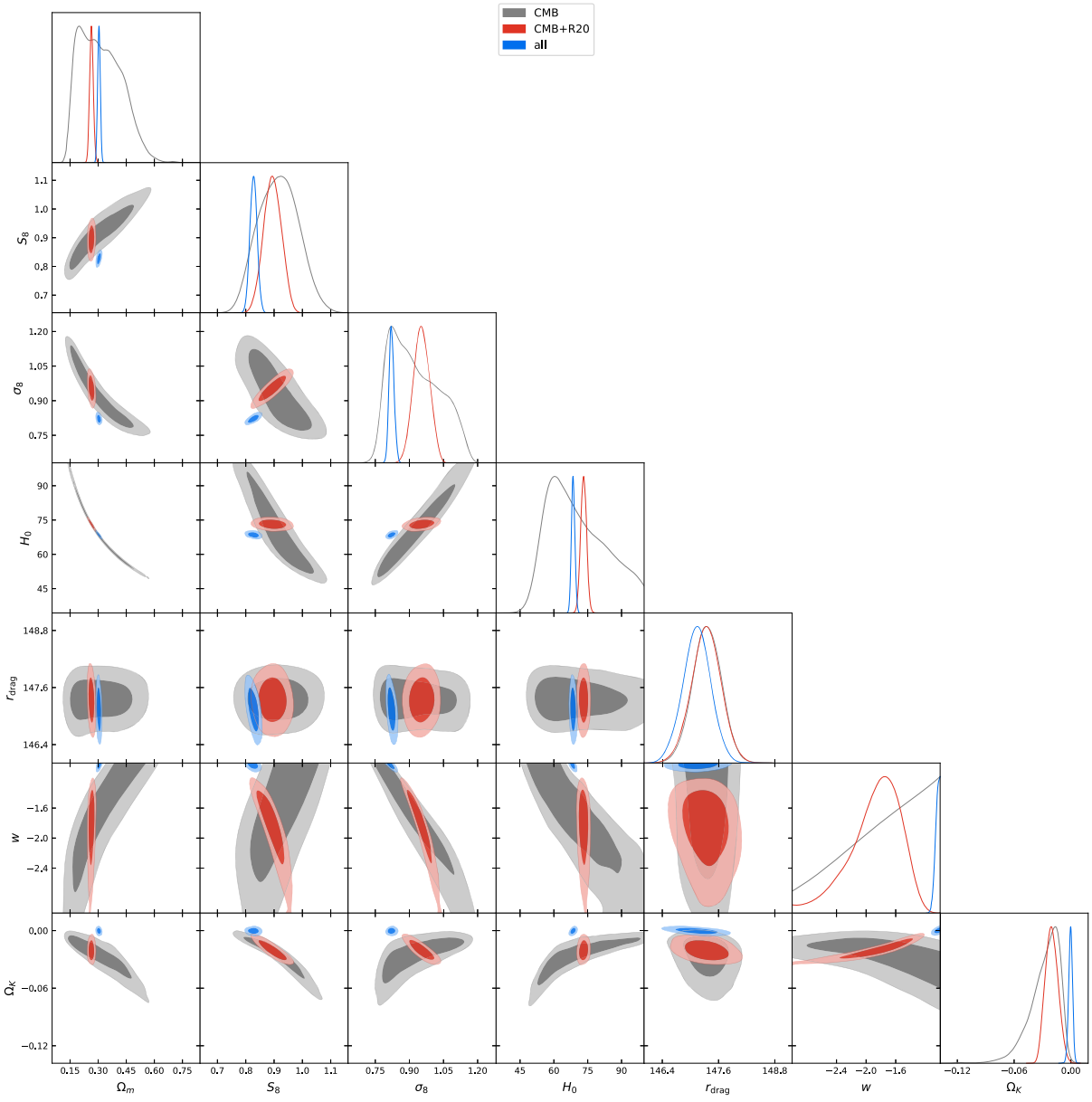

Fig. 14. One dimensional posterior distributions and two dimensional joint contours for the parameter space $\mathcal{P}_{13} \equiv \left\{\Omega_b h^2, \Omega_c h^2, 100\theta_{\rm MC}, \tau, n_s, \ln[10^{10} A_s], w_p, \Omega_k\right\}$ for CMB alone, CMB + R20 and CMB + BAO + Pantheon (referred to as 'all') dataset.

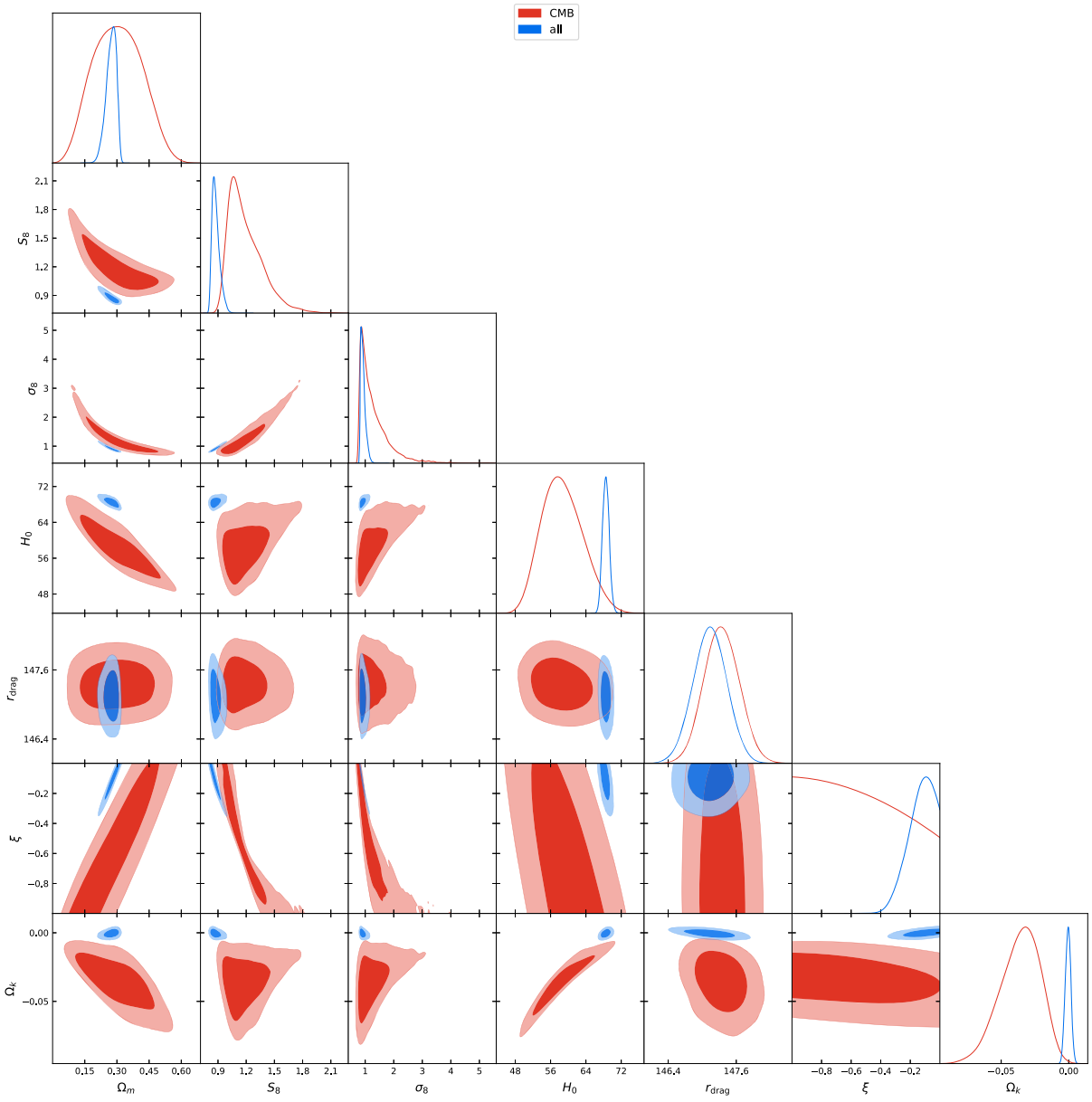

Fig. 15. One dimensional posterior distributions and two dimensional joint contours for the parameter space $\mathcal{P}_{14} \equiv \left\{\Omega_b h^2, \Omega_c h^2, 100\theta_{MC}, \tau, n_s, \ln[10^{10} A_s], \xi_-, \Omega_k\right\}$ for CMB alone, and CMB + BAO + Pantheon (referred to as 'all') dataset.

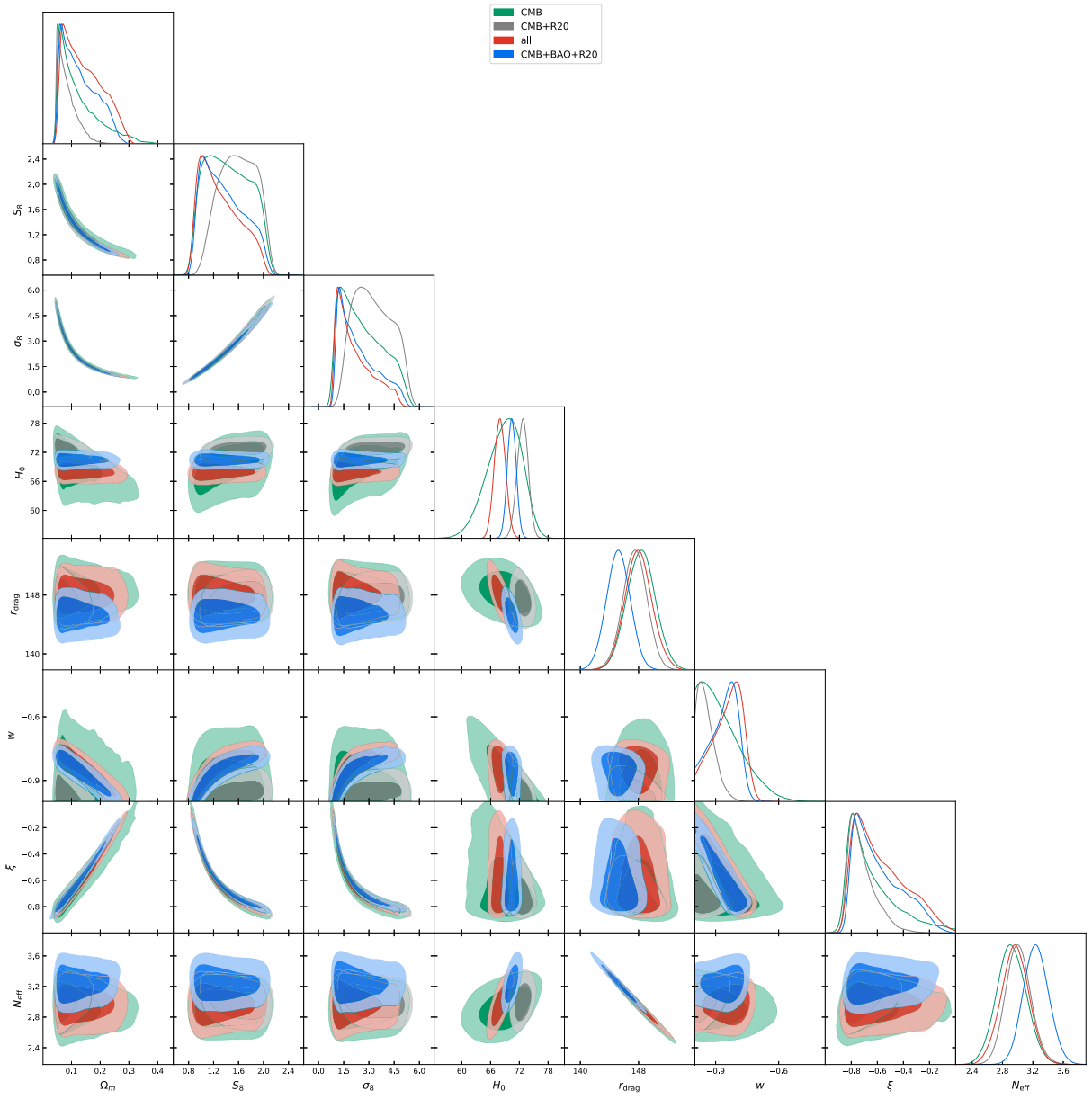

Fig. 16. One dimensional posterior distributions and two dimensional joint contours for the parameter space $\mathcal{P}_{15} \equiv \left\{\Omega_b h^2, \Omega_c h^2, 100\theta_{MC}, \tau, n_s, \ln[10^{10} A_s], N_{eff}, w_q, \xi_-\right\}$ for CMB alone, CMB + R20, CMB + BAO + Pantheon (referred to as 'all'), and CMB + BAO + R20 datasets.

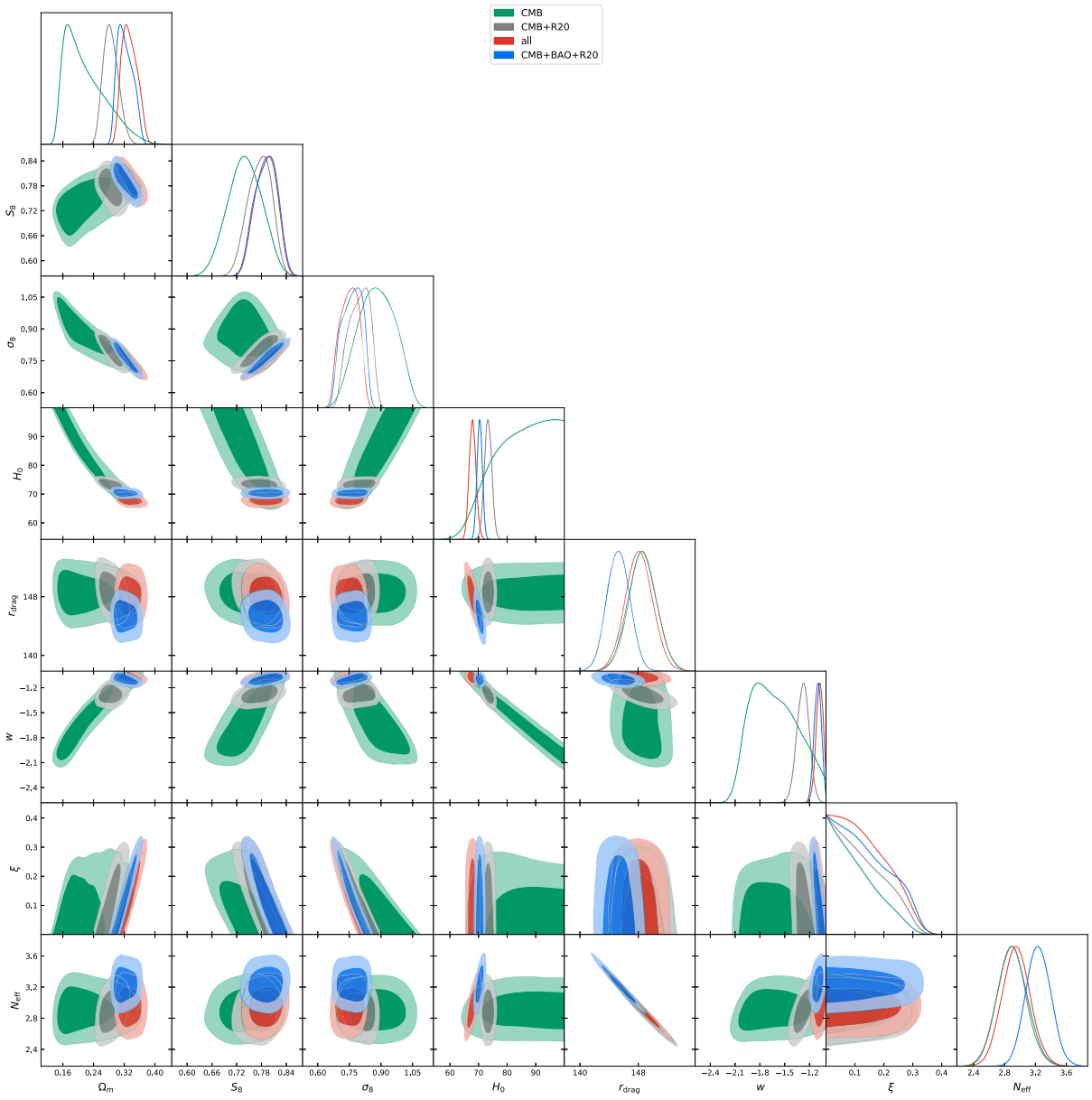

Fig. 17. One dimensional posterior distributions and two dimensional joint contours for the parameter space $\mathcal{P}_{16} \equiv \left\{\Omega_b h^2, \Omega_c h^2, 100\theta_{MC}, \tau, n_s, \ln[10^{10} A_s], N_{eff}, w_p, \xi_+\right\}$ for CMB alone, CMB + R20, CMB + BAO + Pantheon (referred to as 'all'), and CMB + BAO + R20 datasets.

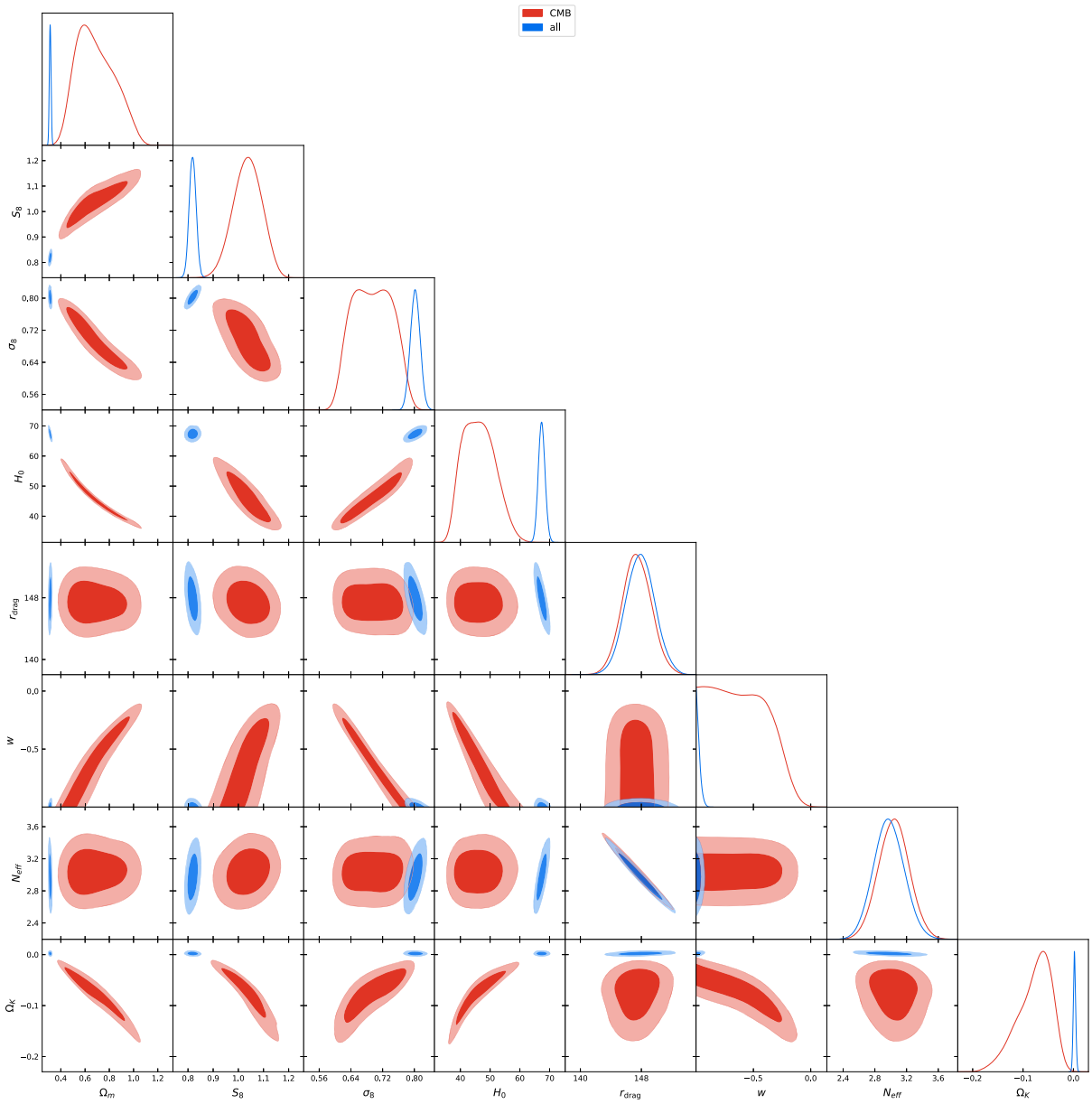

Fig. 18. One dimensional posterior distributions and two dimensional joint contours for the parameter space $\mathcal{P}_{17} \equiv \left\{\Omega_b h^2, \Omega_c h^2, 100\theta_{\rm MC}, \tau, n_s, \ln[10^{10} A_s], N_{\rm eff}, w_q, \Omega_k\right\}$ for CMB alone, and CMB + BAO + Pantheon (referred to as 'all') dataset.

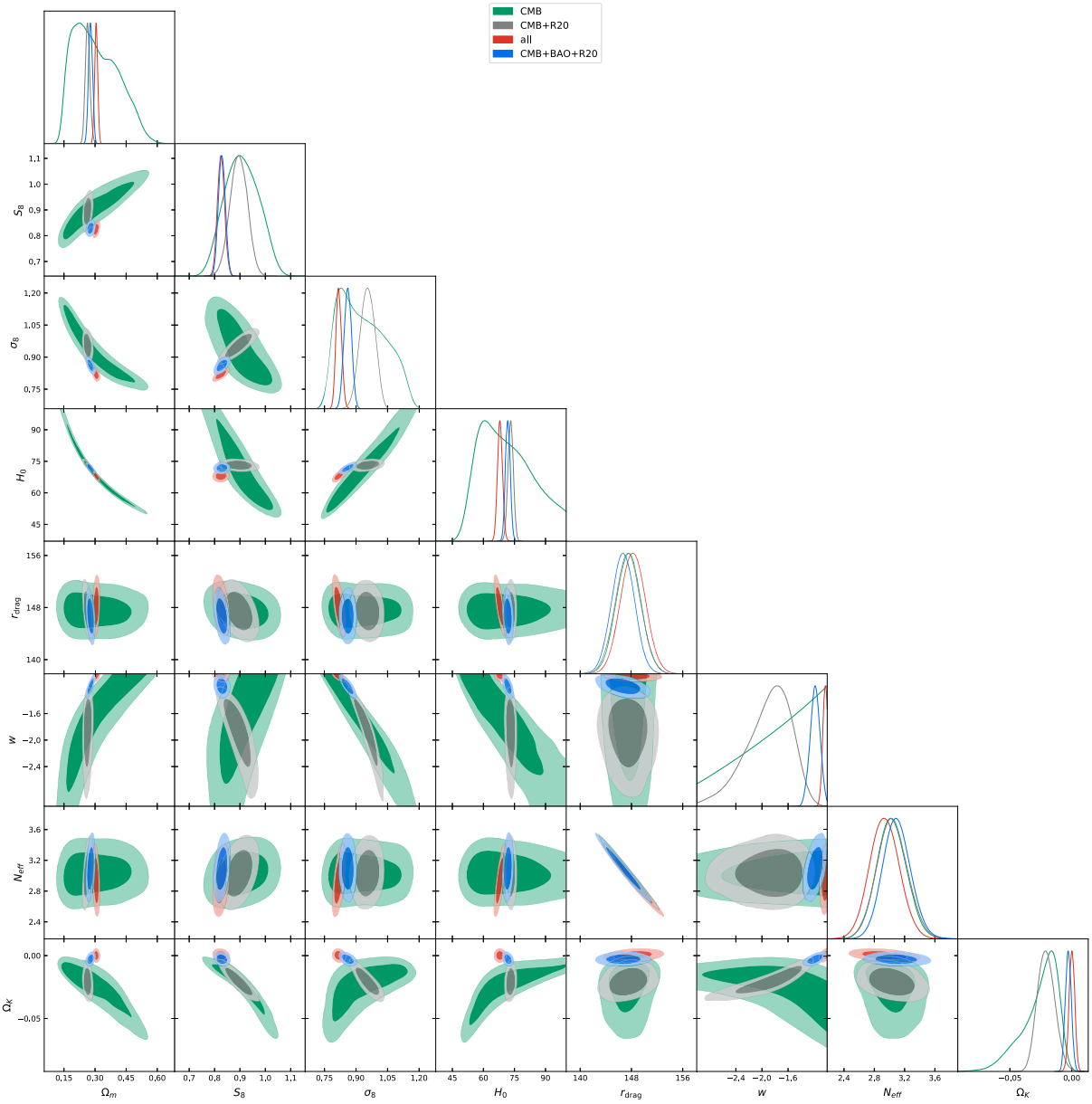

Fig. 19. One dimensional posterior distributions and two dimensional joint contours for the parameter space $\mathcal{P}_{18} \equiv \left\{\Omega_b h^2, \Omega_c h^2, 100\theta_{\rm MC}, \tau, n_s, \ln[10^{10} A_s], N_{\rm eff}, w_p, \Omega_k\right\}$ for CMB alone, CMB + R20, CMB + BAO + Pantheon (referred to as 'all'), and CMB + BAO + R20 datasets.

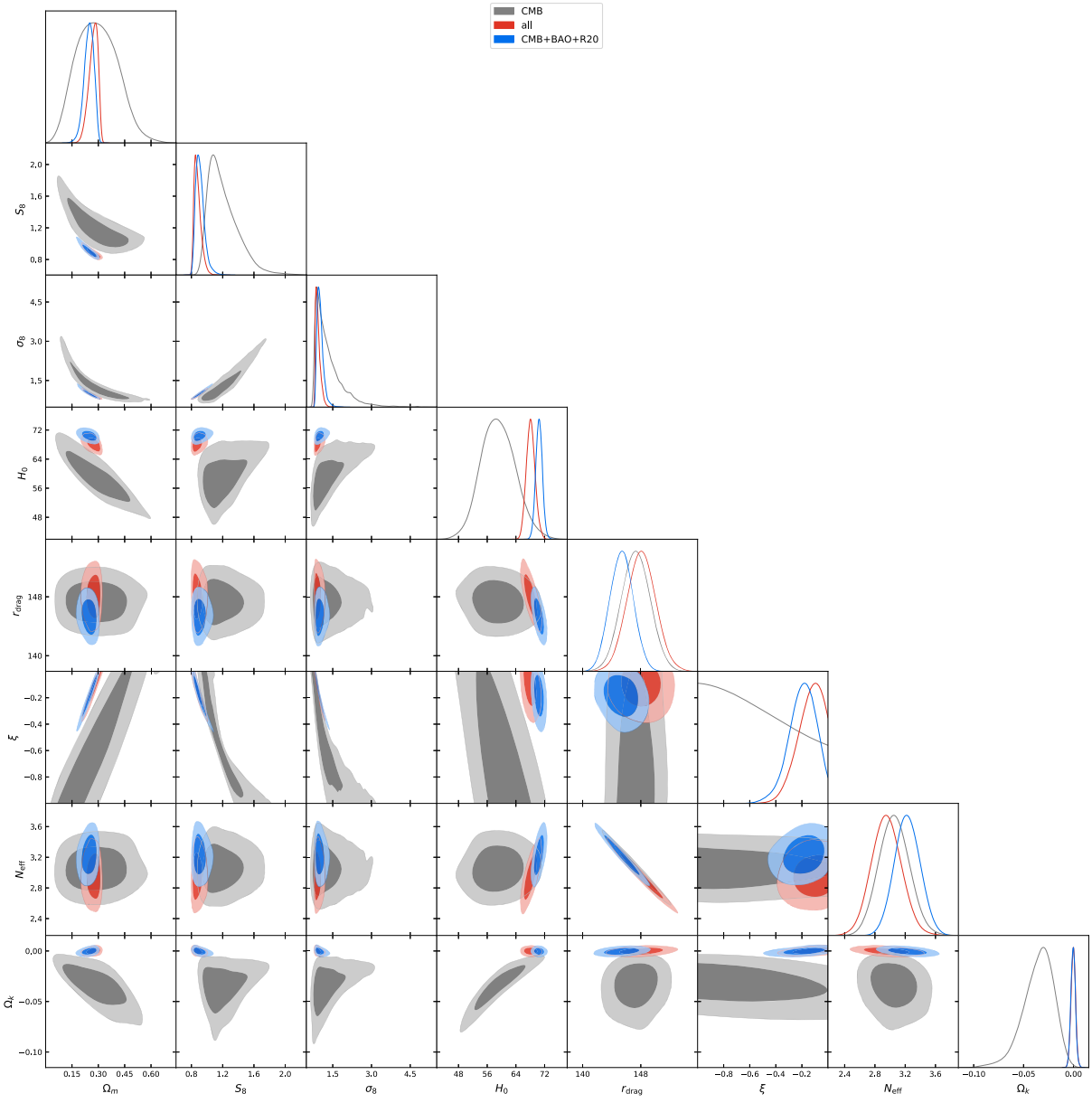

Fig. 20. One dimensional posterior distributions and two dimensional joint contours for the parameter space $\mathcal{P}_{19} \equiv \left\{\Omega_b h^2, \Omega_c h^2, 100\theta_{MC}, \tau, n_s, \ln[10^{10} A_s], N_{\rm eff}, \xi_-, \Omega_k\right\}$ for CMB alone, CMB + BAO + Pantheon (referred to as 'all'), and CMB + BAO + R20 datasets.

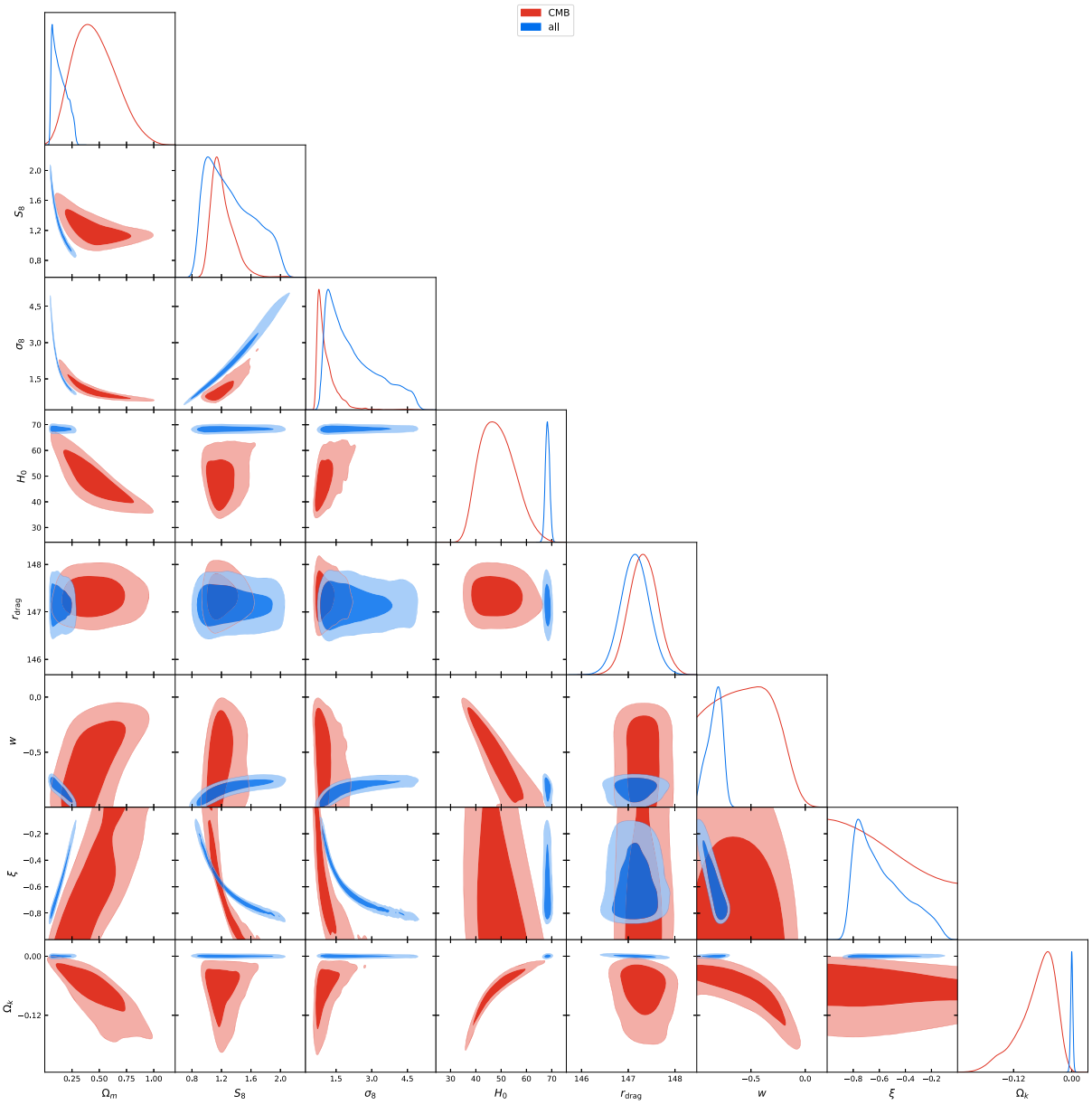

Fig. 21. One dimensional posterior distributions and two dimensional joint contours for the parameter space $\mathcal{P}_{20} \equiv \left\{\Omega_b h^2, \Omega_c h^2, 100\theta_{MC}, \tau, n_s, \ln[10^{10} A_s], w_q, \xi_-, \Omega_k\right\}$ for CMB alone, and CMB + BAO + Pantheon (referred to as 'all') dataset.

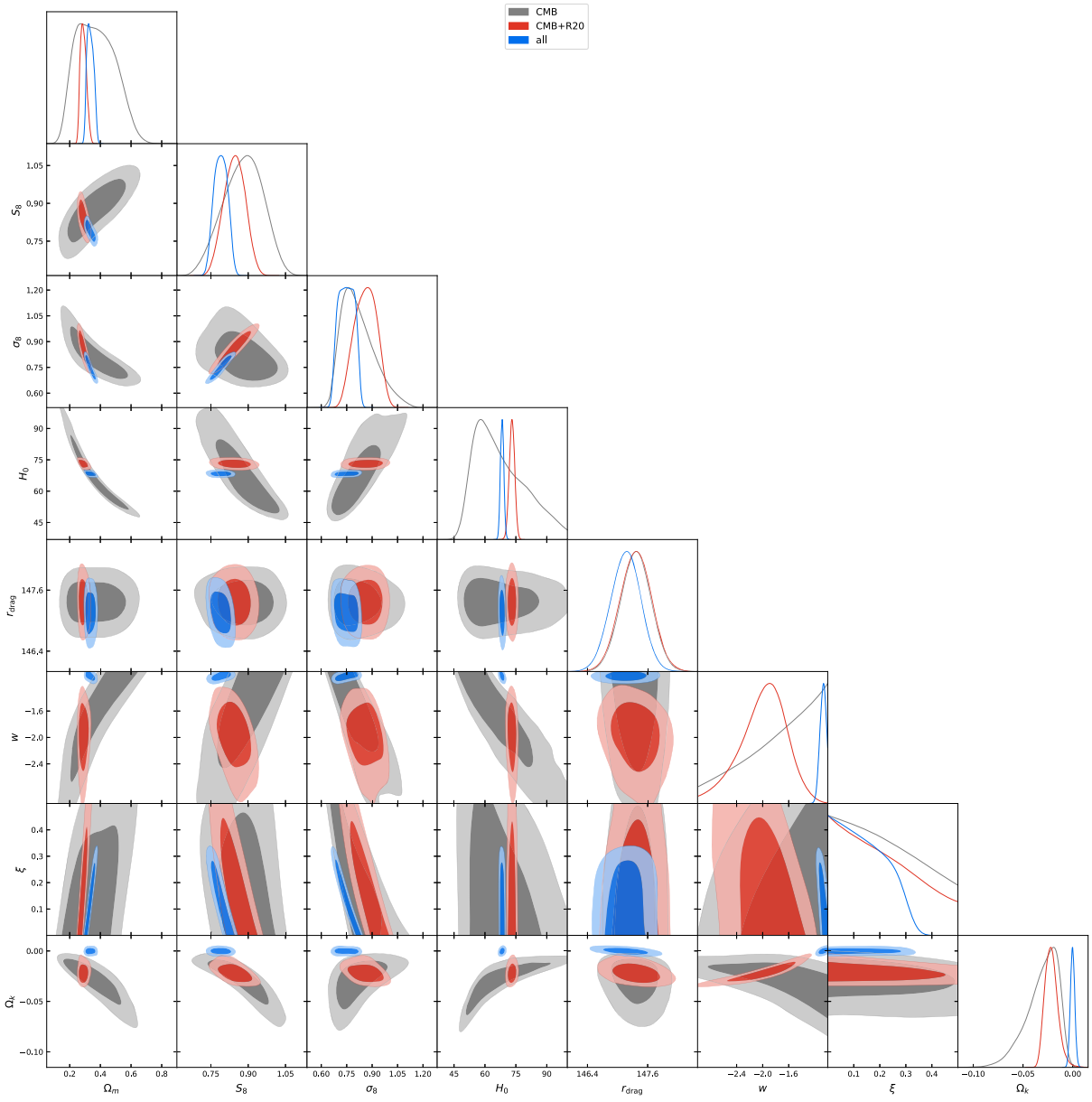

Fig. 22. One dimensional posterior distributions and two dimensional joint contours for the parameter space $\mathcal{P}_{21} \equiv \left\{\Omega_b h^2, \Omega_c h^2, 100\theta_{MC}, \tau, n_s, \ln[10^{10} A_s], w_p, \xi_+, \Omega_k\right\}$ for CMB alone, CMB + R20 and CMB + BAO + Pantheon (referred to as 'all') datasets.

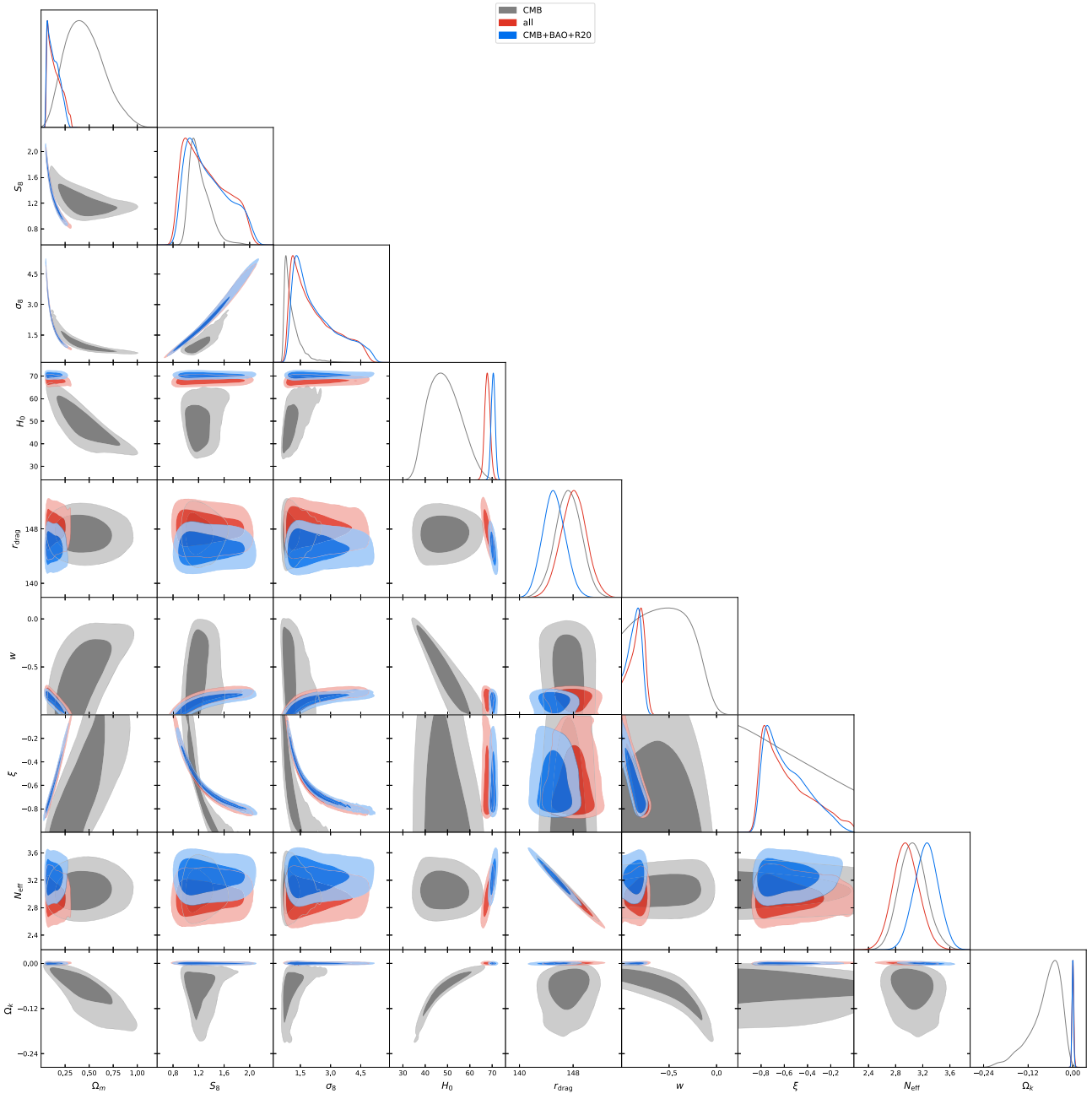

Fig. 23. One dimensional posterior distributions and two dimensional joint contours for the parameter space $\mathcal{P}_{22} \equiv \left\{\Omega_b h^2, \Omega_c h^2, 100\theta_{MC}, \tau, n_s, \ln[10^{10} A_s], N_{\rm eff}, w_q, \xi_-, \Omega_k\right\}$ for CMB alone, CMB + BAO + Pantheon (referred to as 'all'), and CMB + BAO + R20 datasets.

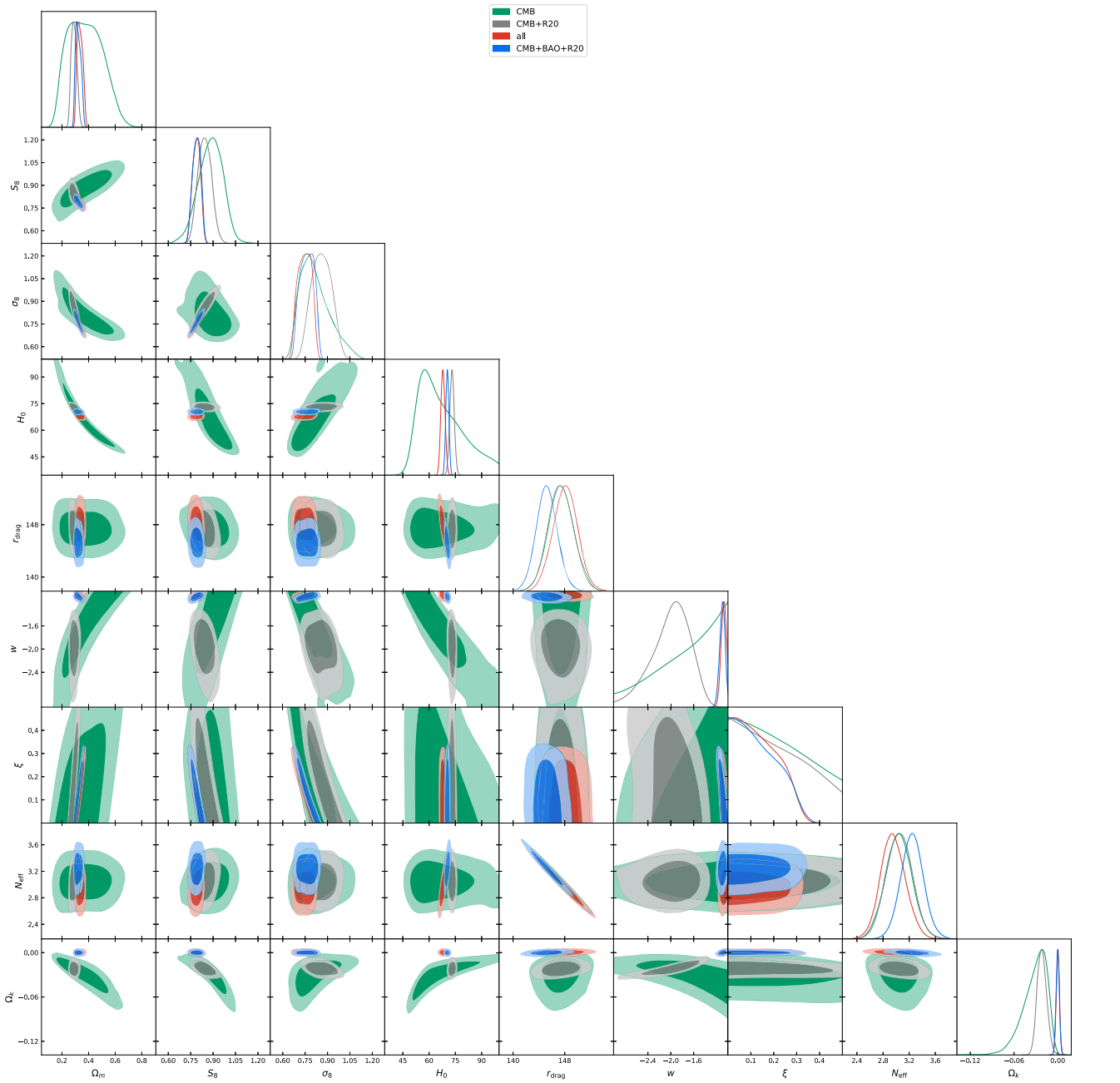

Fig. 24. One dimensional posterior distributions and two dimensional joint contours for the parameter space $\mathcal{P}_{23} \equiv \left\{\Omega_b h^2, \Omega_c h^2, 100\theta_{\rm MC}, \tau, n_s, \ln[10^{10} A_s], N_{\rm eff}, w_p, \xi_+, \Omega_k\right\}$ for CMB alone, CMB + R20, CMB + BAO + Pantheon (referred to as 'all'), and CMB + BAO + R20 datasets.

References

Abbott, T.M.C., et al., DES, 2021. Dark Energy Survey year 3 results: cosmological constraints from galaxy clustering and weak lensing. arXiv:2105.13549 [astro-ph.CO].

Aghanim, N., et al., Planck Collaboration, 2020a. Planck 2018 results VI: cosmological parameters. Astron. Astrophys. 641, A6. https://doi.org/10.1051/0004-6361/201833910. arXiv:1807.06209 [astro-ph.CO].

Aghanim, N., et al., Planck Collaboration, 2020b. Planck 2018 results V: CMB power spectra and likelihoods. Astron. Astrophys. 641, A5. https://doi.org/10.1051/0004-6361/201936386. arXiv:1907.12875 [astro-ph.CO].

Agrawal, P., Cyr-Racine, F.Y., Pinner, D., Randall, L., 2019a. Rock 'n' Roll solutions to the Hubble tension. arXiv:1904.01016 [astro-ph.CO].

Agrawal, P., Obied, G., Vafa, C., 2019b. H_0 tension, Swampland conjectures and the epoch of fading dark matter. arXiv:1906.08261 [astro-ph.CO].

Akita, K., Yamaguchi, M., 2020. A precision calculation of relic neutrino decoupling. J. Cosmol. Astropart. Phys. 08, 012. https://doi.org/10.1088/1475-7516/2020/08/012. arXiv:2005.07047 [hep-ph].

Alam, S., et al., BOSS Collaboration, 2017. The clustering of galaxies in the completed SDSS-III Baryon Oscillation Spectroscopic Survey: cosmological analysis of the DR12 galaxy sample. Mon. Not. R. Astron. Soc. 470 (3), 2617–2652. https://doi.org/10.1093/mnras/stx721. arXiv:1607.03155 [astro-ph.CO].

Amendola, L., 2000. Coupled quintessence. Phys. Rev. D 62, 043511. https://doi.org/10.1103/PhysRevD.62.043511. arXiv:astro-ph/9908023 [astro-ph].

Amirhashchi, H., Yadav, A.K., 2020. Interacting dark sectors in anisotropic universe: observational constraints and H_0 tension. arXiv:2001.03775 [astro-ph.CO].

Anchordoqui, L., Goldberg, H., Nawata, S., Nuñez, C., 2007. Cosmology from string theory. Phys. Rev. D 76, 126005. https://doi.org/10.1103/PhysRevD.76.126005. arXiv:0704.0928 [hep-ph].

Anchordoqui, L.A., 2020. Hubble hullabaloo and string cosmology. arXiv:2005.01217 [astro-ph.CO].

Anchordoqui, L.A., 2021. Decaying dark matter, the H_0 tension, and the lithium problem. Phys. Rev. D 103 (3), 035025. https://doi.org/10.1103/PhysRevD.103.035025. arXiv:2010.09715 [hep-ph].

Anchordoqui, L.A., Goldberg, H., 2012. Neutrino cosmology after WMAP 7-year data and LHC first Z' bounds. Phys. Rev. Lett. 108, 081805. https://doi.org/10.1103/PhysRevLett.108.081805. arXiv:1111.7264 [hep-ph].

Anchordoqui, L.A., Goldberg, H., Steigman, G., 2013. Right-handed neutrinos as the dark radiation: status and forecasts for the LHC. Phys. Lett. B 718, 1162. https://doi.org/10.1016/j.physletb.2012.12.019. arXiv:1211.0186 [hep-ph].

Anchordoqui, L.A., Antoniadis, I., Lüst, D., Soriano, J.F., Taylor, T.R., 2020. H_0 tension and the String Swampland. Phys. Rev. D 101, 083532. https://doi.org/10.1103/PhysRevD.101.083532. arXiv:1912.00242 [hep-th].

Anchordoqui, L.A., Antoniadis, I., Lüst, D., Soriano, J.F., 2021. Dark energy, Ricci-nonflat spaces, and the Swampland. Phys. Lett. B 816, 136199. https://doi.org/10.1016/j.physletb.2021.136199. arXiv:2005.10075 [hep-th].

Arendse, N., Wojtak, R.J., Agnello, A., Chen, G.C.F., Fassnacht, C.D., Sluse, D., Hilbert, S., Millon, M., Bonvin, V., Wong, K.C., et al., 2020. Cosmic dissonance: are new physics or systematics behind a short sound horizon? Astron. Astrophys. 639, A57. https://doi.org/10.1051/0004-6361/201936720. arXiv:1909.07986 [astro-ph.CO].

Asgari, M., et al., KiDS Collaboration, 2020. KiDS-1000 cosmology: cosmic shear constraints and comparison between two point statistics. arXiv:2007.15633 [astro-ph.CO].

Aver, E., Olive, K.A., Skillman, E.D., 2015. The effects of He I λ10830 on helium abundance determinations. J. Cosmol. Astropart. Phys. 07, 011. https://doi.org/10.1088/1475-7516/2015/07/011. arXiv:1503.08146 [astro-ph.CO].

Barrow, J.D., Clifton, T., 2006. Cosmologies with energy exchange. Phys. Rev. D 73, 103520. https://doi.org/10.1103/PhysRevD.73.103520. arXiv:gr-qc/0604063 [gr-qc].

Baumann, D., 2018. Primordial Cosmology. PoS TASI2017, 009. https://doi.org/10.22323/1.305.0009. arXiv:1807.03098 [hep-th].

Baumann, D., Green, D., Wallisch, B., 2016. New target for cosmic axion searches. Phys. Rev. Lett. 117 (17), 171301. https://doi.org/10.1103/PhysRevLett.117.171301. arXiv:1604.08614 [astro-ph.CO].

Benaoum, H.B., Yang, W., Pan, S., Di Valentino, E., 2020. Modified emergent dark energy and its astronomical constraints. arXiv:2008.09098 [gr-qc].

Bennett, J.J., Buldgen, G., De Salas, P.F., Drewes, M., Gariazzo, S., Pastor, S., Wong, Y.Y.Y., 2021. Towards a precision calculation of $N_{\rm eff}$ in the Standard Model II: neutrino decoupling in the presence of flavour oscillations and finite-temperature QED. J. Cosmol. Astropart. Phys. 04, 073. https://doi.org/10.1088/1475-7516/2021/04/073. arXiv:2012.02726 [hep-ph].

Bernal, J.L., Verde, L., Jimenez, R., Kamionkowski, M., Valcin, D., Wandelt, B.D., 2021. The trouble beyond H_0 and the new cosmic triangles. Phys. Rev. D 103 (10), 103533. https://doi.org/10.1103/PhysRevD.103.103533. arXiv:2102.05066 [astro-ph.CO].

Beutler, F., Blake, C., Colless, M., Jones, D.H., Staveley-Smith, L., Campbell, L., Parker, Q., Saunders, W., Watson, F., 2011. The 6dF Galaxy Survey: baryon acoustic oscillations and the local Hubble constant. Mon. Not. R. Astron. Soc. 416, 3017–3032. https://doi.org/10.1111/j.1365-2966.2011.19250.x. arXiv:1106.3366 [astro-ph.CO].

Bolotin, Y.L., Kostenko, A., Lemets, O.A., Yerokhin, D.A., 2014. Cosmological evolution with interaction between dark energy and dark matter. Int. J. Mod. Phys. D 24 (03), 1530007. https://doi.org/10.1142/S0218271815300074. arXiv:1310.0085 [astro-ph.CO].

Bonilla, A., Kumar, S., Nunes, R.C., Pan, S., 2021. Reconstruction of the dark sectors' interaction: a model-independent inference and forecast from GW standard sirens. arXiv:2102.06149 [astro-ph.CO].

Cai, R.G., Wang, A., 2005. Cosmology with interaction between phantom dark energy and dark matter and the coincidence problem. J. Cosmol. Astropart. Phys. 03, 002. https://doi.org/10.1088/1475-7516/2005/03/002. arXiv:hep-th/0411025 [hep-th].

Caldwell, R.R., 2002. A phantom menace? Phys. Lett. B 545, 23–29. https://doi.org/10.1016/S0370-2693(02)02589-3. arXiv:astro-ph/9908168 [astro-ph].

Caldwell, R.R., Dave, R., Steinhardt, P.J., 1998. Cosmological imprint of an energy component with general equation of state. Phys. Rev. Lett. 80, 1582–1585. https://doi.org/10.1103/PhysRevLett.80.1582. arXiv:astro-ph/9708069 [astro-ph].

Caldwell, R.R., Kamionkowski, M., Weinberg, N.N., 2003. Phantom energy and cosmic doomsday. Phys. Rev. Lett. 91, 071301. https://doi.org/10.1103/PhysRevLett.91.071301. arXiv:astro-ph/0302506 [astro-ph].

Camarena, D., Marra, V., 2021. On the use of the local prior on the absolute magnitude of Type Ia supernovae in cosmological inference. Mon. Not. R. Astron. Soc. 504, 5164–5171. https://doi.org/10.1093/mnras/stab1200. arXiv:2101.08641 [astro-ph.CO].

Carroll, S.M., Hoffman, M., Trodden, M., 2003. Can the dark energy equation-of-state parameter w be less than -1? Phys. Rev. D 68, 023509. https://doi.org/10.1103/PhysRevD.68.023509. arXiv:astro-ph/0301273 [astro-ph].

Carroll, S.M., De Felice, A., Trodden, M., 2005. Can we be tricked into thinking that w is less than -1? Phys. Rev. D 71, 023525. https://doi.org/10.1103/PhysRevD.71.023525. arXiv:astro-ph/0408081 [astro-ph].

Chimento, L.P., Richarte, M.G., 2012. Dark matter, dark energy, and dark radiation coupled with a transversal interaction. Phys. Rev. D 86, 103501. https://doi.org/10.1103/PhysRevD.86.103501. arXiv:1210.5505 [gr-qc].

Clemson, T., Koyama, K., Zhao, G.B., Maartens, R., Valiviita, J., 2012. Interacting Dark Energy – constraints and degeneracies. Phys. Rev. D 85, 043007. https://doi.org/10.1103/PhysRevD.85.043007. arXiv:1109.6234 [astro-ph.CO].

Colgáin, E.Ó., Yavartanoo, H., 2019. Testing the Swampland: H_0 tension. Phys. Lett. B 797, 134907. https://doi.org/10.1016/j.physletb.2019.134907. arXiv:1905.02555 [astro-ph.CO].

Comelli, D., Pietroni, M., Riotto, A., 2003. Dark energy and dark matter. Phys. Lett. B 571, 115–120. https://doi.org/10.1016/j.physletb.2003.05.006. arXiv:hep-ph/0302080 [hep-ph].

Cooke, R.J., Pettini, M., Steidel, C.C., 2018. One percent determination of the primordial deuterium abundance. Astrophys. J. 855 (2), 102. https://doi.org/10.3847/1538-4357/aaab53. arXiv:1710.11129 [astro-ph.CO].

Cuesta, A.J., Verde, L., Riess, A., Jimenez, R., 2015. Calibrating the cosmic distance scale ladder: the role of the sound horizon scale and the local expansion rate as distance anchors. Mon. Not. R. Astron. Soc. 448 (4), 3463–3471. https://doi.org/10.1093/mnras/stv261. arXiv:1411.1094 [astro-ph.CO].

de Salas, P.F., Pastor, S., 2016. Relic neutrino decoupling with flavour oscillations revisited. J. Cosmol. Astropart. Phys. 07, 051. https://doi.org/10.1088/1475-7516/2016/07/051. arXiv:1606.06986 [hep-ph].

D'Eramo, F., Ferreira, R.Z., Notari, A., Bernal, J.L., 2018. Hot axions and the H_0 tension. J. Cosmol. Astropart. Phys. 1811, 014. https://doi.org/10.1088/1475-7516/2018/11/014. arXiv:1808.07430 [hep-ph].

Di Valentino, E., 2021. A combined analysis of the H_0 late time direct measurements and the impact on the Dark Energy sector. Mon. Not. R. Astron. Soc. 502 (2), 2065–2073. https://doi.org/10.1093/mnras/stab187. arXiv:2011.00246 [astro-ph.CO].

Di Valentino, E., Mena, O., 2020. A fake interacting dark energy detection? Mon. Not. R. Astron. Soc. 500 (1), L22–L26. https://doi.org/10.1093/mnrasl/slaa175. arXiv:2009.12620 [astro-ph.CO].

Di Valentino, E., Gariazzo, S., Giusarma, E., Mena, O., 2015. Robustness of cosmological axion mass limits. Phys. Rev. D 91 (12), 123505. https://doi.org/10.1103/PhysRevD.91.123505. arXiv:1503.00911 [astro-ph.CO].

Di Valentino, E., Giusarma, E., Lattanzi, M., Mena, O., Melchiorri, A., Silk, J., 2016a. Cosmological Axion and neutrino mass constraints from Planck 2015 temperature and polarization data. Phys. Lett. B 752, 182–185. https://doi.org/10.1016/j.physletb.2015.11.025. arXiv:1507.08665 [astro-ph.CO].

Di Valentino, E., Giusarma, E., Mena, O., Melchiorri, A., Silk, J., 2016b. Cosmological limits on neutrino unknowns versus low redshift priors. Phys. Rev. D 93 (8), 083527. https://doi.org/10.1103/PhysRevD.93.083527. arXiv:1511.00975 [astro-ph.CO].

Di Valentino, E., Melchiorri, A., Mena, O., 2017. Can interacting dark energy solve the H_0 tension? Phys. Rev. D 96 (4), 043503. https://doi.org/10.1103/PhysRevD.96.043503. arXiv:1704.08342 [astro-ph.CO].

Di Valentino, E., Melchiorri, A., Silk, J., 2019. Planck evidence for a closed Universe and a possible crisis for cosmology. Nat. Astron. 4 (2), 196–203. https://doi.org/10.1038/s41550-019-0906-9. arXiv:1911.02087 [astro-ph.CO].

Di Valentino, E., Gariazzo, S., Mena, O., Vagnozzi, S., 2020a. Soundness of dark energy properties. J. Cosmol. Astropart. Phys. 07 (07), 045. https://doi.org/10.1088/1475-7516/2020/07/045. arXiv:2005.02062 [astro-ph.CO].

Di Valentino, E., Melchiorri, A., Mena, O., Vagnozzi, S., 2020b. Interacting dark energy after the latest Planck, DES, and H_0 measurements: an excellent solution to the H_0 and cosmic shear tensions. Phys. Dark Universe 30, 100666. https://doi.org/10.1016/j.dark.2020.100666. arXiv:1908.04281 [astro-ph.CO].

Di Valentino, E., Melchiorri, A., Mena, O., Vagnozzi, S., 2020c. Nonminimal dark sector physics and cosmological tensions. Phys. Rev. D 101 (6), 063502. https://doi.org/10.1103/PhysRevD.101.063502. arXiv:1910.09853 [astro-ph.CO].

Di Valentino, E., et al., 2021a. Cosmology intertwined II: the Hubble constant tension. Astropart. Phys. 131, 102605. https://doi.org/10.1016/j.astropartphys.2021.102605. arXiv:2008.11284 [astro-ph.CO].

Di Valentino, E., et al., 2021b. Cosmology intertwined IV: the age of the universe and its curvature. Astropart. Phys. 131, 102607. https://doi.org/10.1016/j.astropartphys.2021.102607. arXiv:2008.11286 [astro-ph.CO].

Di Valentino, E., et al., 2021c. Cosmology intertwined I: perspectives for the next decade. Astropart. Phys. 131, 102606. https://doi.org/10.1016/j.astropartphys.2021.102606. arXiv:2008.11283 [astro-ph.CO].

Di Valentino, E., et al., 2021d. Cosmology intertwined III: $f\sigma_8$ and S_8. Astropart. Phys. 131, 102604. https://doi.org/10.1016/j.astropartphys.2021.102604. arXiv:2008.11285 [astro-ph.CO].

Di Valentino, E., Melchiorri, A., Mena, O., Pan, S., Yang, W., 2021e. Interacting dark energy in a closed universe. Mon. Not. R. Astron. Soc. 502 (1), L23–L28. https://doi.org/10.1093/mnrasl/slaa207. arXiv:2011.00283 [astro-ph.CO].

Di Valentino, E., Melchiorri, A., Silk, J., 2021f. Investigating cosmic discordance. Astrophys. J. Lett. 908 (1), L9. https://doi.org/10.3847/2041-8213/abe1c4. arXiv:2003.04935 [astro-ph.CO].

Di Valentino, E., Mukherjee, A., Sen, A.A., 2021g. Dark energy with phantom crossing and the H_0 tension. Entropy 23 (4), 404. https://doi.org/10.3390/e23040404. arXiv:2005.12587 [astro-ph.CO].

Di Valentino, E., Mena, O., Pan, S., Visinelli, L., Yang, W., Melchiorri, A., Mota, D.F., Riess, A.G., Silk, J., 2021h. The realm of the Hubble tension – a review of solutions. https://doi.org/10.1088/1361-6382/ac086d. arXiv:2103.01183 [astro-ph.CO], 2021.

Efstathiou, G., 2021. To H0 or not to H0? https://doi.org/10.1093/mnras/stab1588. arXiv:2103.08723 [astro-ph.CO], 2021.

Feng, L., Zhang, J.F., Zhang, X., 2019. Search for sterile neutrinos in a universe of vacuum energy interacting with cold dark matter. Phys. Dark Universe 23, 100261. https://doi.org/10.1016/j.dark.2018.100261. arXiv:1712.03148 [astro-ph.CO].

Ferreira, E.G.M., Quintin, J., Costa, A.A., Abdalla, E., Wang, B., 2017. Evidence for interacting dark energy from BOSS. Phys. Rev. D 95 (4), 043520. https://doi.org/10.1103/PhysRevD.95.043520. arXiv:1412.2777 [astro-ph.CO].

Franca, U., Rosenfeld, R., 2004. Age constraints and fine tuning in VAMP models. Phys. Rev. D 69, 063517. https://doi.org/10.1103/PhysRevD.69.063517. arXiv:astro-ph/0308149 [astro-ph].

Freedman, W.L., 2021. Measurements of the Hubble constant: tensions in perspective. arXiv:2106.15656 [astro-ph.CO].

Froustey, J., Pitrou, C., Volpe, M.C., 2020. Neutrino decoupling including flavour oscillations and primordial nucleosynthesis. J. Cosmol. Astropart. Phys. 12, 015. https://doi.org/10.1088/1475-7516/2020/12/015. arXiv:2008.01074 [hep-ph].

Gao, L.Y., Zhao, Z.W., Xue, S.S., Zhang, X., 2021. Relieving the H_0 tension with a new interacting dark energy model. J. Cosmol. Astropart. Phys. 07, 005. https://doi.org/10.1088/1475-7516/2021/07/005. arXiv:2101.10714 [astro-ph.CO].

Gavela, M.B., Hernandez, D., Lopez Honorez, L., Mena, O., Rigolin, S., 2009. Dark coupling. J. Cosmol. Astropart. Phys. 07, 034. https://doi.org/10.1088/1475-7516/2009/07/034. erratum: J. Cosmol. Astropart. Phys. 05, E01 (2010). arXiv:0901.1611 [astro-ph.CO].

Gavela, M.B., Lopez Honorez, L., Mena, O., Rigolin, S., 2010. Dark coupling and gauge invariance. J. Cosmol. Astropart. Phys. 11, 044. https://doi.org/10.1088/1475-7516/2010/11/044. arXiv:1005.0295 [astro-ph.CO].

Gelman, A., Rubin, D.B., 1992. Inference from iterative simulation using multiple sequences. Stat. Sci. 7, 457–472. https://doi.org/10.1214/ss/1177011136.

Giarè, W., Di Valentino, E., Melchiorri, A., Mena, O., 2020. New cosmological bounds on hot relics: axions & neutrinos. https://doi.org/10.1093/mnras/stab1442. arXiv:2011.14704 [astro-ph.CO], 2020.

Giusarma, E., Di Valentino, E., Lattanzi, M., Melchiorri, A., Mena, O., 2014. Relic Neutrinos, thermal axions and cosmology in early 2014. Phys. Rev. D 90 (4), 043507. https://doi.org/10.1103/PhysRevD.90.043507. arXiv:1403.4852 [astro-ph.CO].

Gogoi, A., Sharma, R.K., Chanda, P., Das, S., 2021. Early mass-varying neutrino dark energy: nugget formation and Hubble anomaly. Astrophys. J. 915 (2), 132. https://doi.org/10.3847/1538-4357/abfe5b. arXiv:2005.11889 [astro-ph.CO].

Gómez-Valent, A., Pettorino, V., Amendola, L., 2020. Update on coupled dark energy and the H_0 tension. Phys. Rev. D 101 (12), 123513. https://doi.org/10.1103/PhysRevD.101.123513. arXiv:2004.00610 [astro-ph.CO].

Gómez-Valent, A., Zheng, Z., Amendola, L., Pettorino, V., Wetterich, C., 2021. Early dark energy in the pre- and post-recombination epochs. arXiv:2107.11065 [astro-ph.CO].

Guo, J.J., Zhang, J.F., Li, Y.H., He, D.Z., Zhang, X., 2018. Probing the sign-changeable interaction between dark energy and dark matter with current observations. Sci. China, Phys. Mech. Astron. 61 (3), 030011. https://doi.org/10.1007/s11433-017-9131-9. arXiv:1710.03068 [astro-ph.CO].

Hamana, T., et al., 2020. Cosmological constraints from cosmic shear two-point correlation functions with HSC survey first-year data. Publ. Astron. Soc. Jpn. 72 (1), 16. https://doi.org/10.1093/pasj/psz138. arXiv:1906.06041 [astro-ph.CO].

Handley, W., 2021. Curvature tension: evidence for a closed universe. Phys. Rev. D 103 (4), L041301. https://doi.org/10.1103/PhysRevD.103.L041301. arXiv:1908.09139 [astro-ph.CO].

He, J.H., Wang, B., Abdalla, E., 2009. Stability of the curvature perturbation in dark sectors' mutual interacting models. Phys. Lett. B 671, 139–145. https://doi.org/10.1016/j.physletb.2008.11.062. arXiv:0807.3471 [gr-qc].

Hill, J.C., McDonough, E., Toomey, M.W., Alexander, S., 2020. Early dark energy does not restore cosmological concordance. Phys. Rev. D 102 (4), 043507. https://doi.org/10.1103/PhysRevD.102.043507. arXiv:2003.07355 [astro-ph.CO].

Hou, Z., Keisler, R., Knox, L., Millea, M., Reichardt, C., 2013. How massless neutrinos affect the cosmic microwave background damping tail. Phys. Rev. D 87, 083008. https://doi.org/10.1103/PhysRevD.87.083008. arXiv:1104.2333 [astro-ph.CO].

Hu, W., Sugiyama, N., 1996. Small scale cosmological perturbations: an analytic approach. Astrophys. J. 471, 542–570. https://doi.org/10.1086/177989. arXiv:astro-ph/9510117 [astro-ph].

Jackson, B.M., Taylor, A., Berera, A., 2009. On the large-scale instability in interacting dark energy and dark matter fluids. Phys. Rev. D 79, 043526. https://doi.org/10.1103/PhysRevD.79.043526. arXiv:0901.3272 [astro-ph.CO].

Jacques, T.D., Krauss, L.M., Lunardini, C., 2013. Additional light sterile neutrinos and cosmology. Phys. Rev. D 87 (8), 083515. https://doi.org/10.1103/PhysRevD.87.083515. Erratum: Phys. Rev. D 88 (10), 109901 (2013). arXiv:1301.3119 [astro-ph.CO].

Jedamzik, K., Pogosian, L., Zhao, G.B., 2021. Why reducing the cosmic sound horizon alone can not fully resolve the Hubble tension. Commun. Phys. 4, 123. https://doi.org/10.1038/s42005-021-00628-x. arXiv:2010.04158 [astro-ph.CO].

Knox, L., Millea, M., 2020. Hubble constant hunter's guide. Phys. Rev. D 101 (4), 043533. https://doi.org/10.1103/PhysRevD.101.043533. arXiv:1908.03663 [astro-ph.CO].

Kolb, E.W., Turner, M.S., 1990. The Early Universe. Front. Phys. 69, 1–547.

Kumar, S., 2021. Remedy of some cosmological tensions via effective phantom-like behavior of interacting vacuum energy. arXiv:2102.12902 [astro-ph.CO].

Kumar, S., Nunes, R.C., 2016. Probing the interaction between dark matter and dark energy in the presence of massive neutrinos. Phys. Rev. D 94 (12), 123511. https://doi.org/10.1103/PhysRevD.94.123511. arXiv:1608.02454 [astro-ph.CO].

Kumar, S., Nunes, R.C., 2017. Echo of interactions in the dark sector. Phys. Rev. D 96 (10), 103511. https://doi.org/10.1103/PhysRevD.96.103511. arXiv:1702.02143 [astro-ph.CO].

Kumar, S., Nunes, R.C., Yadav, S.K., 2019. Dark sector interaction: a remedy of the tensions between CMB and LSS data. Eur. Phys. J. C 79 (7), 576. https://doi.org/10.1140/epjc/s10052-019-7087-7. arXiv:1903.04865 [astro-ph.CO].

Lewis, A., 2013. Efficient sampling of fast and slow cosmological parameters. Phys. Rev. D 87 (10), 103529. https://doi.org/10.1103/PhysRevD.87.103529. arXiv:1304.4473 [astro-ph.CO].

Lewis, A., Bridle, S., 2002. Cosmological parameters from CMB and other data: a Monte Carlo approach. Phys. Rev. D 66, 103511. https://doi.org/10.1103/PhysRevD.66.103511. arXiv:astro-ph/0205436 [astro-ph].

Lewis, A., Challinor, A., Lasenby, A., 2000. Efficient computation of CMB anisotropies in closed FRW models. Astrophys. J. 538, 473–476. https://doi.org/10.1086/309179. arXiv:astro-ph/9911177 [astro-ph].

Li, H.L., Zhang, J.F., Feng, L., Zhang, X., 2017. Reexploration of interacting holographic dark energy model: cases of interaction term excluding the Hubble parameter. Eur. Phys. J. C 77 (12), 907. https://doi.org/10.1140/epjc/s10052-017-5473-6. arXiv:1711.06159 [astro-ph.CO].

Li, Y.H., Zhang, X., 2014. Large-scale stable interacting dark energy model: cosmological perturbations and observational constraints. Phys. Rev. D 89 (8), 083009. https://doi.org/10.1103/PhysRevD.89.083009. arXiv:1312.6328 [astro-ph.CO].

Lin, W., Chen, X., Mack, K.J., 2021. Early-Universe-physics insensitive and uncalibrated cosmic standards: constraints on Ω_m and implications for the Hubble tension. arXiv:2102.05701 [astro-ph.CO].

Lucca, M., 2021a. Dark energy-dark matter interactions as a solution to the S_8 tension. arXiv:2105.09249 [astro-ph.CO].

Lucca, M., 2021b. Multi-interacting dark energy and its cosmological implications. arXiv:2106.15196 [astro-ph.CO].

Lucca, M., Hooper, D.C., 2020. Shedding light on dark matter-dark energy interactions. Phys. Rev. D 102 (12), 123502. https://doi.org/10.1103/PhysRevD.102.123502. arXiv:2002.06127 [astro-ph.CO].

Mangano, G., Miele, G., Pastor, S., Pinto, T., Pisanti, O., Serpico, P.D., 2005. Relic neutrino decoupling including flavor oscillations. Nucl. Phys. B 729, 221. https://doi.org/10.1016/j.nuclphysb.2005.09.041. arXiv:hep-ph/0506164.

Martinelli, M., Hogg, N.B., Peirone, S., Bruni, M., Wands, D., 2019. Constraints on the interacting vacuum–geodesic CDM scenario. Mon. Not. R. Astron. Soc. 488 (3), 3423–3438. https://doi.org/10.1093/mnras/stz1915. arXiv:1902.10694 [astro-ph.CO].

Morris, M.S., Thorne, K.S., Yurtsever, U., 1988. Wormholes, time machines, and the weak energy condition. Phys. Rev. Lett. 61, 1446–1449. https://doi.org/10.1103/PhysRevLett.61.1446.

Mukherjee, P., Banerjee, N., 2021. Nonparametric reconstruction of interaction in the cosmic dark sector. Phys. Rev. D 103 (12), 123530. https://doi.org/10.1103/PhysRevD.103.123530. arXiv:2105.09995 [astro-ph.CO].

Murgia, R., Gariazzo, S., Fornengo, N., 2016. Constraints on the coupling between dark energy and dark matter from CMB data. J. Cosmol. Astropart. Phys. 1604, 014. https://doi.org/10.1088/1475-7516/2016/04/014. arXiv:1602.01765 [astro-ph.CO].

Nunes, R.C., Di Valentino, E., 2021. Dark sector interaction and the supernova absolute magnitude tension. arXiv:2107.09151 [astro-ph.CO].

Nunes, R.C., Pan, S., Saridakis, E.N., 2016. New constraints on interacting dark energy from cosmic chronometers. Phys. Rev. D 94 (2), 023508. https://doi.org/10.1103/PhysRevD.94.023508. arXiv:1605.01712 [astro-ph.CO].

Paliathanasis, A., Pan, S., Yang, W., 2019. Dynamics of nonlinear interacting dark energy models. Int. J. Mod. Phys. D 28 (12), 1950161. https://doi.org/10.1142/S021827181950161X. arXiv:1903.02370 [gr-qc].

Paliathanasis, A., Leon, G., Khyllep, W., Dutta, J., Pan, S., 2021. Interacting quintessence in light of generalized uncertainty principle: cosmological perturbations and dynamics. Eur. Phys. J. C 81 (7), 607. https://doi.org/10.1140/epjc/s10052-021-09362-8. arXiv:2104.06097 [gr-qc].

Pan, S., Sharov, G.S., 2017. A model with interaction of dark components and recent observational data. Mon. Not. R. Astron. Soc. 472 (4), 4736–4749. https://doi.org/10.1093/mnras/stx2278. arXiv:1609.02287 [gr-qc].

Pan, S., Bhattacharya, S., Chakraborty, S., 2015. An analytic model for interacting dark energy and its observational constraints. Mon. Not. R. Astron. Soc. 452 (3), 3038–3046. https://doi.org/10.1093/mnras/stv1495. arXiv:1210.0396 [gr-qc].

Pan, S., Mukherjee, A., Banerjee, N., 2018. Astronomical bounds on a cosmological model allowing a general interaction in the dark sector. Mon. Not. R. Astron. Soc. 477 (1), 1189–1205. https://doi.org/10.1093/mnras/sty755. arXiv:1710.03725 [astro-ph.CO].

Pan, S., Yang, W., Di Valentino, E., Saridakis, E.N., Chakraborty, S., 2019a. Interacting scenarios with dynamical dark energy: observational constraints and alleviation of the H_0 tension. Phys. Rev. D 100 (10), 103520. https://doi.org/10.1103/PhysRevD.100.103520. arXiv:1907.07540 [astro-ph.CO].

Pan, S., Yang, W., Singha, C., Saridakis, E.N., 2019b. Observational constraints on sign-changeable interaction models and alleviation of the H_0 tension. Phys.

Rev. D 100 (8), 083539. https://doi.org/10.1103/PhysRevD.100.083539. arXiv:1903.10969 [astro-ph.CO].
Pan, S., de Haro, J., Yang, W., Amorós, J., 2020a. Understanding the phenomenology of interacting dark energy scenarios and their theoretical bounds. Phys. Rev. D 101 (12), 123506. https://doi.org/10.1103/PhysRevD.101.123506. arXiv:2001.09885 [gr-qc].
Pan, S., Sharov, G.S., Yang, W., 2020b. Field theoretic interpretations of interacting dark energy scenarios and recent observations. Phys. Rev. D 101 (10), 103533. https://doi.org/10.1103/PhysRevD.101.103533. arXiv:2001.03120 [astro-ph.CO].
Pan, S., Yang, W., Paliathanasis, A., 2020c. Non-linear interacting cosmological models after Planck 2018 legacy release and the H_0 tension. Mon. Not. R. Astron. Soc. 493 (3), 3114–3131. https://doi.org/10.1093/mnras/staa213. arXiv:2002.03408 [astro-ph.CO].
Peebles, P.J.E., Ratra, B., 1988. Cosmology with a time variable cosmological constant. Astrophys. J. Lett. 325, L17. https://doi.org/10.1086/185100.
Perivolaropoulos, L., Skara, F., 2021. Challenges for ΛCDM: an update. arXiv:2105.05208 [astro-ph.CO].
Pettorino, V., Amendola, L., Wetterich, C., 2013. How early is early dark energy? Phys. Rev. D 87, 083009. https://doi.org/10.1103/PhysRevD.87.083009. arXiv:1301.5279 [astro-ph.CO].
Poulin, V., Smith, T.L., Grin, D., Karwal, T., Kamionkowski, M., 2018. Cosmological implications of ultralight axionlike fields. Phys. Rev. D 98 (8), 083525. https://doi.org/10.1103/PhysRevD.98.083525. arXiv:1806.10608 [astro-ph.CO].
Poulin, V., Smith, T.L., Karwal, T., Kamionkowski, M., 2019. Early dark energy can resolve the Hubble tension. Phys. Rev. Lett. 122 (22), 221301. https://doi.org/10.1103/PhysRevLett.122.221301. arXiv:1811.04083 [astro-ph.CO].
Ratra, B., Peebles, P.J.E., 1988. Cosmological consequences of a rolling homogeneous scalar field. Phys. Rev. D 37, 3406. https://doi.org/10.1103/PhysRevD.37.3406.
Raveri, M., Hu, W., Sethi, S., 2019. Swampland conjectures and late-time cosmology. Phys. Rev. D 99 (8), 083518. https://doi.org/10.1103/PhysRevD.99.083518. arXiv:1812.10448 [hep-th].
Riess, A.G., 2019. The expansion of the universe is faster than expected. Nat. Rev. Phys. 2 (1), 10–12. https://doi.org/10.1038/s42254-019-0137-0. arXiv:2001.03624 [astro-ph.CO].
Riess, A.G., Casertano, S., Yuan, W., Macri, L.M., Scolnic, D., 2019. Large magellanic cloud Cepheid standards provide a 1% foundation for the determination of the Hubble constant and stronger evidence for physics beyond ΛCDM. Astrophys. J. 876 (1), 85. https://doi.org/10.3847/1538-4357/ab1422. arXiv:1903.07603 [astro-ph.CO].
Riess, A.G., Casertano, S., Yuan, W., Bowers, J.B., Macri, L., Zinn, J.C., Scolnic, D., 2021. Cosmic distances calibrated to 1% precision with Gaia EDR3 parallaxes and Hubble Space Telescope photometry of 75 Milky Way cepheids confirm tension with ΛCDM. Astrophys. J. Lett. 908 (1), L6. https://doi.org/10.3847/2041-8213/abdbaf. arXiv:2012.08534 [astro-ph.CO].
Ross, A.J., Samushia, L., Howlett, C., Percival, W.J., Burden, A., Manera, M., 2015. The clustering of the SDSS DR7 main Galaxy sample – I: a 4 per cent distance measure at $z = 0.15$. Mon. Not. R. Astron. Soc. 449 (1), 835–847. https://doi.org/10.1093/mnras/stv154. arXiv:1409.3242 [astro-ph.CO].
Salvatelli, V., Marchini, A., Lopez-Honorez, L., Mena, O., 2013. New constraints on coupled dark energy from the Planck satellite experiment. Phys. Rev. D 88 (2), 023531. https://doi.org/10.1103/PhysRevD.88.023531. arXiv:1304.7119 [astro-ph.CO].
Salvatelli, V., Said, N., Bruni, M., Melchiorri, A., Wands, D., 2014. Indications of a late-time interaction in the dark sector. Phys. Rev. Lett. 113 (18), 181301. https://doi.org/10.1103/PhysRevLett.113.181301. arXiv:1406.7297 [astro-ph.CO].
Saridakis, E.N., et al., CANTATA, 2021. Modified gravity and cosmology: an update by the CANTATA network. arXiv:2105.12582 [gr-qc].
Sawicki, I., Vikman, A., 2013. Hidden negative energies in strongly accelerated universes. Phys. Rev. D 87 (6), 067301. https://doi.org/10.1103/PhysRevD.87.067301. arXiv:1209.2961 [astro-ph.CO].
Schöneberg, N., Abellán, G.F., Sánchez, A.P., Witte, S.J., Poulin, c.V., Lesgourgues, J., 2021. The H_0 olympics: a fair ranking of proposed models. arXiv:2107.10291 [astro-ph.CO].
Scolnic, D.M., Jones, D.O., Rest, A., Pan, Y.C., Chornock, R., Foley, R.J., Huber, M.E., Kessler, R., Narayan, G., Riess, A.G., et al., 2018. The complete light-curve sample of spectroscopically confirmed SNe Ia from Pan-STARRS1 and cosmological constraints from the combined Pantheon sample. Astrophys. J. 859 (2), 101. https://doi.org/10.3847/1538-4357/aab9bb. arXiv:1710.00845 [astro-ph.CO].
Sekiguchi, T., Takahashi, T., 2021. Early recombination as a solution to the H_0 tension. Phys. Rev. D 103 (8), 083507. https://doi.org/10.1103/PhysRevD.103.083507. arXiv:2007.03381 [astro-ph.CO].
Sharov, G.S., Bhattacharya, S., Pan, S., Nunes, R.C., Chakraborty, S., 2017. A new interacting two fluid model and its consequences. Mon. Not. R. Astron. Soc. 466 (3), 3497–3506. https://doi.org/10.1093/mnras/stw3358. arXiv:1701.00780 [gr-qc].
Shirokov, S.I., Baryshev, Y.V., 2020. A crucial test of the phantom closed cosmological model. Mon. Not. R. Astron. Soc. 499 (1), L101–L104. https://doi.org/10.1093/mnrasl/slaa167. arXiv:2009.10215 [astro-ph.CO].
Sinha, S., 2021. Differentiating dark interactions with perturbation. Phys. Rev. D 103 (12), 123547. https://doi.org/10.1103/PhysRevD.103.123547. arXiv:2101.08959 [astro-ph.CO].
Steigman, G., Schramm, D.N., Gunn, J.E., 1977. Cosmological limits to the number of massive leptons. Phys. Lett. B 66, 202–204. https://doi.org/10.1016/0370-2693(77)90176-9.
Tröster, T., et al., 2020. Cosmology from large-scale structure: constraining ΛCDM with BOSS. Astron. Astrophys. 633, L10. https://doi.org/10.1051/0004-6361/201936772. arXiv:1909.11006 [astro-ph.CO].
Vagnozzi, S., 2020. New physics in light of the H_0 tension: an alternative view. Phys. Rev. D 102 (2), 023518. https://doi.org/10.1103/PhysRevD.102.023518. arXiv:1907.07569 [astro-ph.CO].
Vagnozzi, S., Di Valentino, E., Gariazzo, S., Melchiorri, A., Mena, O., Silk, J., 2020. Listening to the BOSS: the galaxy power spectrum take on spatial curvature and cosmic concordance. arXiv:2010.02230 [astro-ph.CO].
Väliviita, J., Palmgren, E., 2015. Distinguishing interacting dark energy from wCDM with CMB, lensing, and baryon acoustic oscillation data. J. Cosmol. Astropart. Phys. 1507, 015. https://doi.org/10.1088/1475-7516/2015/07/015. arXiv:1504.02464 [astro-ph.CO].
Valiviita, J., Majerotto, E., Maartens, R., 2008. Instability in interacting dark energy and dark matter fluids. J. Cosmol. Astropart. Phys. 07, 020. https://doi.org/10.1088/1475-7516/2008/07/020. arXiv:0804.0232 [astro-ph].
van Uitert, E., et al., 2018. KiDS+GAMA: cosmology constraints from a joint analysis of cosmic shear, galaxy–galaxy lensing, and angular clustering. Mon. Not. R. Astron. Soc. 476 (4), 4662–4689. https://doi.org/10.1093/mnras/sty551. arXiv:1706.05004 [astro-ph.CO].
Verde, L., Treu, T., Riess, A., 2019. Tensions between the Early and the Late Universe. https://doi.org/10.1038/s41550-019-0902-0. arXiv:1907.10625 [astro-ph.CO], 2019.
vom Marttens, R.F., Casarini, L., Hipólito-Ricaldi, W.S., Zimdahl, W., 2017. CMB and matter power spectra with non-linear dark-sector interactions. J. Cosmol. Astropart. Phys. 01, 050. https://doi.org/10.1088/1475-7516/2017/01/050. arXiv:1610.01665 [astro-ph.CO].
von Marttens, R., Casarini, L., Mota, D.F., Zimdahl, W., 2019. Cosmological constraints on parametrized interacting dark energy. Phys. Dark Universe 23, 100248. https://doi.org/10.1016/j.dark.2018.10.007. arXiv:1807.11380 [astro-ph.CO].
von Marttens, R., Gonzalez, J.E., Alcaniz, J., Marra, V., Casarini, L., 2020. A model-independent reconstruction of dark sector interactions. arXiv:2011.10846 [astro-ph.CO].
Wang, B., Abdalla, E., Atrio-Barandela, F., Pavon, D., 2016. Dark matter and dark energy interactions: theoretical challenges, cosmological implications and observational signatures. Rept. Prog. Phys. 79 (9), 096901. https://doi.org/10.1088/0034-4885/79/9/096901. arXiv:1603.08299 [astro-ph.CO].
Wang, L.F., He, D.Z., Zhang, J.F., Zhang, X., 2021. Constraints on interacting dark energy model from lensed quasars: relieving the H_0 tension from 5.3σ to 1.7σ. arXiv:2102.09331 [astro-ph.CO].
Weinberg, S., 2013. Goldstone bosons as fractional cosmic neutrinos. Phys. Rev. Lett. 110 (24), 241301. https://doi.org/10.1103/PhysRevLett.110.241301. arXiv:1305.1971 [astro-ph.CO].
Wetterich, C., 1988. Cosmology and the fate of dilatation symmetry. Nucl. Phys. B 302, 668–696. https://doi.org/10.1016/0550-3213(88)90193-9. arXiv:1711.03844 [hep-th].
Wetterich, C., 1995. The Cosmon model for an asymptotically vanishing time dependent cosmological 'constant'. Astron. Astrophys. 301, 321–328. arXiv:hep-th/9408025 [hep-th].
Yang, W., Xu, L., 2014a. Cosmological constraints on interacting dark energy with redshift-space distortion after Planck data. Phys. Rev. D 89 (8), 083517. https://doi.org/10.1103/PhysRevD.89.083517. arXiv:1401.1286 [astro-ph.CO].
Yang, W., Xu, L., 2014b. Testing coupled dark energy with large scale structure observation. J. Cosmol. Astropart. Phys. 08, 034. https://doi.org/10.1088/1475-7516/2014/08/034. arXiv:1401.5177 [astro-ph.CO].
Yang, W., Xu, L., 2014c. Coupled dark energy with perturbed Hubble expansion rate. Phys. Rev. D 90 (8), 083532. https://doi.org/10.1103/PhysRevD.90.083532. arXiv:1409.5533 [astro-ph.CO].
Yang, W., Banerjee, N., Pan, S., 2017a. Constraining a dark matter and dark energy interaction scenario with a dynamical equation of state. Phys. Rev. D 95 (12), 123527. https://doi.org/10.1103/PhysRevD.95.123527. arXiv:1705.09278 [astro-ph.CO].
Yang, W., Pan, S., Mota, D.F., 2017b. Novel approach toward the large-scale stable interacting dark-energy models and their astronomical bounds. Phys. Rev. D 96 (12), 123508. https://doi.org/10.1103/PhysRevD.96.123508. arXiv:1709.00006 [astro-ph.CO].
Yang, W., Mukherjee, A., Di Valentino, E., Pan, S., 2018a. Interacting dark energy with time varying equation of state and the H_0 tension. Phys. Rev. D 98 (12), 123527. https://doi.org/10.1103/PhysRevD.98.123527. arXiv:1809.06883 [astro-ph.CO].
Yang, W., Pan, S., Barrow, J.D., 2018b. Large-scale stability and astronomical constraints for coupled dark-energy models. Phys. Rev. D 97 (4), 043529. https://doi.org/10.1103/PhysRevD.97.043529. arXiv:1706.04953 [astro-ph.CO].
Yang, W., Pan, S., Di Valentino, E., Nunes, R.C., Vagnozzi, S., Mota, D.F., 2018c. Tale of stable interacting dark energy, observational signatures, and the H_0 tension. J. Cosmol. Astropart. Phys. 1809, 019. https://doi.org/10.1088/1475-7516/2018/09/019. arXiv:1805.08252 [astro-ph.CO].

Yang, W., Mena, O., Pan, S., Di Valentino, E., 2019a. Dark sectors with dynamical coupling. Phys. Rev. D 100 (8), 083509. https://doi.org/10.1103/PhysRevD.100.083509. arXiv:1906.11697 [astro-ph.CO].

Yang, W., Pan, S., Paliathanasis, A., 2019b. Cosmological constraints on an exponential interaction in the dark sector. Mon. Not. R. Astron. Soc. 482 (1), 1007–1016. https://doi.org/10.1093/mnras/sty2780. arXiv:1804.08558 [gr-qc].

Yang, W., Pan, S., Xu, L., Mota, D.F., 2019c. Effects of anisotropic stress in interacting dark matter – dark energy scenarios. Mon. Not. R. Astron. Soc. 482 (2), 1858–1871. https://doi.org/10.1093/mnras/sty2789. arXiv:1804.08455 [astro-ph.CO].

Yang, W., Di Valentino, E., Mena, O., Pan, S., 2020a. Dynamical dark sectors and neutrino masses and abundances. Phys. Rev. D 102 (2), 023535. https://doi.org/10.1103/PhysRevD.102.023535. arXiv:2003.12552 [astro-ph.CO].

Yang, W., Di Valentino, E., Mena, O., Pan, S., Nunes, R.C., 2020b. All-inclusive interacting dark sector cosmologies. Phys. Rev. D 101 (8), 083509. https://doi.org/10.1103/PhysRevD.101.083509. arXiv:2001.10852 [astro-ph.CO].

Yang, W., Di Valentino, E., Pan, S., Basilakos, S., Paliathanasis, A., 2020c. Metastable dark energy models in light of *Planck* 2018 data: alleviating the H_0 tension. Phys. Rev. D 102 (6), 063503. https://doi.org/10.1103/PhysRevD.102.063503.

Yang, W., Pan, S., Di Valentino, E., Wang, B., Wang, A., 2020d. Forecasting interacting vacuum-energy models using gravitational waves. J. Cosmol. Astropart. Phys. 05, 050. https://doi.org/10.1088/1475-7516/2020/05/050. arXiv:1904.11980 [astro-ph.CO].

Yang, W., Pan, S., Nunes, R.C., Mota, D.F., 2020e. Dark calling Dark: interaction in the dark sector in presence of neutrino properties after Planck CMB final release. J. Cosmol. Astropart. Phys. 04, 008. https://doi.org/10.1088/1475-7516/2020/04/008. arXiv:1910.08821 [astro-ph.CO].

Yang, W., Di Valentino, E., Pan, S., Mena, O., 2021a. A complete model of phenomenologically emergent dark energy. Phys. Dark Universe 31, 100762. https://doi.org/10.1016/j.dark.2020.100762. arXiv:2007.02927 [astro-ph.CO].

Yang, W., Di Valentino, E., Pan, S., Wu, Y., Lu, J., 2021b. Dynamical dark energy after Planck CMB final release and H_0 tension. Mon. Not. R. Astron. Soc. 501 (4), 5845–5858. https://doi.org/10.1093/mnras/staa3914. arXiv:2101.02168 [astro-ph.CO].

Yang, W., Pan, S., Aresté Saló, L., de Haro, J., 2021c. Theoretical and observational bounds on some interacting vacuum energy scenarios. Phys. Rev. D 103 (8), 083520. https://doi.org/10.1103/PhysRevD.103.083520. arXiv:2104.04505 [astro-ph.CO].

Yang, W., Pan, S., Di Valentino, E., Mena, O., Melchiorri, A., 2021d. 2021-H_0 odyssey: closed, phantom and interacting dark energy cosmologies. arXiv:2101.03129 [astro-ph.CO].

Yao, Y., Meng, X.H., 2021. Relieve the H0 tension with a new coupled generalized three-form dark energy model. Phys. Dark Universe 33, 100852. https://doi.org/10.1016/j.dark.2021.100852. arXiv:2011.09160 [astro-ph.CO].

Yao, Y.H., Meng, X.H., 2020. A new coupled three-form dark energy model and implications for the H_0 tension. Phys. Dark Universe 30, 100729. https://doi.org/10.1016/j.dark.2020.100729.

Zyla, P.A., et al., Particle Data Group, 2020. Review of particle physics. PTEP 2020 (8), 083C01. https://doi.org/10.1093/ptep/ptaa104.